12-2011

Optimization-Based Power Management of Hybrid Power Systems with Applications in Advanced Hybrid Electric Vehicles and Wind Farms with Battery Storage

Hoseinali Borhan
Clemson University, hborhan@gmail.com

Optimization-Based Power Management of Hybrid Power Systems with Applications in Advanced Hybrid Electric Vehicles and Wind Farms with Battery Storage

---

A Doctoral Dissertation
Presented to
the Graduate School of
Clemson University

In Partial Fulfillment
of the Requirements for the Degree
Doctor of Philosophy
Mechanical Engineering

---

by
Hoseinali Borhan
December 2011

Accepted by:
Dr. Ardalan Vahidi, Committee Chair
Dr. Mario A. Rotea
Dr. John Wagner
Dr. Mohammed Daqaq
Dr. Martin Schmoll

Abstract

Modern hybrid electric vehicles and many stationary renewable power generation systems combine multiple power generating and energy storage devices to achieve an overall system-level efficiency and flexibility which is higher than their individual components. The power or energy management control, "brain" of these "hybrid" systems, determines adaptively and based on the power demand the power split between multiple subsystems and plays a critical role in overall system-level efficiency. This dissertation proposes that a receding horizon optimal control (aka Model Predictive Control) approach can be a natural and systematic framework for formulating this type of power management controls. More importantly the dissertation develops new results based on the classical theory of optimal control that allow solving the resulting optimal control problem in real-time, in spite of the complexities that arise due to several system nonlinearities and constraints. The dissertation focus is on two classes of hybrid systems: hybrid electric vehicles in the first part and wind farms with battery storage in the second part.

The first part of the dissertation proposes and fully develops a real-time optimization-based power management strategy for hybrid electric vehicles. Current industry practice uses rule-based control techniques with "else-then-if" logic and look-up maps and tables in the power management of production hybrid vehicles. These algorithms are not guaranteed to result in the best possible fuel economy and there exists a gap between their performance and a minimum possible fuel economy benchmark. Furthermore, considerable time and effort are spent calibrating the control system in the vehicle development phase, and there is little flexibility in real-time handling of constraints and re-optimization of the system operation in the event of changing operating conditions and varying parameters. In addition, a proliferation of different powertrain configurations may result in the need for repeated control system redesign. To address these shortcomings, we formulate the power management problem as a nonlinear and constrained optimal control problem. Solution of this optimal control problem in real-time on chronometric- and memory- constrained automotive microcontrollers is quite challenging; this computational complexity is due to the highly nonlinear dynamics of the

powertrain subsystems, mixed-integer switching modes of their operation, and time-varying and nonlinear hard constraints that system variables should satisfy. The main contribution of the first part of the dissertation is that it establishes methods for systematic and step-by step improvements in fuel economy while maintaining the algorithmic computational requirements in a real-time implementable framework. More specifically a linear time-varying model predictive control approach is employed first which uses sequential quadratic programming to find sub-optimal solutions to the power management problem. Next the objective function is further refined and broken into a short and a long horizon segments; the latter approximated as a function of the state using the connection between the Pontryagin minimum principle and Hamilton-Jacobi-Bellman equations. The power management problem is then solved using a nonlinear MPC framework with a dynamic programming solver and the fuel economy is further improved.

Typical simplifying academic assumptions are minimal throughout this work, thanks to close collaboration with research scientists at Ford research labs and their stringent requirement that the proposed solutions be tested on high-fidelity production models. Simulation results on a high-fidelity model of a hybrid electric vehicle over multiple standard driving cycles reveal the potential for substantial fuel economy gains. To address the control calibration challenges, we also present a novel and fast calibration technique utilizing parallel computing techniques.

The second part of this dissertation presents an optimization-based control strategy for the power management of a wind farm with battery storage. The strategy seeks to minimize the error between the power delivered by the wind farm with battery storage and the power demand from an operator. In addition, the strategy attempts to maximize battery life. The control strategy has two main stages. The first stage produces a family of control solutions that minimize the power error subject to the battery constraints over an optimization horizon. These solutions are parameterized by a given value for the state of charge at the end of the optimization horizon. The second stage screens the family of control solutions to select one attaining an optimal balance between power error and battery life. The battery life model used in this stage is a weighted Amp-hour (Ah) throughput model. The control strategy is modular, allowing for more sophisticated optimization models in the first stage, or more elaborate battery life models in the second stage. The strategy is implemented in real-time in the framework of Model Predictive Control (MPC).

Dedication

To my lovely wife and twin girls ***Fereshteh, Parnia***, and ***Ava*** and my parents.

Acknowledgments

I own an enormous debt of gratitude to my PhD advisor, Prof. Ardalan Vahidi, who introduced me to the interesting research area of model predictive control and hybrid electric vehicles and taught me how to apply the theory and do research on real complex engineering problems. I have benefited tremendously not only from his broad knowledge but also from his creative big-picture viewpoint in thinking of concrete issues. I am really grateful for his generous support and patient guidance on every stage of my PhD progress.

I also wish to express my gratitude to my PhD co-advisor, Prof. Mario A. Rotea, Head of Mechanical Engineering Department at the University of Texas at Dallas, who supervised me during a research internship at this university. He introduced me to the interesting research area of wind energy and energy storage systems. I have benefited a great deal from his valuable knowledge in control theory and his abstract thinking in analyzing problems.

The first part of this dissertation was supported by a University Research Program (URP) grant from Ford Motor Company for about four years. I would like to thank Dr. Anthony Phillips, Mr. Ming Kuang, and Dr. Stefano Di Cairano from the Research and Advanced Engineering of Ford Motor Company, and Prof. Ilya V. Kolmanovsky who is currently with the University of Michigan, Ann Arbor for their valuable discussions and feedbacks during this research. I also wish to thank Dr. Wei Liang and Mr. Ryan McGee from Ford Motor Company who helped me in the implementation and calibration of the developed controller over a high-fidelity model of a Ford hybrid vehicle during a research internship at Ford Motor Company. The second part of this dissertation was supported by a research grant from the Department of Energy at the University of Texas at Dallas and partly by an NSF grant at Clemson University. I also wish to thank Dr. Daniel Viassolo from Vestas Technology for his feedbacks and discussions on this part of research.

My special thanks to my PhD committee members, Profs. Wagner and Daqaq from ME Dept. and Prof. Schmoll from Dept. of Math. Sciences; my family; and my friends at Clemson especially Mr. and Mrs. Lotfi, Mrs. Katherine Smith, and Dr. Chen Zhang who all supported me in any respect during my PhD.

Publications

1. H. Borhan, A. Vahidi, A. Phillips, M. Kuang, Ilya V. Kolmanovsky, and S. Di Cairano "MPC-based Energy Management of a Power-Split Hybrid Electric Vehicle", IEEE Transactions on Control Systems Technology, in press. (Article first published online. doi:10.1109/TCST.2011.2134852), 2011

2. H. Borhan, M. Rotea, and D. Viassolo "Optimization-Based Power Management of a Wind Farm with Battery Storage", submitted to the Journal of Wind Energy, 2011

3. H. Borhan and A. Vahidi "MPC-Based Energy Management of a Power-Split Hybrid Electric Vehicle with Combined Battery and Ultracapacitor Energy Storage", submitted to the International Journal of Powertrain (IJPT), 2011

4. H. Borhan, W. Liang, A. Vahidi, A. Phillips, M. Kuang, S. Di Cairano, and R. McGee "Nonlinear Model Predictive Control of a Power-Split Hybrid Electric Vehicle: Influence of Inclusion of Powertrain Dynamics", ASME Dynamic Systems and Control Conference, Arlington, VA, USA, 2011

5. H. Borhan, C. Zhang, A. Vahidi, A. Phillips, M. Kuang, and S. Di Cairano, "Nonlinear Model Predictive Control for Power-Split Hybrid Electric Vehicles", 49th IEEE Conference of Decision and Control (CDC), Atlanta, GA, USA, 2010

6. H. Borhan and A. Vahidi, "Model Predictive Control of a Power-Split Hybrid Electric Vehicle with Combined Battery and Ultracapacitor Energy Storage", American Control Conference (ACC), Baltimore, MD, USA, 2010

7. H. Borhan, A. Vahidi, A. Phillips, M. Kuang, and Ilya V. Kolmanovsky, "Predictive Energy Management of a Power-Split Hybrid Electric Vehicle", American Control Conference (ACC), St. Louis, MO, USA, 2009

Table of Contents

List of Tables

List of Figures

Chapter 1

Introduction

1.1 Motivation and Background

The soaring rate of the energy consumption in the U.S. and worldwide, and the limited energy resources, is constantly challenging us to research and develop energy generating and consumption systems with higher efficiency and increased reliability. The 2009 U.S. flow of energy presented in reference [14], shows that around 37% of energy in the U.S. comes from petroleum; around 71% of this energy is consumed in transportation with a low overall efficiency of less than 30%. Another fact that can be observed from this data is that in the electrical generation sector, around 68% of the generated energy is lost where part of this is due to the difference between the time of supply and demand. For example, the wind energy which currently constitutes around 9% of the renewable energy resources in the U.S. is an intermittent and variable source of energy making its integration to the grid a challenging task [24, 15].

In order to reduce the loss of energy in transportation and also to increase the reliability of the electrical power generated from renewable energy resources including wind energy, one effective solution is addition of a battery storage system to the vehicles' powertrain and to the renewable energy generators. Addition the battery storage provides an extra degree of freedom to both meet the demand power by an operator more reliably and also to operate the combined system more efficiently. Figure 1.1 schematically shows a hybrid power system in which a primary power generator is combined with a battery storage[1]. The primary power generator utilizes energy resources such as petroleum-based fuels or renewable energy

[1]Note that in Figure 1.1, P_{ppg} represents the power of the primary power generator; P_{bs} represents the power of the battery storage; and P_{out} represents the output power available for consumption.

resources to meet power demands and also to charge the battery storage when needed. The battery power source is used to assist the primary power generator in meeting the power demand such that the overall efficiency and load matching are improved. Hybrid electric vehicles and also wind farms with battery storage are two examples of hybrid power systems which are studied in this thesis.

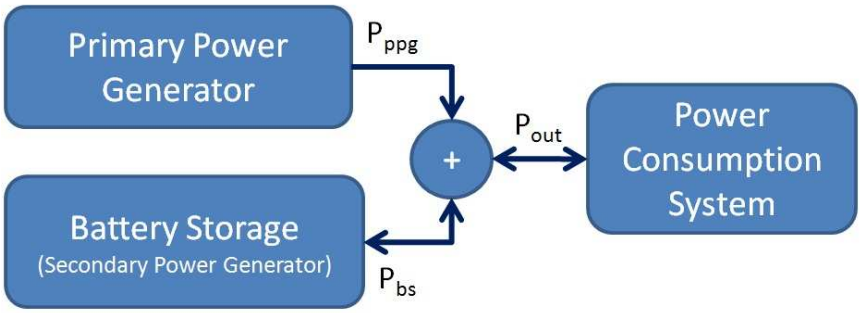

Figure 1.1: Schematic View of a Hybrid Power System

In a hybrid power system, a power (energy) management strategy is required to control the flow of power (energy) between the multiple power sources such that certain performance objectives are optimized while an operator's power demand and the constraints of the system are enforced. A schematic view of a hybrid power system with a power management control block is shown in Figure 1.2[2]. The power management control of hybrid electric vehicles and also wind farms with battery storage systems are reviewed in the following sections.

1.2 Hybrid Electric Vehicles and the Power Management Control

A hybrid electric vehicle (HEV) combines the power of an internal combustion engine with a battery storage [17]. In these vehicles, the battery can be charged or discharged to assist the engine in driving the vehicle. Furthermore, in the braking mode, the kinetic energy of the vehicle dissipated in the conventional vehicles can be partially captured in the battery. A particularly challenging problem for hybrid electric vehicles is their power management algorithm that manages the flow of mechanical and electrical powers in the system. The HEV power management objective is to minimize the total fuel consumption such that the driver demand power is delivered while all system and component level constraints are enforced.

Improvement of fuel economy in hybrid electric vehicles strongly depends on the employed power

[2]Note that in Figure 1.2, *SOC* is the state of charge of the battery storage; P_{ref} is the reference power from an operator; and u_1 and u_2 are the control inputs.

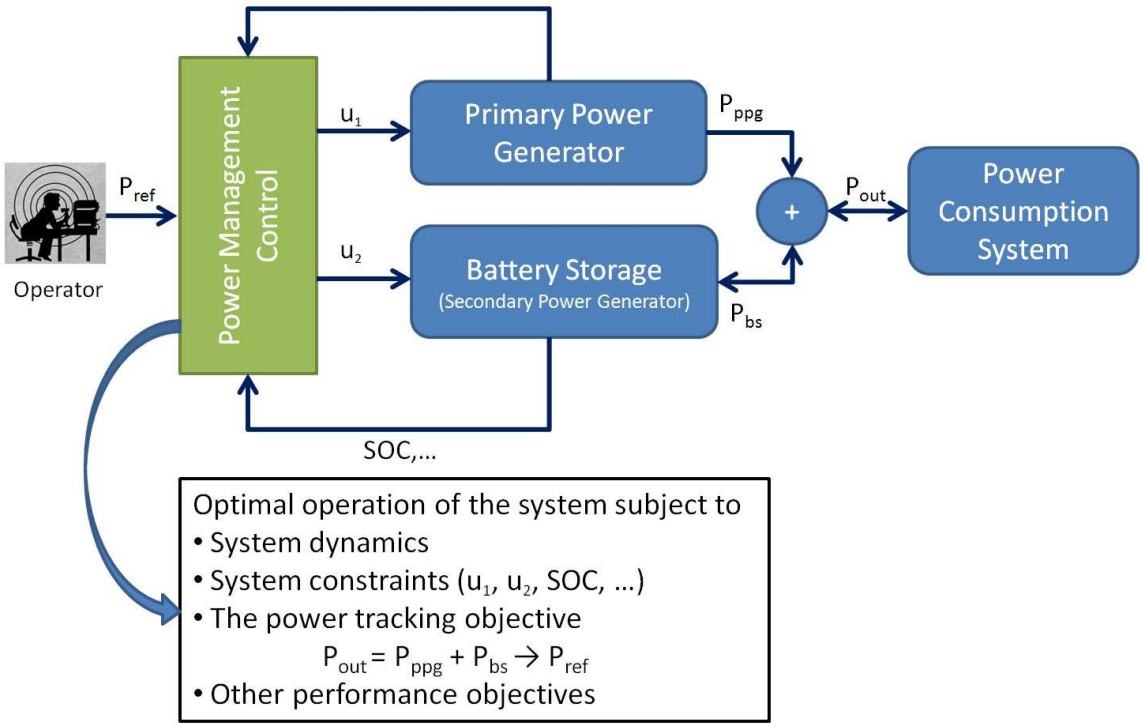

Figure 1.2: Power Management Control

(energy) management strategy. When formulated in an optimal control framework, the HEV power management problem becomes a nonlinear, constrained, and dynamic optimization problem, due to the nonlinearities of the dynamic model of the powertrain and several equality and inequality constraints on the states and on the control inputs. In the past, researchers have used numerical solutions, e.g. based on dynamic programming (DP), as in references [19, 43], or have simplified the dynamic optimization problem to an equivalent instantaneous optimization which is called Equivalent Consumption Minimization Strategy (ECMS), as in references [46, 47, 45]. Comprehensive reviews of these optimal control methods, along with heuristic rule-based strategies, can be found in reference [45] and [51]. If we assume to have the full knowledge of the future driving conditions, the globally optimal solution for a model of the HEV can be derived with dynamic programming (DP). However, the DP solutions are dependent on usually unknown future power demands, and are computationally demanding when a long horizon is considered. Furthermore, even for a known driving cycle, the optimal control obtained by DP cannot be applied directly to the vehicle because of the differences between the model which is used for the DP calculations and the real vehicle or high-fidelity models [10]. Because of these issues, DP solutions have only been used as a benchmark for the best achievable fuel economy on an HEV. In order to develop an optimization-based strategy which can be applied in real-time, in the ECMS

approach an instantaneous optimization method is proposed in references [46, 47, 40]. The ECMS approach introduces an equivalent fuel cost for the battery discharge. This equivalent fuel cost is added to the fuel consumption to define a total fuel cost. Although ECMS can be applied in real-time as a causal controller, the decisions are instantaneous because the dynamics of the system are not considered in the optimization.

A compromise between the computational cost and none-causality of the globally optimal DP control and the faster, causal, but instantaneous ECMS control can be formed in a power management strategy based on Model Predictive Control (MPC). This is the subject of the first part of this thesis; the results that will be presented have appeared in a series of conference and journal publications by the author and his collaborators. In reference [28], a linear time-varying (LTV) MPC for the power management of a power-split HEV[3] is formulated by the author and his collaborators. In this formulation, by defining a quadratic cost function over a prediction horizon, linear MPC methods are implemented for the HEV power management in real-time. Later in reference [27], we have reformulated the MPC fuel minimization problem to include not only the fuel cost over the prediction horizon but also an approximate cost-to-go beyond the planning horizon represented as a terminal cost in the MPC. In this formulation, the relationship between the Hamilton-Jacobi-Bellman (HJB) equation and the Pontryagin's minimum principle is used to show how to tune the approximate cost-to-go function [27], [44], [53]. The simulation results of this MPC over a high-fidelity model of the HEV with respect to both the LTV MPC and the PSAT software show noticeable improvements [27, 29]. However, because the powertrain dynamics are ignored in the MPC calculations, heuristic strategies should still be defined to penalize the engine transients in the cost function. In reference [10], by adding an additional state (engine speed) to the MPC, we have included the powertrain inertial dynamics in the MPC optimization. It is shown that without any heuristic engine start and stop strategy, the fuel economy of the MPC can be further improved with respect to the MPC with only battery dynamics.

1.3 Wind Farms with Battery Storage and the Power Management Control

Wind energy is a promising source of renewable energy that has grown rapidly in the U.S. and abroad. Given the intermittent nature of the wind, the output power of a wind farm is variable creating grid integration issues. Battery storage systems have been proposed [24] to mitigate the effect of the variable wind

[3] A power-split HEV is an advanced hybrid electric vehicle with an electrically continues transmission system. More details are presented in Chapter 2.

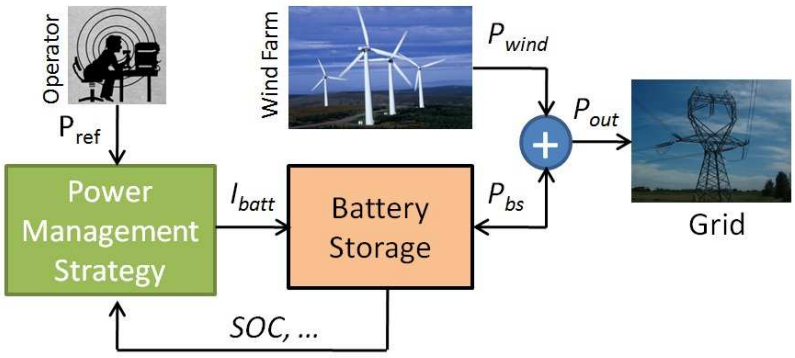

Figure 1.3: Wind farm with battery storage system

resource and deliver a firm and reliable power over a given time period. A schematic view of a wind farm with battery storage is presented in Figure 1.3, which shows how the wind farm power is combined with the battery storage power to deliver power to the grid as close as possible to the reference power specified by an operator. Costs associated to battery storage maintenance and replacements are quite large. Therefore, for an economically feasible project, special attention should be placed on the way the storage is operated. In addition, costs increase as storage size increases, which highlight the importance of operating the storage in the most efficient fashion.

A power management system is required to operate the battery storage. There are two main objectives in developing the power management system:

1. **Power error objective:** Minimize the power error between the combined output power (P_{out}) of the wind farm with the battery storage and an operator reference power (P_{ref}); see Figure 1.3.

2. **Battery life objective:** Extend the battery life in order to reduce the maintenance and replacement costs.

In reference [21], a rule-based strategy is developed for power dispatching of a wind farm with battery storage. This reference considers a feedback control scheme to incorporate the operating constraints of the battery including the state of charge (SOC) and current. The goal of the strategy is to use the battery storage in order to dispatch the wind farm to the grid on an hourly basis. Later, in reference [6], the authors develop a solution to the problem introduced in [21] using Model Predictive Control (MPC). The problems considered in [21] and [6] address the power error minimization objective (objective 1) primarily. The battery life extension objective (objective 2) is addressed in an indirect fashion, by constraining battery current and

SOC. There is not explicit life model of the storage system in the formulation presented in these references.

The second part of the dissertation describes an optimization-based strategy for the power management problem of battery storage in a wind farm. Power management is achieved by commanding the instantaneous current to the battery storage. This current command is generated via optimization and seeks to reduce power error (objective 1) while extending battery life (objective 2). *Modularity* is one of the most appealing features of the proposed strategy. With minimal changes, the formulation can accommodate more sophisticated optimization models as well as more elaborated battery life models.

The joint optimization of power error and battery life leads to an optimal control problem, which in general is not simple to be solved in real-time. We manage the complexity of this problem by decomposing it into three subproblems solved in three separate stages. In the first stage, a family of control solutions (i.e., battery current profiles) is generated by minimizing the power error objective with battery constraints over an optimization horizon. The family of control solutions is parameterized with a set of pre-defined terminal values for the battery state of charge (SOC) at the end of the optimization horizon. In the second stage, a battery life model is applied to the family of solutions in order to calculate the loss of battery life for each member of the family. Finally in the third stage, by means of a pre-defined cost function that combines power error and loss of battery life, the family of solutions is screened and the control current with the best balance between power error reduction and battery life extension is selected. The strategy is performed in the framework of Model Predictive Control (MPC) [34] and the effectiveness of the strategy is shown by closed-loop simulations using actual wind farm power data.

The power management strategy is demonstrated via simulations using the setup shown schematically in Figure 1.3. In this setup, the wind farm consists of a number of wind turbine generators with total installed capacity equal to 150 MW. The wind power data used in simulations come from an actual farm located in the state of Texas. The battery storage consists of a number of lead-acid batteries combined in series and parallel to produce enough power and energy to the system. We have selected the lead- acid technology for the storage since it is one of the cost effective options for large-scale storage applications such as wind farms. However, the strategy can be easily applied on other battery technologies.

1.4 Thesis Overview

In the first part of this dissertation, optimization-based strategies are developed for the real-time power management of a power-split HEV. Current practice uses rule-based control techniques with logics

and look-up maps and tables in the power management of production hybrid vehicles. These algorithms are not guaranteed to result in the best possible fuel economy and there exists a gap between their performance and a maximum possible fuel economy benchmark. Furthermore, considerable time and effort are spent calibrating the control system in the vehicle development phase, and there is little flexibility in real-time handling of constraints and re-optimization of the system operation in the event of changing operating conditions and varying parameters. Therefore, optimization-based control strategies are required to facilitate closer-to-optimal power management of the HEV, while easing the calibration process. To systematically design and calibrate the power management control of a power-split HEV, first the objective of minimizing fuel consumption is formulated as a nonlinear and constrained optimal control problem. Then in order to solve this optimal control problem in real-time, MPC-based power management strategies are developed and applied on high-fidelity HEV models.

The outline of the first part of this dissertation which includes chapters 2-6 is as follows: First in Chapter 2, control-oriented modeling of the power-split HEV is presented. This model is used to design the strategy with Model Predictive Control (MPC). It is shown that a power-split HEV has two control inputs and depending on the level of accuracy, the control-oriented model may have one state, the battery state of charge, or two states, the battery state of charge and the engine speed. In Chapter 3, a quadratic cost function is defined for the power management problem of the HEV and a linear time-varying (LTV) MPC method is applied to solve the control problem in real-time. The simulation results over a high-fidelity model of a power-split HEV are shown to be comparable with or better than a rule-based controller. In Chapter 4, in order to improve the fuel economy of the LTV MPC, a new form of cost function is derived and a nonlinear MPC approach with a dynamic programming (DP) solver is employed to solve the control problem in real-time. The closed-loop simulation results over the high-fidelity model of the HEV are presented showing noticeable improvement with respect to both the rule-based controller and also the LTV MPC. In Chapter 5, the nonlinear MPC is applied to a high-fidelity model of an HEV from Ford Motor Company. Furthermore, it is shown that the engine speed dynamics, especially in engine start/stop transients, have a considerable effect on the fuel economy. Therefore, the engine speed dynamics is incluced in the model of the MPC and a 2-state MPC with a DP solver is applied over the Ford high-fidelity model. The simulation results show that with the 2-state MPC strategy, the MPC fuel economy is further improved. In Chapter 6, a summary of the HEV research findings and the potential future works are presented.

In the second part of this dissertation, an optimization-based strategy is developed for the real-time power management of a wind farm with battery storage in order to optimize the power error minimization

and battery life extension objectives discussed in Section 1.3. The complexity of the problem is managed by decomposing the controller into two main stages. In the first stage, a family of optimal solutions are generated by solving a one-state power error minimization problem over an optimization horizon. The solutions are parameterized by a set of pre-defined SOCs at the end of the optimization horizon. In the second stage, the family of solutions are screened by a battery life model in order to select a control solution that attains an optimal balance between the power error and battery life. The strategy is implemented in the framework of Model Predictive Control.

The outline of the second part of this dissertation which includes chapters 7-9 is as follows: First in Chapter 7, the control objectives of the power management problem for the wind farm with battery storage are modeled for the control design. Then in Chapter 8, an MPC-based power management strategy is developed to solve the control problem in real-time. In this strategy, first a family of control solutions are generated over a prediction horizon. Then, based on a battery life model, the family of solutions are screened and a control signal to the battery storage that balances the control objectives is calculated. The simulation results over real wind farm data are presented showing the effectiveness of the strategy. Finally in Chapter 9, a summary and potential future works based on the findings in the second part of the dissertation are presented.

Part 1:

Optimization-Based Power Management of an Advanced Hybrid Electric Vehicle

Chapter 2

Control-Oriented Modeling of a Power-Split HEV

Hybrid Electric Vehicles (HEVs) are characterized by their powertrain system which combines an internal combustion engine (ICE) with a high voltage battery. They have better fuel efficiency than conventional vehicles due to energy recovery from regenerative braking and higher powertrain efficiency with battery assistance. Among possible configurations of a hybrid electric powertrain, power-split (parallel-series) which provides both series and parallel functionality is produced by several auto-makers. Toyota Prius, Ford Fusion Hybrid, and Ford Escape Hybrid are among the HEVs which have a power-split powertrain. We select this type of hybrid vehicle in this research. Figure 1 shows the main components of a power-split HEV. In this configuration, the engine and the generator are connected to the planet carrier and sun gear of a planetary gear set or speed coupler, respectively. The output of the speed coupler is combined with a second motor/generator through a torque coupler to power the vehicle driveline. In addition, a battery provides another degree of freedom to save or deliver energy. Thus, there are two degrees of freedom for the power management of these HEVs. The two degrees of freedom and different modes of operation of a power-split HEV allow the vehicle to operate more efficiently and consequently to have reduced fuel consumption.

In this section, a control-oriented model for the power management of a power-split HEV is derived. The derivations are based on our work presented in [28, 29] and the related publications in the literature including [33], [12]. This model will be used in designing our model-based power management strategies based on model predictive control. In Figure 1, a schematic diagram of a power-split HEV components is

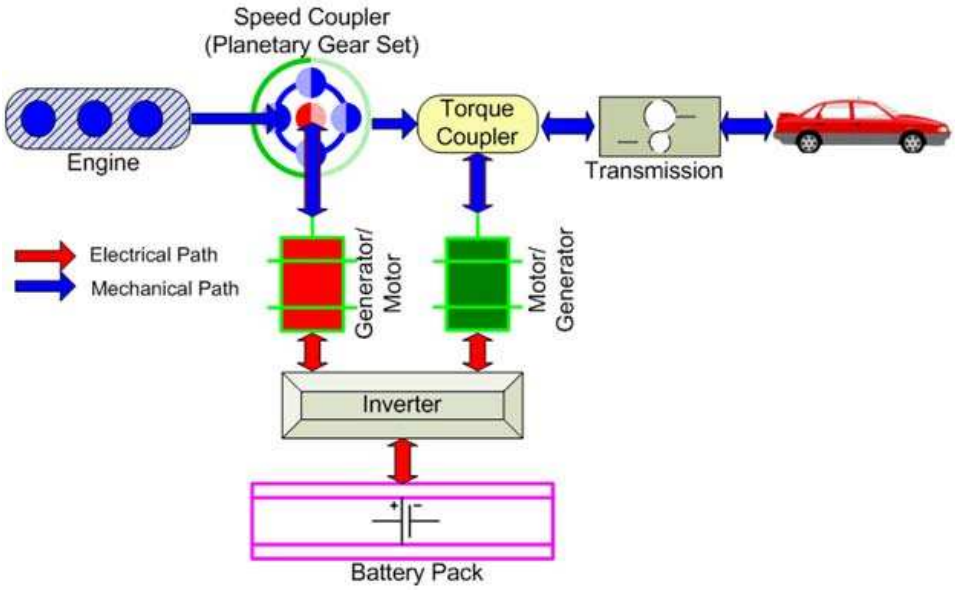

Figure 2.1: A Power-Split HEV Configuration

shown. As it is shown in the figure, The HEV powertrain can be divided into chassis, transaxle, engine, and electrical subsystems. An internal combustion engine, the main source of HEV power, converts the fuel chemical power into the mechanical energy to drive the vehicle. In the transaxle, a planetary gear set combines power of the engine and the generator. A torque coupler combines the power of the motor and that of the ring gear of the planetary gear set. Furthermore, there is a final drive that reduces the output speed of the powertrain. In the electrical system, there are two electrical machines, referred to as the generator and the motor, and a high voltage battery package. The battery can either drive the vehicle or store energy. Both the motor and generator may work in motoring and generating modes. The governing equations for each subsystem is presented next.

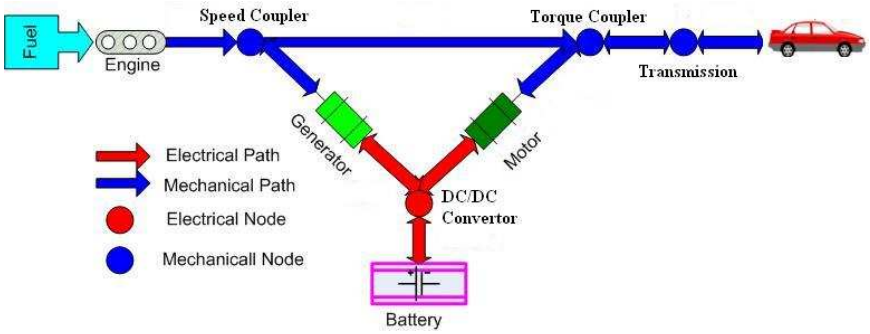

Figure 2.2: A Power-Split HEV Configuration

2.1 The Powertrain Model

As it is shown in Figure 2.3, the power-split powertrain, also called electric-continuously variable transmission, includes a planetary gear set (speed coupler) which combines the power of engine, motor, and generator. This power coupling can be accomplished such that the engine operating point becomes independent of the vehicle operating conditions. Neglecting the inertia of pinion gears in the planetary gear set and assuming that all the connecting shafts in the powertrain are rigid, the dynamics of the powertrain can be obtained applying Newton's motion laws

$$\begin{aligned} J_{gen}\frac{d\omega_{gen}}{dt} &= T_{gen} - F \cdot N_S \\ J_{eng}\frac{d\omega_{eng}}{dt} &= T_{eng} + F \cdot (N_S + N_R) \\ J_{mot}\frac{d\omega_{mot}}{dt} &= T_{mot} - \rho_{m2r} \cdot N_r \cdot F - \rho_{m2d} \cdot T_{out} \end{aligned} \tag{2.1}$$

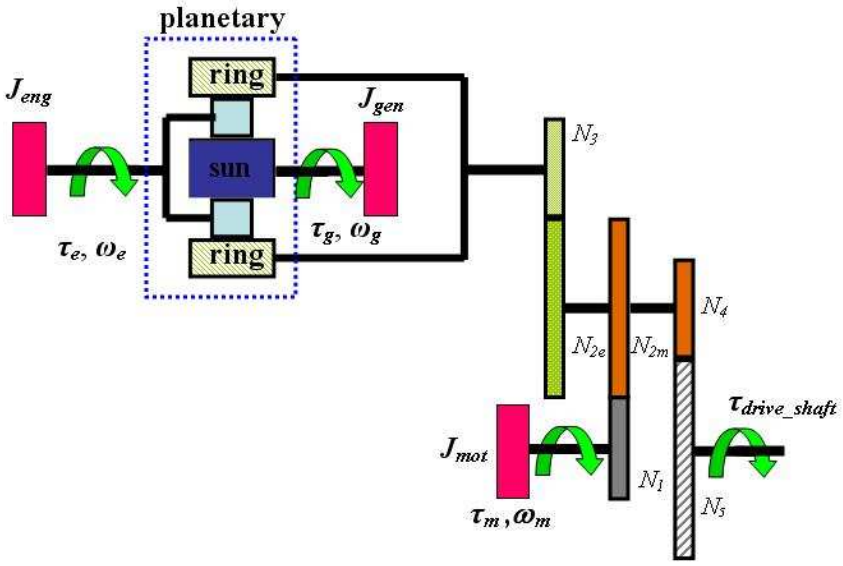

Figure 2.3: A Ford Power-split HEV driveline [10]

where J_{gen} is the lumped inertia of the generator and the sun gear; J_{eng} is the lumped inertia of the engine and the carrier gear; and J_{mot} is the inertia of the motor. In equations (2.1), N_S and N_R are the radii of the sun and ring gears; T_{eng}, T_{gen}, and T_{mot} are the engine, generator, and motor torques, respectively; ω_{eng}, ω_{gen}, and ω_{mot} are the engine, generator, and motor speeds, respectively; and T_{out} is the powertrain output torque on the wheel. Also in equations (2.1), F is the interaction force between the different gears and ρ_{m2r} and ρ_{m2d}

are defined by (Figure 2.3)

$$\rho_{m2r} = \frac{N_{2e}}{N_3} \cdot \frac{N_1}{N_{2m}}, \rho_{m2d} = \frac{N_1}{N_{2m}} \cdot \frac{N_4}{N_5} \tag{2.2}$$

There are also two kinematic equality constraints between velocities

$$N_S \omega_{gen} + N_R \omega_{ring} = (N_S + N_R)\, \omega_{eng} \tag{2.3}$$

where

$$\omega_{ring} = \rho_{m2r} \cdot \omega_{mot};\ \omega_{mot} = \frac{V}{r_w \cdot \rho_{m2d}} \tag{2.4}$$

In (2.4), V is the vehicle velocity with dynamics described by

$$m\frac{dV}{dt} = \frac{T_{out} + T_b}{r_w} - \frac{1}{2}A_{veh}c_d V^2 - f_r mg\cos(\theta) + mg\sin(\theta) \tag{2.5}$$

In equation (2.5), m and A_{veh} are the mass and frontal area of the vehicle, respectively, r_w is the wheel radius, f_r is the coefficient of rolling resistance, c_d is the air drag coefficient, θ is the road grade, and g is the gravity acceleration.

2.2 The Electrical Subsystem Model

The battery state of charge (SOC) has been considered as the main state in optimal control of an HEV and its dynamics can be represented by [51]

$$\frac{dSOC}{dt} = -\frac{V_{oc} - \sqrt{V_{oc}^2 - 4P_{batt}R_{batt}}}{2C_{batt}R_{batt}} \tag{2.6}$$

where

$$P_{batt} = P_{mot} + P_{gen} + P_{motor}^{loss} + P_{gen}^{loss} \tag{2.7}$$

and

$$P_{mot} = T_{mot} \cdot \omega_{mot}; P_{gen} = T_{gen} \cdot \omega_{gen} \tag{2.8}$$

In these equations, V_{oc}, R_{batt}, and C_{batt} are the battery open-circuit voltage, the internal resistance, and the ca-

pacity, respectively; P_{batt} is the battery power; P_{mot} and P_{gen} are the motor and generator power, respectively; and P_{motor}^{loss} and P_{gen}^{loss} are the motor and generator power losses, respectively. In this model, a positive battery power ($P_{batt} > 0$) indicates the battery is discharging and a negative battery power ($P_{batt} < 0$) indicates the battery is charging. As it is shown in Figure 2.4, empirical maps are used to calculate the power loss of the motor and generator as functions of their corresponding torque and speed.

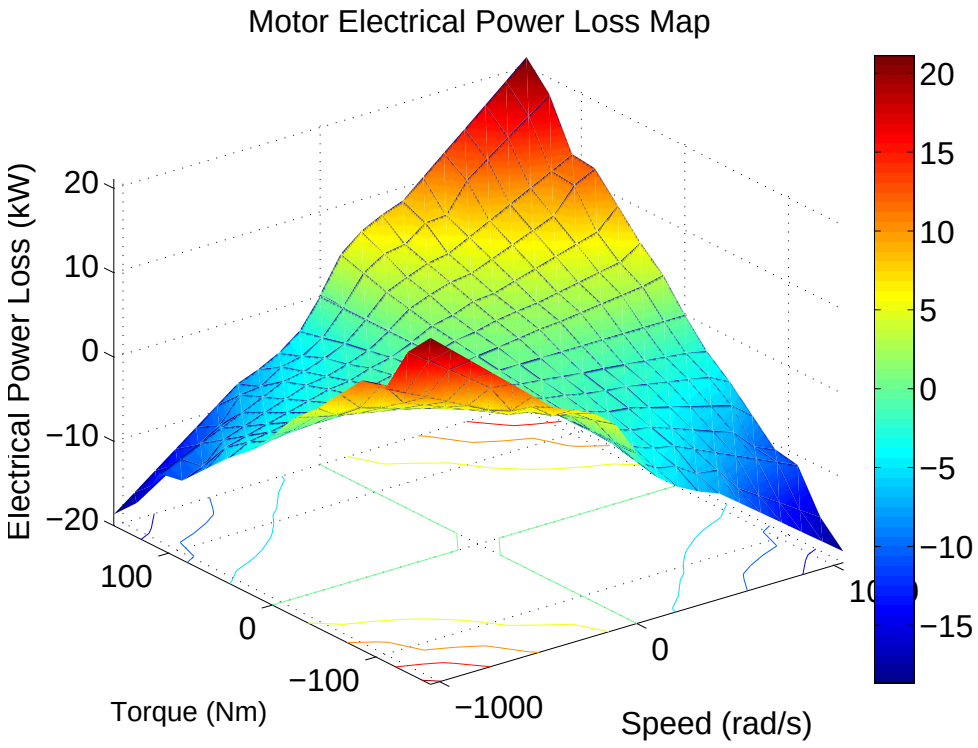

Figure 2.4: Motor Power Loss Map (Toyota Prius PSAT model [31]

The model of the electrical system is constrained by

$$\begin{aligned} SOC^{\min} \leq SOC \leq SOC^{\max};\ P_{batt}^{\min} \leq P_{batt} \leq P_{batt}^{\max} \\ T_{mot}^{\min} \leq T_{mot} \leq T_{mot}^{\max};\ \omega_{mot}^{\min} \leq \omega_{mot} \leq \omega_{mot}^{\max} \\ T_{gen}^{\min} \leq T_{gen} \leq T_{gen}^{\max};\ \omega_{gen}^{\min} \leq \omega_{gen} \leq \omega_{gen}^{\max} \end{aligned} \tag{2.9}$$

where $\cdot^{\min}$ and $\cdot^{\max}$ denote the minimum and maximum bounds which may be variable. As presented in Figure

2.5, empirical maps are used to calculate the maximum and minimum torques of the motor and generator as functions of their corresponding torque and speed.

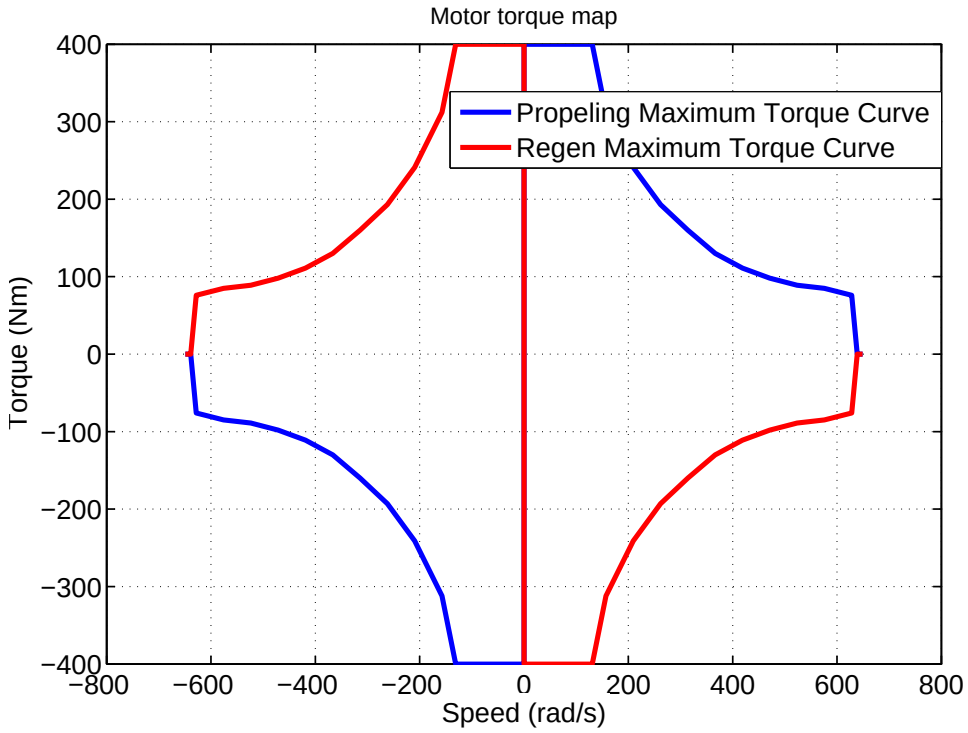

Figure 2.5: Motor maximum torque (Toyota Prius PSAT model [31])

2.3 The Engine Model

In the control-oriented model, the thermal and fluid dynamics of the engine are ignored with respect to the inertial dynamics of the engine presented in equation (2.1). An empirical map of the engine is used to relate the fuel consumption rate, $\dot{m}_f$, to the engine speed and torque as (see Figure 2.6)

$$\dot{m}_f = \varphi(\omega_{eng}, T_{eng}) \tag{2.10}$$

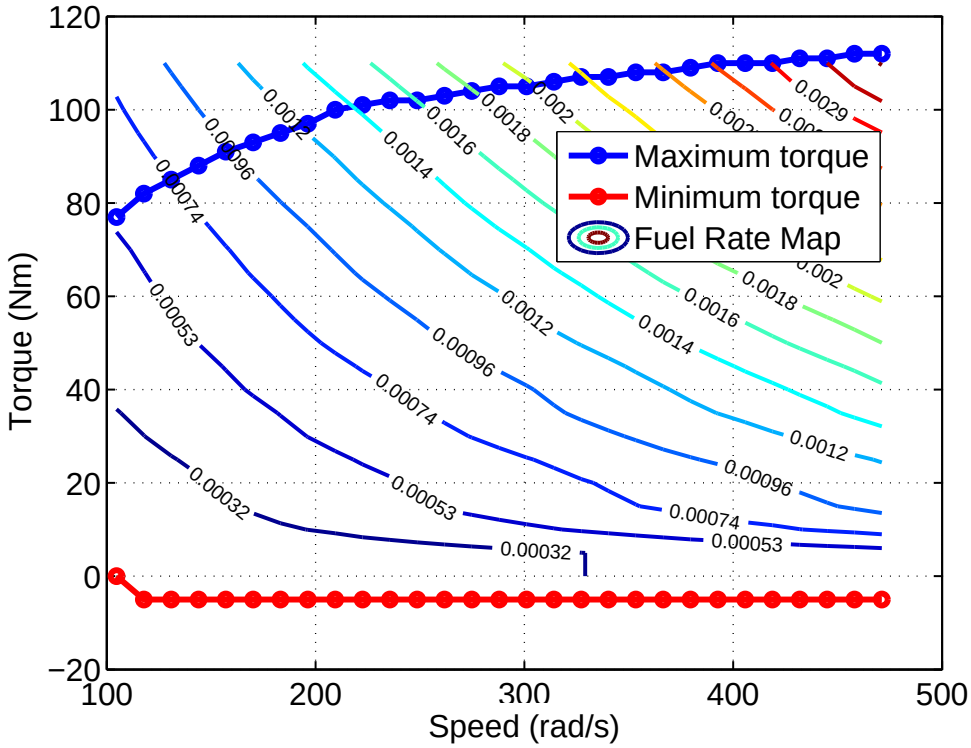

Figure 2.6: Engine fuel rate and maximum torque (Toyota Prius PSAT model [31])

The model of the engine is constrained by

$$T_{eng}^{\min} \leq T_{eng} \leq T_{eng}^{\max};\ \omega_{eng}^{\min} \leq \omega_{eng} \leq \omega_{eng}^{\max} \tag{2.11}$$

where empirical maps are used to calculate the maximum and minimum torques of the engine as functions of engine torque and speed as presented in Figure 2.6.

2.4 The Augmented Model

The drivability constraint requires that the total torque at the wheels, which is the sum of the powertrain output torque, T_{out}, and the friction brake torque[1], T_b, to be equal to the driver demanded torque, T_{driver}

$$T_{out} + T_b = T_{driver} \tag{2.12}$$

Assuming that the above drivability constraint holds at each time, the vehicle speed dynamics presented in equation (2.5) can be removed from the control-oriented model (it does not add an additional state to the control model). The vehicle velocity dynamics will be used later to predict vehicle speed profile from an initial vehicle velocity and a driver torque profile. By combining the above equations and considering the driveability constraint, the *control-oriented model* is obtained as

$$\begin{aligned} \dot{x} &= f(x,u,v) \\ y &= g(x,u,v) \end{aligned} \tag{2.13}$$

where

$$x = \begin{bmatrix} SOC \\ \omega_{eng} \end{bmatrix},\ u = \begin{bmatrix} T_{eng} \\ T_{gen} \end{bmatrix},\ v = \begin{bmatrix} T_{driver} \\ V \end{bmatrix}$$

and

$$y = \begin{bmatrix} \dot{m}_f \\ P_{batt} \\ \omega_{gen} \\ T_{mot} \end{bmatrix}$$

in equation (2.13), x is the state vector, u is the input vector (optimization variables), v is the measured disturbance, and y is the output vector. f is defined by

$$f = \begin{bmatrix} f_1(x,u,v) \\ f_2(x,u,v) \end{bmatrix}, \tag{2.14}$$

[1]The HEV has a conventional braking system in addition to the regenerative braking system. The braking power drained by the conventional brakes follows a different energy path,since it does not recharge the battery.

where

$$f_1 = -\frac{V_{OC}-\sqrt{V_{OC}^2-4P_{batt}R_{batt}}}{2C_{batt}R_{batt}} \tag{2.15}$$

$$\begin{aligned} f_2 = &(\frac{1}{J_{Lumped}}T_{eng} + \left(\frac{N_S+N_R}{N_S}\right)T_{gen} + \left(\frac{J_{gen}}{mr_w\rho_{m2d}}\right)\left(\frac{N_SN_R+N_R^2}{N_S^2}\right) \\ &\times(\frac{T_{driver}}{r_w} - \frac{1}{2}A_{veh}c_dV^2 - f_rmg\cos(\theta) + mg\sin(\theta))) \end{aligned} \tag{2.16}$$

and $J_{Lumped} = J_{eng} + J_{gen}\left(\frac{N_S+N_R}{N_S}\right)^2$. The computation of y by g in (2.13), i.e. of $\dot{m}_f$, P_{batt}, and ω_{gen} is defined by (2.10), (2.7), (**??**), and T_{mot} is obtained by

$$\begin{aligned} T_{mot} = &\rho_{m2r}\left(\frac{N_R}{N_S+N_R}\right)(J_{eng}f_2 - T_{eng}) + \rho_{m2d}(T_{driver} - T_b) \\ &+ \left(\frac{J_{mot}}{r_w\rho_{m2d}m}\right)(\frac{T_{driver}}{r_w} - \frac{1}{2}A_{veh}c_dV^2 - f_rmg\cos(\theta) + mg\sin(\theta)) \end{aligned} \tag{2.17}$$

Since this model has two state variables, we call it the 2-state (control-oriented) model. If we ignore the inertial dynamics of the motor, the generator, and the engine (powertrain), a computationally simplified model with just battery SOC dynamics is obtained, we refer to it by 1-state (control-oriented) model [28, 29, 26]. The 1-state control oriented model can be represented in the state-space as

$$\begin{aligned} \dot{x} &= f(x,u,v) \\ y &= g(x,u,v) \end{aligned} \tag{2.18}$$

where

$$x = SOC,\ u = \begin{bmatrix} T_{eng} \\ \omega_{eng} \end{bmatrix},\ v = \begin{bmatrix} T_{driver} \\ V \end{bmatrix}$$

and

$$y = \begin{bmatrix} \dot{m}_f \\ P_{batt} \\ \omega_{gen} \\ T_{mot} \\ T_{gen} \end{bmatrix}$$

In the next three chapters, the designs of an MPC with these control-oriented models for the power

management of the HEV are presented and simulated over high-fidelity models of the HEV.

Chapter 3

HEV Optimization-Based Power Management with Linear Time-Varying MPC

In this chapter, the power management problem is formulated as a linear MPC problem and a quadratic programming method is used to solve it in real-time. For this purpose, a quadratic cost function is chosen

$$J = \int_t^{t+\Delta t} (w_f \cdot (\dot{m}_f(\tau))^2 + w_{SOC} \cdot (SOC(\tau) - SOC_r)^2) d\tau \tag{3.1}$$

where Δt is the prediction horizon, and w_f and w_{SOC} are the penalty weights. Based on the derived 1-State control-oriented model and the constraints in equations (2.18), (2.9) and (2.11), the moving horizon optimal control problem at each time is defined by

$$\begin{aligned} &\min_{\substack{u(\tau) \\ t \le \tau \le t+\Delta t}} \int_t^{t+\Delta t} (w_f \cdot (\dot{m}_f(\tau))^2 + w_{SOC} \cdot (SOC(\tau) - SOC_r)^2) d\tau \\ &S\dot{O}C = f(u(\tau), v(\tau)) \\ &SOC_{\min} \le SOC(\tau) \le SOC_{\max}, u(\tau) \in U, y(\tau) \in Y \end{aligned} \tag{3.2}$$

where U and Y are the admissible sets of inputs and outputs according to equations (2.9) and (2.11). Note that SOC at time t in optimal control problem presented in equations (3.2) is the measured value of the state at current time and is known. This quadratic finite-horizon optimal control problem can be solved using the linear MPC approach as explained in the following sections.

3.1 Linear Model Predictive Control

LTV-MPC control strategy is based on the standard MPC method for the linear systems, which is briefly explained first. More details can be found in [34, 52]. In the standard MPC, a finite-horizon quadratic cost functional penalizes deviation of the system outputs y from the corresponding references r. In its more general form, the associated optimization problem can be formulated in discrete-time as

$$\begin{aligned} &\min_{\Delta U} J = \sum_{i=0}^{N-1} \|u(k+i) - u_{target}(k)\|^2_{w_i^u} + \\ &\|\Delta u(k+i)\|^2_{w_i^{\Delta u}} + \|y(k+i+1|k) - r(k+i+1)\|^2_{w_{i+1}^y} + \rho_\varepsilon \varepsilon^2 \end{aligned} \tag{3.3}$$

subject to

$$\begin{cases} x(k+i+1|k) = Ax(k+i|k) + B_u u(k+i) + B_v v(k+i) \\ y(k+i|k) = Cx(k+i|k) + D_v v(k+i) \end{cases}$$

$$u_i^{\min} \le u(k+i) \le u_i^{\max}$$

$$\Delta u_i^{\min} \le \Delta u(k+i) \le \Delta u_i^{\max}$$

$$-\varepsilon + y_i^{\min} \le y(k+i+1|k) \le y_i^{\max} + \varepsilon$$

$$\Delta u(k+i) = 0 \; for \; i = M, ..., N$$

$$\varepsilon \ge 0$$

where N is the prediction horizon, M is the control horizon, $\Delta U = [\Delta u(k), ..., \Delta u(k+M-1)]^T$ is the sequence of input increments to be optimized, v is the vector of known inputs or measured disturbances, w_i^u, $w_i^{\Delta u}$, w_{i+1}^y and ρ_ε are the weighting factors at the i^{th} sample time, $x(k+i|k) \in R^n$ is the predicted state vector, $u(k+i) \in R^m$ is the vector of the manipulated variables, $y(k+i|k)$ is the vector of the predicted outputs, $r(k)$ is the vector of the output references, $u_{target}(k)$ is the input steady-state references, and ε is the softening or slack variable used to avoid infeasibility. Using the discrete model of the system, the outputs over a finite future

horizon are predicted by

$$
\begin{aligned}
&y(k+i+1|k) = C[A^{i+1}x(k) + \\
&\sum_{l=0}^{i} A^{i}B_u \left(u(k-1) + \sum_{j=0}^{l} \Delta u(k+j) \right) + \\
&B_v v(k+l)] + D_v v(k)
\end{aligned}
\tag{3.4}
$$

Substituting predicted trajectories of the outputs into the performance index J and output constraints, the optimization problem can be formulated as a Quadratic Program (QP) with linear inequality constraints

$$
[\Delta U^*, \varepsilon] = \arg\min_{\Delta U, \varepsilon} \left(\frac{1}{2} \Delta U^T H \Delta U + F^T \Delta U \right) \tag{3.5}
$$

subject to

$$
G_u \Delta U + G_\varepsilon \varepsilon \leq W
$$

where H, F, G_u, G_ε, and W are constant matrices and functions of references, measured inputs, input targets, the last control input, and the measured or estimated states at current sample time [34, 52]. After solving QP problem (3.5) and obtaining the optimal input sequence ΔU^*, the control input to the plant is obtained by

$$
u(k) = u(k-1) + \Delta u^*(k) \tag{3.6}
$$

3.2 LTV-MPC Power Management Strategy

In the LTV-MPC approach, the nonlinear prediction model (2.18) is linearized at each sample time around the current operating conditions and the linearized model is used to formulate the linear MPC problem (3.3). Then the control inputs are obtained by solving the linear MPC at that sample time. The stability and disturbance rejection properties for this approach are addressed in the literature as in [4, 56, 37, 32]. In the power management based on the LTV-MPC, the following actions are performed at each sampling time (k):

- Measurement/estimation of system state, $(SOC(k))$.
- Prediction of the torque demand and vehicle speed (measured disturbance) over the prediction horizon. For short prediction horizons, if preview information are not available, constant vehicle speed with an exponentially decaying driver torque as it is presented in Section 3.3, or constant demand torque as it

is used in Chapter 5 or reference [10] can be applied to calculate the measured disturbance along the prediction horizon.

- Linearization of the nonlinear model around the current operating conditions to obtain a linear system

$$\begin{cases} \dot{x} = \tilde{A}x + \tilde{B}_u u + \tilde{B}_v v + \tilde{F} \\ y = \tilde{C}x + \tilde{D}_u u + \tilde{D}_v v + \tilde{G} \end{cases} \tag{3.7}$$

where

$$\begin{aligned} \tilde{A} &= \left(\frac{\partial f}{\partial x}\right)_{(x_0,u_0,v_0)}; \tilde{B}_u = \left(\frac{\partial f}{\partial u}\right)_{(x_0,u_0,v_0)} \\ \tilde{B}_v &= \left(\frac{\partial f}{\partial v}\right)_{(x_0,u_0,v_0)}; \tilde{C} = \left(\frac{\partial g}{\partial x}\right)_{(x_0,u_0,v_0)} \\ \tilde{D}_u &= \left(\frac{\partial g}{\partial u}\right)_{(x_0,u_0,v_0)}; \tilde{D}_v = \left(\frac{\partial g}{\partial v}\right)_{(x_0,u_0,v_0)} \\ \tilde{F} &= f(u_0,v_0) - \tilde{A}x_0 - \tilde{B}_u u_0 - \tilde{B}_v v_0 \\ \tilde{G} &= g(x_0,u_0,v_0) - \tilde{C}x_0 - \tilde{D}_u u_0 - \tilde{D}_v v_0 \end{aligned} \tag{3.8}$$

x_0, u_0 and v_0 are the current values of the state, input and known or measured inputs to the system, respectively and $g(x_0,u_0,v_0)$ is the vector of the current measurements of the outputs. In order to remove input-output direct feedthrough in accordance to the standard MPC formulation presented in Section 3.1, the linearized system is augmented with fast filters with time constant T_f, chosen to be at least 5-10 times faster than the fastest time constant of the plant. The augmented linearized system can be represented as

$$\begin{aligned} \begin{bmatrix} \dot{x} \\ \dot{x}_a \end{bmatrix} &= \underbrace{\begin{bmatrix} 0_{1\times1} & \tilde{B}_u \\ 0_{3\times1} & -1/T_f I_{3\times3} \end{bmatrix}}_{A^c} \begin{bmatrix} x \\ x_a \end{bmatrix} + \\ &\underbrace{\begin{bmatrix} 0_{1\times3} \\ 1/T_f I_{3\times3} \end{bmatrix}}_{B_u^c} u + \underbrace{\begin{bmatrix} \tilde{B}_v & I_{1\times1} & 0_{1\times6} \\ 0_{3\times2} & 0_{3\times1} & 0_{3\times6} \end{bmatrix}}_{B_v^c} \begin{bmatrix} v \\ \tilde{F} \\ \tilde{G} \end{bmatrix} \\ [y] &= \underbrace{\begin{bmatrix} \tilde{C} & \tilde{D}_u \end{bmatrix}}_{C^c} \begin{bmatrix} x \\ x_a \end{bmatrix} + \underbrace{\begin{bmatrix} \tilde{D}_v & 0_{6\times1} & I_{6\times6} \end{bmatrix}}_{D_v^c} \begin{bmatrix} v \\ \tilde{F} \\ \tilde{G} \end{bmatrix} \end{aligned} \tag{3.9}$$

- Time discretization of (3.9) with sampling period $T_s = 1$ second and application of the classical linear MPC (3.3) to the resulting model to compute the control input, as explained in Section 3.1.
- If the MPC requested power, $T_{eng} \times \omega_{eng}$, is greater than zero, the MPC decisions are applied to the plant; otherwise, the engine is turned off and T_{eng} and ω_{eng} are set to zero.

3.3 Simulation Conditions

The design parameters of the MPC are the penalty weights and prediction and control horizons. In addition, in this work, the time constant τ_d in the torque model (3.10) is another tuning parameter. Via various simulations and observations over different driving conditions, some of which are presented in the next section, these parameters are tuned. In the simulations, the sampling period of MPC is 1 second and the prediction and control horizons are chosen to be 5 steps. Also the performance index weights and the demanded torque time constant are chosen to be $w_{SOC} = 1, w_f = 50$, and $\tau_d = 1$ second. The fast filter time constant is $T_f = 0.01$ second.

In order to implement the power management strategy, the control system is decomposed into two levels. The first or supervisory level finds the optimum values for the two degrees of freedom of the problem, engine speed and torque, at each sampling time. These optimal values are posed as references to a second, low-level controller. This controller determines the engine, motor, generator, and friction brake torques based on the references set by the supervisory controller. A block-diagram of the closed-loop system is shown in Figure 3.1. In the low-level controller, standard control loops are used for reference tracking.

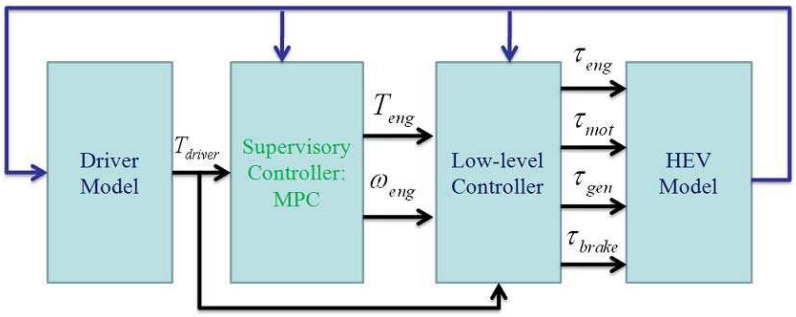

Figure 3.1: Hierarchial Control System

A high-fidelity model of Toyota Prius extracted from the database of Powertrain Simulation Analysis Toolkit (PSAT) commercial software [31] is employed in the closed-loop model presented in Figure 3.1.

PSAT is a state-of-the-art flexible powertrain simulation software developed by Argonne National Laboratory with the support of automotive manufacturers and sponsored by the U.S. Department of Energy (DOE). It runs in a MATLAB/Simulink environment and provides access to dynamic models of different mechanical and electrical components of several hybrid vehicle configurations. The level of details in PSAT component models and its forward simulation approach ensures a reliable estimation of fuel economy. The modeling accuracy of PSAT has been validated against production HEVs such as the Honda Insight [22] and the Toyota Prius [41]. Another model that we will use to analyze the power management strategy later in this dissertation is based on a high-fidelity model of Ford Fusion HEV developed at Ford Motor Company. The future driver torque demand, which is usually unknown, is assumed to be exponentially decreasing over the prediction horizon [28]

$$T_{driver}(k+i) = T_{driver}(k)e^{\left(\frac{-i\tau}{\tau_d}\right)} \qquad i = 1,\ 2,\ \cdots,\ P \tag{3.10}$$

where $T_{driver}(k)$ is the known value of the driver torque demand at the beginning of the prediction horizon, τ is the sample time and τ_d determines the decay rate. Due to the frequent variations of the torque demand in a driving cycle and the integrative nature of the system dynamics with respect to the torque, the assumption of a decaying torque demand was found to be more reasonable and lead to better results than a constant-torque assumption (which is the standard assumption in MPC for measured disturbances). The effectiveness of (3.10) has been later confirmed by simulations. By using the above driver torque model and by numerical integration of the vehicle longitudinal dynamics (2.5) over the future time horizon, the future velocity profile is predicted.

3.4 LTV-MPC Simulation Results

Before showing the simulation results over standard (long) drive cycles, we discuss first a driving scenario that includes a 0 to 70 (km/hour) acceleration, a constant 70 (km/hour) cruise, and then deceleration to a stop. The results are presented in Figures 3.2-3.3.

As seen in Figure 3.3, during acceleration (15 to 35 seconds), the motor provides the initial torque before the engine is engaged and then it continues to assist the engine. The generator provides negative or reaction torque that increases transmission of engine torque to the wheels. This operation is called positive-split [12]. Later, during the cruise mode (35 to 60 seconds), the controller reduces the generator speed to negative values and the generator operates in motoring mode. During this mode, the vehicle speed is

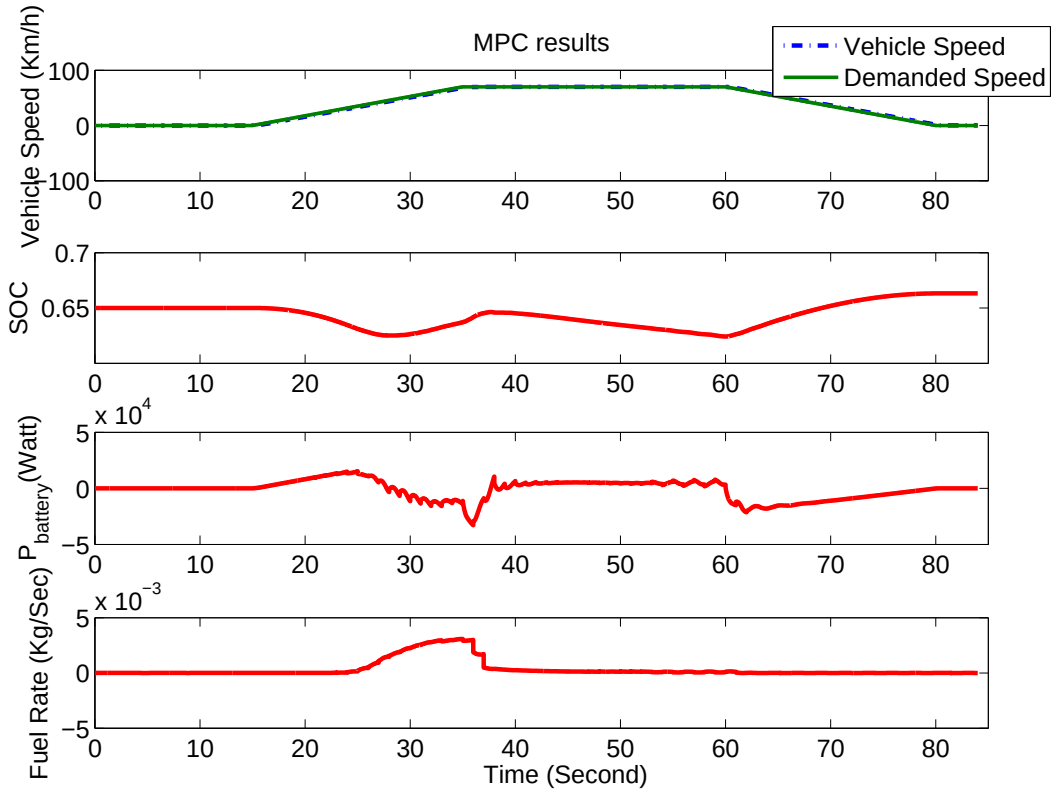

Figure 3.2: LTV-MPC results with acceleration-cruise-brake cycle.

relatively high and the power demand is low; negative generator speed reduces the engine speed according to equation (2.3). This mode is called negative-split [12]. During deceleration, the motor operates in the generating mode and energy is recuperated into the battery. This mode is the regenerative braking mode. The ripples in the battery power and fuel consumption rate plots are due to the discrete-time MPC updates.

To demonstrate the LTV-MPC strategy performance quantitatively, we ran simulations over standard city and highway driving cycles using the detailed model extracted from PSAT. At each sample time, the MPC constraints are updated based on the feedback from the plant model. The target SOC is set to 0.7 which is the default value in PSAT for this HEV. The upper and lower limits of SOC are set to 0.5 and 0.8, respectively. Other constraints are updated as functions of operating points based on the on-line feedback from the PSAT model. The MPC prediction model and tuning parameters are kept unchanged as described before. The MPC controller issues its optimal evaluation of engine torque and speed which are passed to the lower level controller. Figure 3.4 shows the simulation results over a standard urban driving cycle called UDDS cycle and Figure 3.5 shows the simulation results over a standard highway driving cycle called Highway FET. In

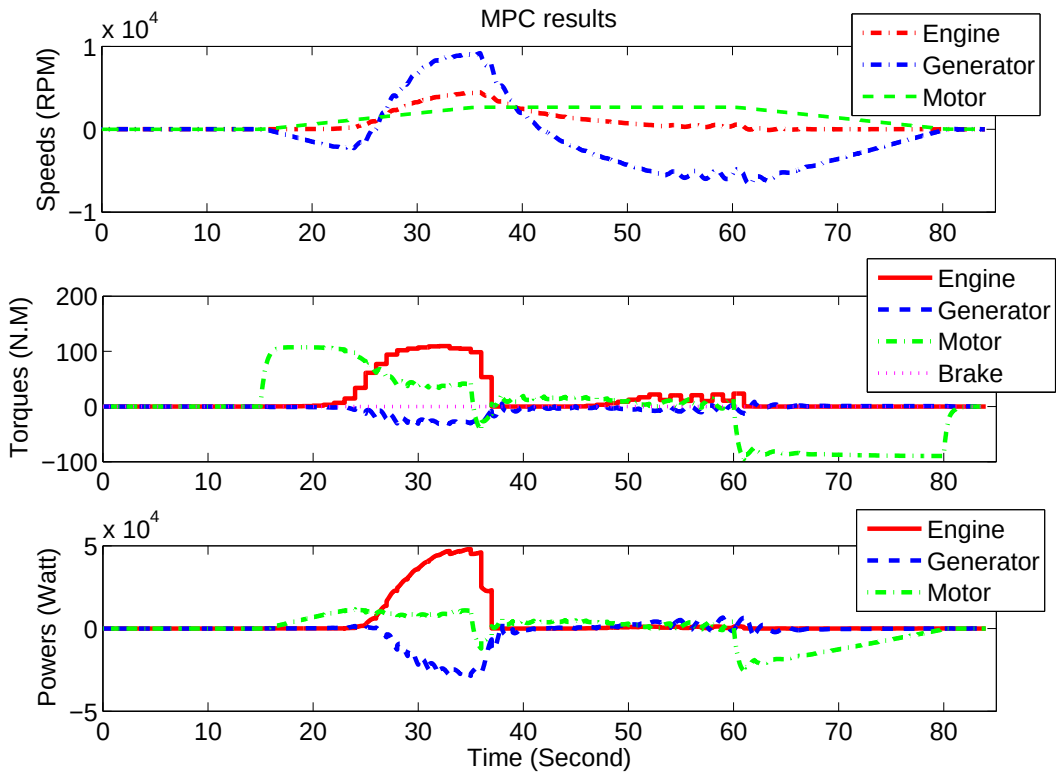

Figure 3.3: LTV-MPC results with acceleration-cruise-brake cycle.

order to remove the effect of different initial and final SOCs on the fuel economy, we ran the simulations over the same cycle multiple times until the system reaches a charge balance.

It is observed that the vehicle speed reference profile from the standard cycles is followed while all the constraints on the system are enforced. Furthermore, Table 3.1 compares the fuel economy and the initial and final battery state of charge for both LTV MPC and rule-based controller of PSAT. It can be observed that the LTV-MPC fuel economy results are comparable with those of the PSAT. *We attribute the lower fuel economy of the LTV-MPC for the UDDS cycle with respect to that of PSAT to the model error introduced by linearization of the control-oriented model. Furthermore, the feasible reference for the fuel consumption rate cannot be zero most of the time.* Because of these issues, we observed that even increasing the prediction and control horizons of the LTV-MPC with the current quadratic cost functional cannot noticeably improve the fuel economy. In [9], a piecewise linear approximation of the fuel consumption map is used for an ERAD HEV configuration, resulting in a hybrid MPC approach, that requires the solution of mixed-integer programs. In Chapter 4, we develop a nonlinear MPC approach that does not require linearizations and uses

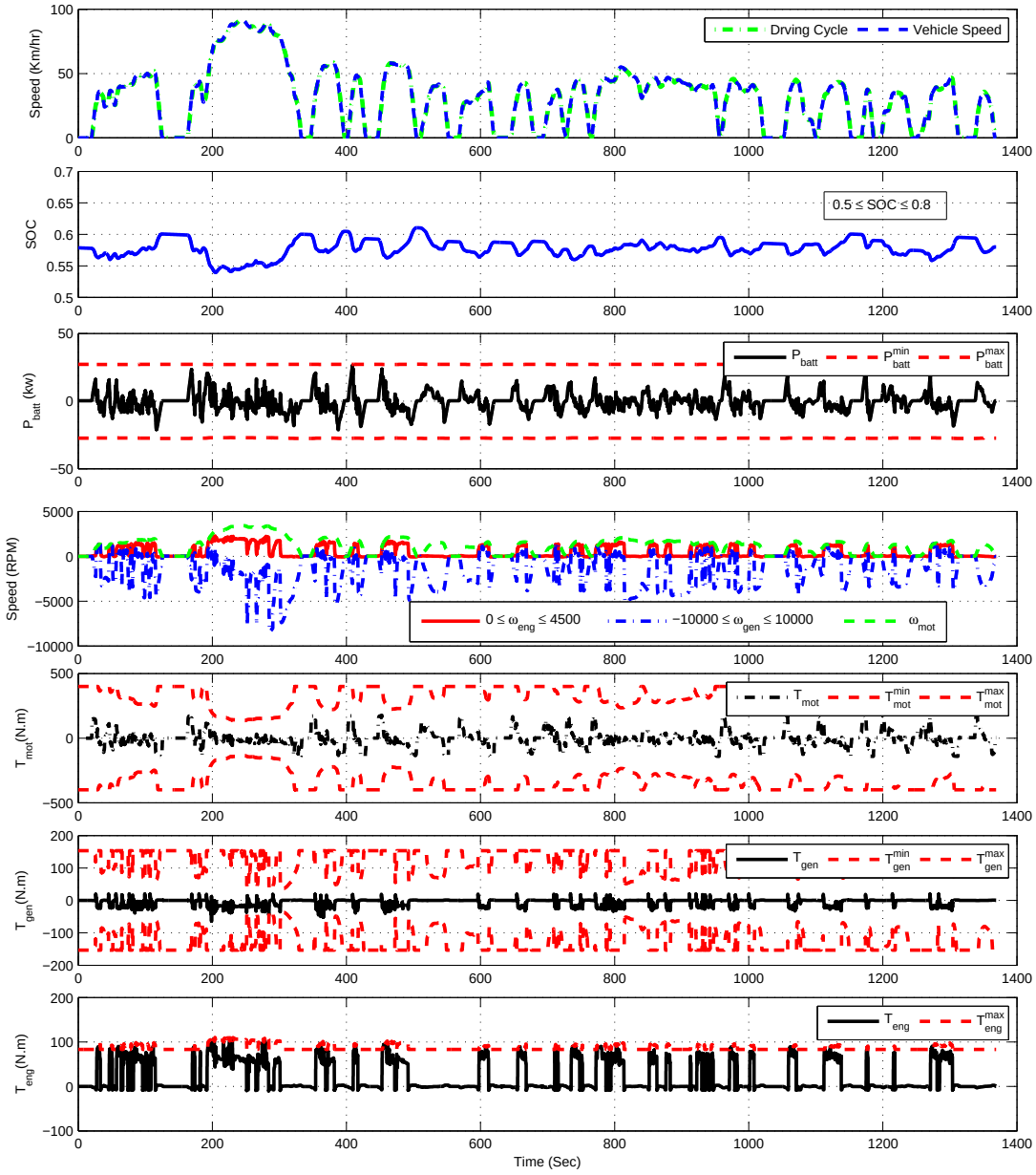

Figure 3.4: The LTV-MPC strategy results over UDDS cycle

a different cost function to improve fuel economy. In Appendix A, the effect of combining a supercapacitor with the battery in the performance of a power-split HEV is discussed with the LTV-MPC strategy.

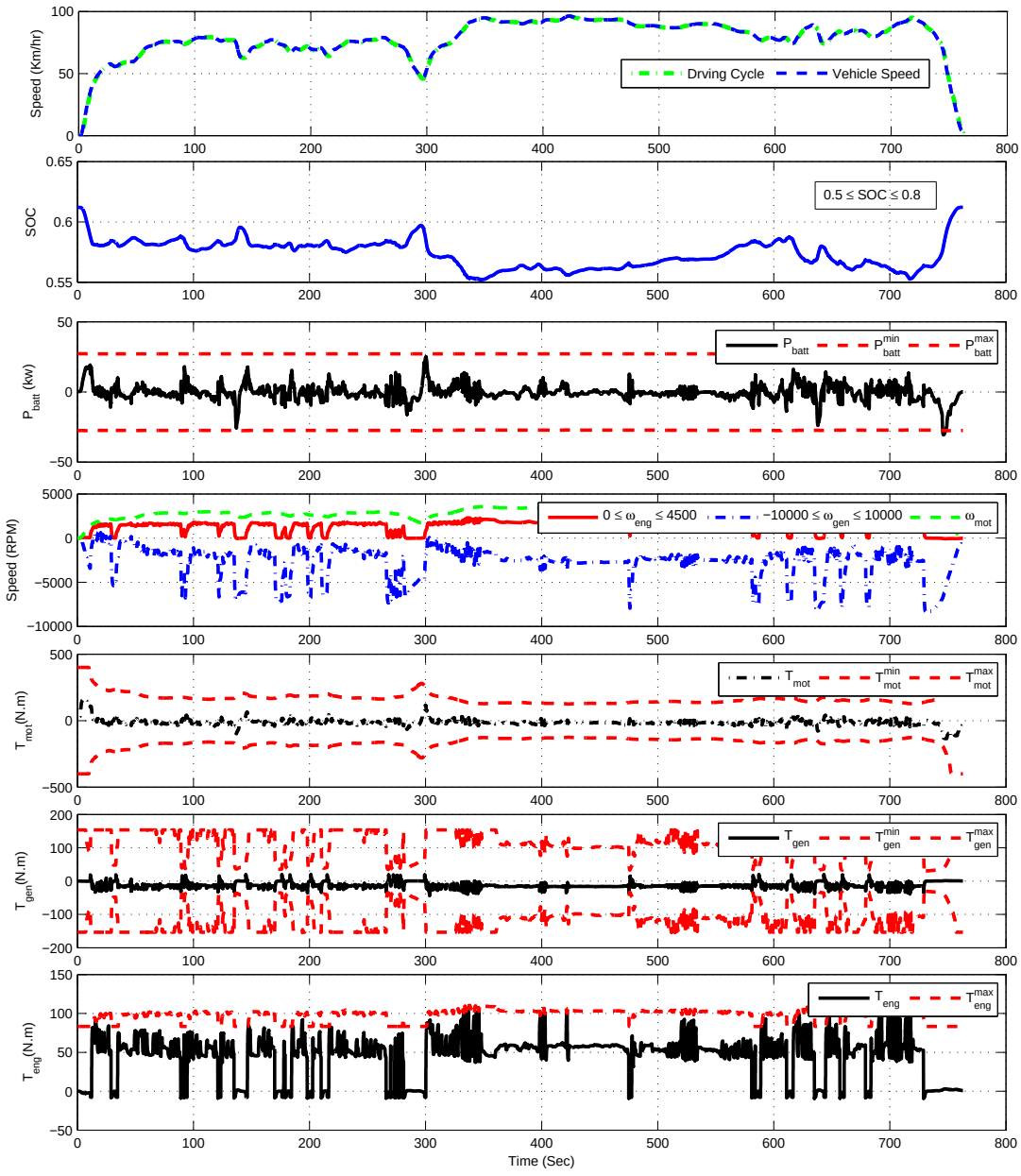

Figure 3.5: The LTV-MPC strategy results over Highway FET cycle

Table 3.1: LTV-MPC and PSAT results over the PSAT model

UDDS cycle			
Controller	*Initial SOC*	*Final SOC*	$FuelEconomy\ (mpg)$
LTV-MPC	0.70	0.59	84.31
	0.59	0.59	**73.02**
PSAT	0.70	0.67	78.55
	0.67	0.67	**76.03**
Highway FET cycle			
Controller	*Initial SOC*	*Final SOC*	$FuelEconomy\ (mpg)$
LTV-MPC	0.70	0.63	70.1
	0.63	0.63	**66.12**
PSAT	0.70	0.64	69.43
	0.63	0.63	**65.52**

Chapter 4

HEV Optimization-Based Power Management with Nonlinear MPC

To systematically improve the fuel economy of a power-split hybrid, we formulated the power management problem as a nonlinear optimization problem. In the previous chapter, the nonlinear powertrain model and the constraints were linearized at each sample time and a receding horizon linear MPC strategy is employed to minimize a quadratic cost function. Simulation results of the linear MPC over multiple driving cycles indicated comparable results with the PSAT base-controller. Although the proposed linear MPC algorithm, proposed in the previous chapter, is causal and has the potential for real-time implementation, more fuel economy improvement is desirable with respect to the base-controller. In this chapter, by applying the principles of optimal control theory, a new form of the cost function is proposed. The derivations and simulation results are reviewed in the following sections. It will be shown that the new nonlinear MPC can improve the fuel economy noticeably. Furthermore, the important effect of the engine speed transients on fuel economy is shown and addition of the engine speed (powertrain) inertial dynamics to the MPC model is proposed.

4.1 Nonlinear MPC Power Management

The linear time-varying MPC problem introduced in the last chapter produced results close to those of the PSAT software. However there seems to be room for further improvement in fuel economy. One reason

that the fuel economy gains are not as much as expected may be attributed to the LTV MPC cost function in (3.1). This cost function does not penalize the total fuel used over an entire cycle. With the experience we have gained when working with the LTV MPC formulation, we believe a better formulation of the cost function is possible; one that penalizes the approximation of the total fuel used over an entire cycle. The total fuel cost over an entire cycle which starts at time t_0 and ends at time t_f can be obtained by

$$J = \int_{t_0}^{t_f} \dot{m}_f(u(t))dt + h(SOC(t_f)) \tag{4.1}$$

where $h(SOC(t_f))$ penalizes the deviation of SOC at the end of the cycle from a reference value, SOC_r. As was previously discussed in Section 3, the objective of the power management strategy is to minimize a cost function (here (4.1)) while satisfying the dynamical equations (2.18) and the constraints (2.9) and (2.11). However in real applications, the driving conditions over long time horizons are not generally known in advance and, furthermore, the parameters of the model and of the constraints may vary. Moreover, the solution of the optimal control problem over a long horizon is computationally demanding. To address these issues, we propose to use Bellman's Principle of Optimality [25] to split the above optimal control problem into a (integrated) stage cost and an approximated minimum fuel cost from the end of the prediction horizon to the end of the drive cycle. We then propose to solve the problem using the receding horizon framework. At time $t \leq t_f$, the cost function is

$$J(u, SOC(t), t) = \int_{t}^{t_f} \dot{m}_f(u(\tau))d\tau + h(SOC(t_f)) \tag{4.2}$$

where $SOC(t)$ is any admissible state value at time t. Note that the performance metric depends on the values of $SOC(t)$[1], t, and the control inputs over the interval $[t,\ t_f]$. The minimum cost or cost-to-go is obtained by

$$J^*(SOC(t), t) = \min_{\substack{u(\tau) \\ t \leq \tau \leq t_f}} \{ \int_{t}^{t_f} \dot{m}_f(u(\tau))d\tau + h(SOC(t_f)) \} \tag{4.3}$$

subject to the constraints (2.9) and (2.11) and dynamics (2.18). By dividing the time interval $[t,\ t_f]$ one can

[1]Note that the SOC is the only dynamical state of the system. This explains the variables in the cost-to-go in (4.2).

write

$$J^*(SOC(t),t) = \min_{\substack{u(\tau) \\ t\le\tau\le t_f}} \{ \int_t^{t+\Delta t} \dot{m}_f(u(\tau))d\tau + \int_{t+\Delta t}^{t_f} \dot{m}_f(u(\tau))d\tau + h(SOC(t_f))\} \tag{4.4}$$

where Δt is a chosen time horizon. Bellman's principle of optimality requires that

$$J^*(SOC(t),t) = \min_{\substack{u(\tau) \\ t\le\tau\le t+\Delta t}} \{ \int_t^{t+\Delta t} \dot{m}_f(u(\tau))d\tau + J^*(SOC(t+\Delta t),t+\Delta t)\} \tag{4.5}$$

The minimum fuel cost over the interval $[t+\Delta t, t_f]$, i.e. $J^*(SOC(t+\Delta t),t+\Delta t)$, is not in general a known function of SOC. In the next section, we show how this function can be approximated, hence enabling us to solve the above fuel minimization problem in a receding horizon approach.

4.2 Approximation of the Cost-To-Go Function

In this section, we attempt to derive an approximation for the minimum fuel cost as a function of the battery's state of charge. An approximation of the cost-to-go will be sufficient because the optimal solutions are recalculated in a receding horizon manner at each time step. Assuming that a Taylor series expansion of $J^*(SOC(t+\Delta t),t+\Delta t)$ around $SOC^*(t+\Delta t)$ can be made, we obtain

$$J^*(SOC(t+\Delta t),t+\Delta t) = J^*(SOC^*(t+\Delta t),t+\Delta t) + \frac{\partial J^*}{\partial SOC}(SOC^*(t+\Delta t),t+\Delta t)\cdot\Delta SOC + O(\Delta SOC^2) \tag{4.6}$$

where $\Delta SOC = (SOC(t+\Delta t) - SOC^*(t+\Delta t))$. As shown in Appendix B, by observing the relationship between the Pontryagin's minimum principle and HJB equations as represented in [25], if SOC^* denotes the optimal trajectory from current time t and initial state $SOC(t)$ to the end of the trip, we can rewrite equation (4.6) as

$$J^*(SOC(t+\Delta t),t+\Delta t) \cong J^*(SOC^*(t+\Delta t),t+\Delta t) + \lambda(SOC(t),t)\cdot(SOC(t+\Delta t) - SOC^*(t+\Delta t)) \tag{4.7}$$

where

$$\lambda(SOC(t),t) = \frac{\partial J^*}{\partial SOC}(SOC(t),t) \tag{4.8}$$

By adding and subtracting the constant reference value SOC_r, to and from the last term of equation (4.7) we obtain

$$J^*(SOC(t+\Delta t),t+\Delta t) \cong \alpha(SOC(t),t) + \lambda(SOC(t),t)\cdot(SOC(t+\Delta t) - SOC_r) \tag{4.9}$$

where, $\alpha(SOC(t),t)$ is

$$\begin{aligned} \alpha = J^*(SOC^*(t+\Delta t),t+\Delta t) + \\ \lambda(SOC(t),t)\cdot(SOC_r - SOC^*(t+\Delta t)) \end{aligned} \tag{4.10}$$

Substituting (4.9) into cost function (4.5) we get

$$J^*(SOC(t),t) = \min_{\substack{u(\tau) \\ t\le\tau\le t+\Delta t}} \{\alpha(SOC(t),t) + \int_t^{t+\Delta t} \dot{m}_f(u(\tau))d\tau + \lambda(SOC(t),t)\cdot(SOC(t+\Delta t) - SOC_r)\} \tag{4.11}$$

Since α in (4.11) is not a function of the control inputs, it does not affect the selection of the optimal control inputs. So the optimal control over the interval $[t,\ t+\Delta t]$ can be found by solving the following finite-time optimal control problem

$$\begin{aligned} &\min_{\substack{u(\tau) \\ t\le\tau\le t+\Delta t}} \{\int_t^{t+\Delta t} \dot{m}_f d\tau + \lambda(SOC(t),t)\cdot(SOC(t+\Delta t) - SOC_r)\} \\ &S\dot{O}C = f(u(\tau), v(\tau)) \\ &SOC_{\min} \le SOC(\tau) \le SOC_{\max}, u(\tau) \in U, y(\tau) \in Y \end{aligned} \tag{4.12}$$

where U and Y are the sets of admissible inputs and outputs according to (2.9) and (2.11). We will solve this

finite-horizon optimal control problem in a receding horizon manner as explained in the next section.

As shown in Appendices B and C, the parameter λ is related to both the equivalent factor in the ECMS method and the rate of change of minimum cost with respect to the *SOC*. An admissible range for λ can be obtained as explained in the ECMS literature [20] or from the DP solutions over different driving cycles [44]. In what follows, it is shown that λ can be approximated by a tunable piecewise linear function over the admissible range. Using equation (4.8) and assuming sufficient smoothness of J^*, the Taylor series expansion of the function λ around the SOC_r yields

$$\lambda(SOC(t),t) = \frac{\partial J^*}{\partial SOC}(SOC_r,t) + \frac{\partial^2 J^*}{\partial SOC^2}(SOC_r,t)(SOC(t) - SOC_r) + O(\Delta SOC_r^2) \tag{4.13}$$

where $\Delta SOC_r = (SOC(t) - SOC_r) \ll 1$. By defining $\lambda_0 = \frac{\partial J^*}{\partial SOC}(SOC_r,t)$ and $\mu = \frac{\partial^2 J^*}{\partial SOC^2}(SOC_r,t)$ as two tuning design parameters and ignoring the higher order terms we obtain

$$\lambda(SOC(t),t) \cong \lambda_0 + \mu \Delta SOC_r \tag{4.14}$$

which approximates λ as an affine function of the state.

4.3 Nonlinear Model Predictive Control

Because the new receding horizon cost is a nonlinear and non-quadratic function of the control inputs, the LTV MPC approach cannot be used and a general nonlinear MPC solution is required. Here a general nonlinear MPC framework is explained. More details about Nonlinear MPC can be found in [34, 52]. Consider the following discrete-time nonlinear system,

$$x(k+1) = f(x(k), u(k)) \tag{4.15}$$

where $f(.,.) : R^n \times R^m \rightarrow R^n$ is the state update function or map, $x \in R^n$ is the state vector, and $u \in R^m$ is the control input. System (4.15) is subject to the following state and input constraints

$$x(k) \in X,\ u(k) \in U \tag{4.16}$$

Given the prediction horizon $N \in Z^+$, we consider the cost function $J(.,.) : R^n \times R^{Nm} \rightarrow R^+$ defined by

$$J(x(k),U(k)) = \sum_{i=0}^{N-1} l(x(k+i),u(k+i)) + L(x(k+N)) \tag{4.17}$$

where $U(k) = [u(k),\cdots,u(k+N-1)]$ is a sequence of inputs over the prediction horizon N, $x(k+i)$ for $i = 0,\cdots,N$ is the state trajectory obtained by applying the control sequence $U(k)$ to the system (4.15), starting from the initial state $x(k) = x(t)$, $l(.,.) : R^n \times R^m \rightarrow R^+$ is the stage cost, and $L(.) : R^n \rightarrow R^+$ is the terminal cost.

At each sampling time k, the following finite time optimal control problem is solved:

$$\min_{U(k)} J(x(k),U(k)) = \sum_{i=0}^{N-1} l(x(k+i),u(k+i)) + L(x(k+N)) \tag{4.18}$$

subject to

$$\begin{aligned} x(k+1) &= f(x(k),u(k),v(k)) \\ x(k+i) &\in X \\ u(k+i) &\in U \\ x(k) &= x(t) \end{aligned} \tag{4.19}$$

Assuming that $U^*(k) = [u^*(k),\cdots,u^*(k+N-1)]$ is the optimal solution of the optimization problem (4.18), the control input to be applied to the plant is obtained by

$$u(x(k)) = u^*(k) \tag{4.20}$$

At the next sampling time, this process is repeated to calculate MPC inputs over a shifted horizon. In order to solve the optimal control problem presented in (4.18), we use the method of dynamic programming which is explained in the next section.

4.4 The Method of Dynamic Programming (DP)

Once the optimal control problem is defined, the next task is to calculate the control inputs that minimize the cost function. Two main methods of accomplishing the minimization are the minimum principle of Pontryagin and the method of dynamic programming (DP) developed by R. E. Bellman [25]. The variational

approach of Pontryagin leads to a nonlinear two-point boundary value problem that is hard to solve in general. On the other hand, DP leads to discrete functional equations that can be solved using digital computers. We propose to employ DP to solve the nonlinear MPC problem. The details of derivations of DP equations are not presented but we review the final equations here. More details are available in most optimal control reference books such as [25]. By applying the principle of optimality backward over the control horizon (4.18), the following recurrence relation is obtained:

$$J^*_{k+N-j}(x(k+N-j)) = \min_{u(k+N-j)} \{l(x(k+N-j),u(k+N-j)) + J^*_{k+N-(j-1)}(f(x(k+N-j),u(k+N-j)))\} \tag{4.21}$$

where $j = 1,2,\cdots,N$ and the initial value is

$$J^*_{k+N}(x(k+N)) = L(x(k+N)) \tag{4.22}$$

Equation (4.21) is the recurrence relation that can be solved backward by discretizing the states and input over their admissible sets. For more details about the computational procedure, please refer to section 3.8 of [25]. Dynamic programming can be used to solve an optimal control problem numerically but its main drawback is increased computational time and memory requirement for high-dimensional systems. Bellman calls this difficulty the "curse of dimensionality". For our power management problem, we observed that the computational time for one-state dynamics is acceptable for real-time implementation but for two-state dynamics, the computational time even with a DP solver we programmed in C++ is higher than real-time. There are explicit or off-line methods to reduce the computational time of the nonlinear MPC with online solver which are out of the scope of this research. In order to investigate the MPC performance and analyze fuel economy values, online DP solvers are computationally acceptable (it was observed that the computational time of the 1-state MPC is real-time and the one of 2-state MPC is about two times of the real-time over a PC).

4.5 The Nonlinear MPC Power Management

The optimal control problem in (4.12) will be first discretized with sampling time T_s and then will be solved in a receding horizon strategy using dynamic programming. More specifically, the following actions are performed at each sampling time (k):

- The constraints are updated using the feedback from the HEV model.
- The future torque demand and vehicle speed (measured disturbances) unknown over the prediction horizon, are initialized at the current value and predicted along the predicted horizon. For short prediction horizons, if preview information are not available, constant vehicle speed with an exponentially decaying driver torque as it is presented in Section 3.3, or constant demand torque as it is used in Chapter 5 or reference [10] can be applied to calculate the measured disturbance along the prediction horizon.
- As it was explained in Section 4.2, the parameter λ is calculated according to equation (4.14).
- Using dynamic programming, the updated MPC problem (4.12) is solved numerically over the prediction horizon. Since the MPC prediction horizon is usually short compared to the whole drive cycle, the computations can be done in real-time.
- Consistent with standard MPC framework, the first input in the sequence of the calculated optimal inputs over the prediction horizon is applied to the plant if the MPC requested power, $T_{eng} \times \omega_{eng}$, is greater than zero; otherwise the engine is turned off and T_{eng} and ω_{eng} are set to zero.

The above steps are repeated by receding the prediction horizon one step forward. Repeating these calculations for every new measurement yields a state feedback control law.

4.6 Nonlinear MPC Simulation Results over the PSAT High-Fidelity Model

To quantitatively demonstrate the validity of the nonlinear MPC strategy, we ran simulations over multiple standard driving cycles. Figure 4.1 shows the simulation results over a standard urban driving cycle called UDDS cycle and Figure 4.2 shows the simulation results over a standard highway driving cycle called Highway FET. In order to remove the effect of different initial and final SOCs on the fuel economy, we ran the simulations over the same cycle multiple times until the system reaches a charge balance. Furthermore, Table 4.1 compares the fuel economy and the initial and final SOCs of the LTV-MPC controller, the rule-based controller of PSAT, and the nonlinear MPC controller. The fuel economy values with equal initial and final SOCs are used to compare the performance of different controllers. Table 4.1 shows that over both city

and highway driving cycles, the nonlinear MPC controller achieves an improved fuel economy with respect to the LTV-MPC strategy and the rule-based controller.

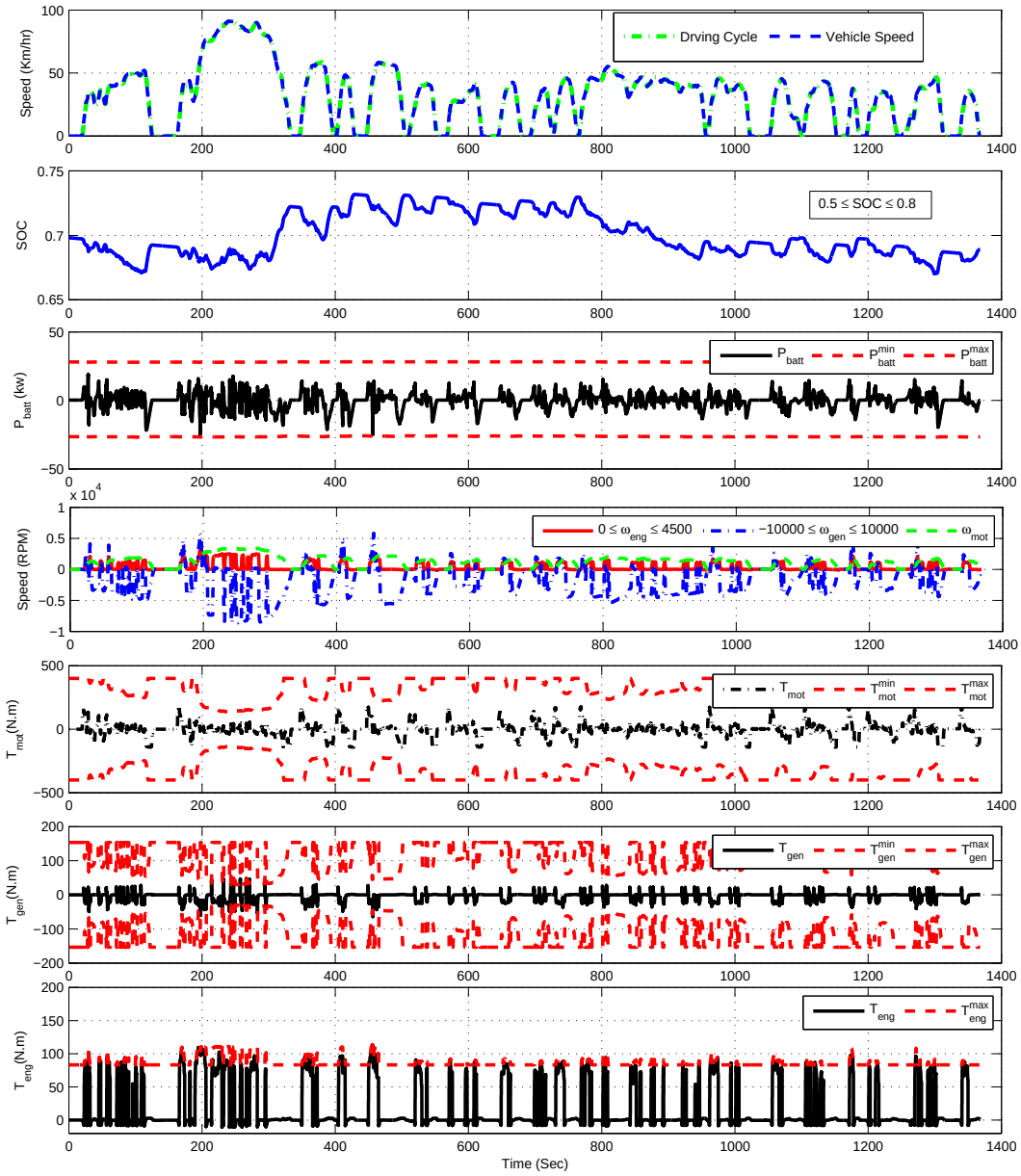

Figure 4.1: The Nonlinear MPC strategy results over UDDS cycle

In order to analyze the performance of the nonlinear MPC over more driving scenarios, more stan-

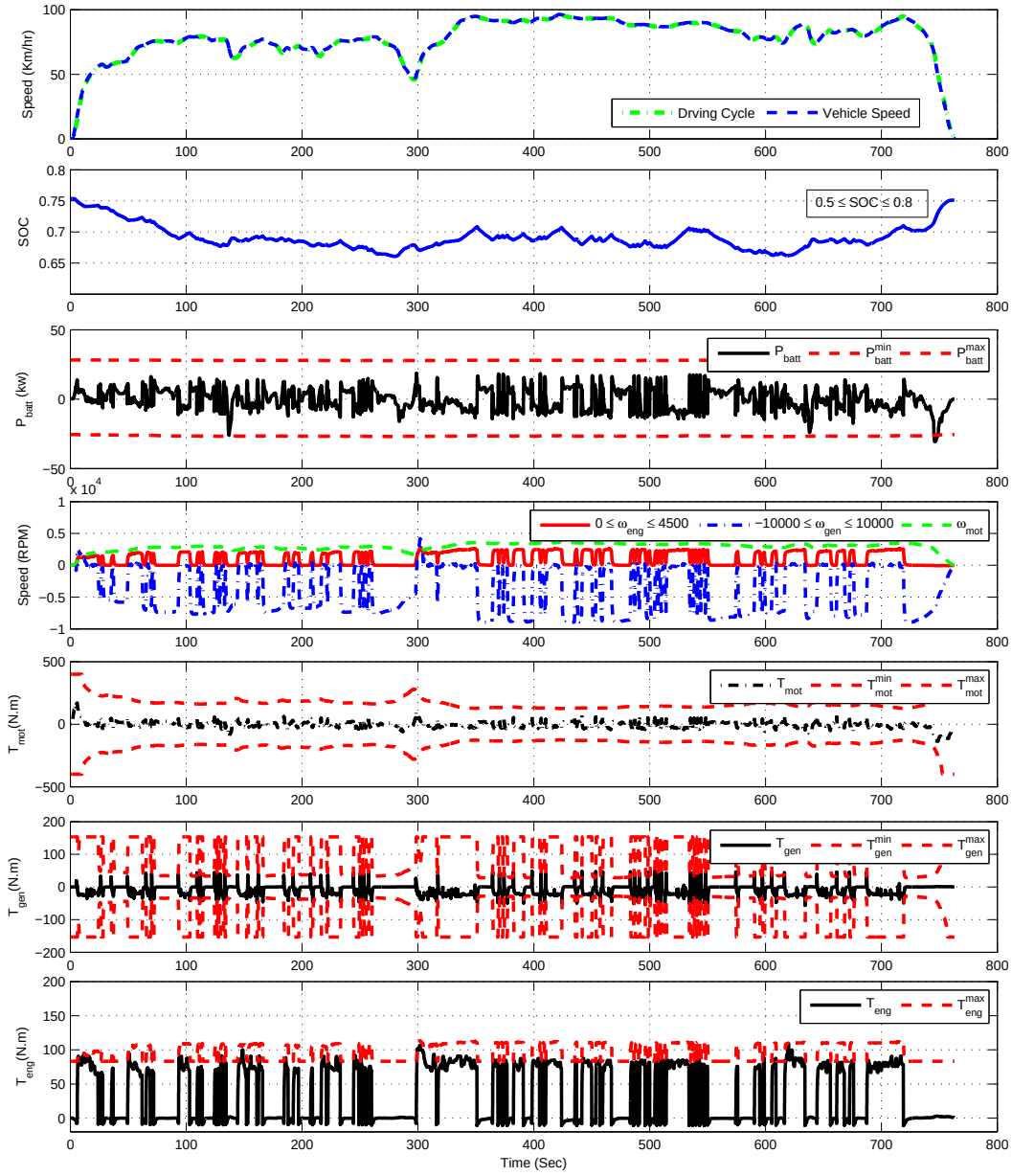

Figure 4.2: The nonlinear MPC strategy results over Highway FET cycle

dard driving cycles are selected and the MPC strategy are applied for the power management of the HEV. Table 4.2 presents the results of the nonlinear MPC and the rule-based controller of the PSAT for the additional driving cycles. It is observed that the nonlinear MPC strategy consistently shows better fuel economy

Table 4.1: MPC and PSAT controller results (See Figure 4 of Appendix A for cycles)

UDDS cycle			
Controller	*Initial SOC*	*Final SOC*	$FuelEconomy\ (mpg)$
LTV-MPC	0.70	0.59	84.31
	0.59	0.59	**73.02**
PSAT	0.70	0.67	78.55
	0.67	0.67	**76.03**
Nonlinear MPC	0.70	0.68	82.37
	0.68	0.68	**80.1**
Highway FET cycle			
Controller	*Initial SOC*	*Final SOC*	$FuelEconomy\ (mpg)$
LTV-MPC	0.70	0.63	70.1
	0.63	0.63	**66.12**
PSAT	0.70	0.64	69.43
	0.63	0.63	**65.52**
Nonlinear MPC	0.70	0.74	69.63
	0.74	0.74	**72.2**

with respect to the rule-based controller.

Table 4.2: MPC and PSAT controller results (See Figure 4 of Appendix A for cycles)

US06 cycle			
Controller	*Initial SOC*	*Final SOC*	$FuelEconomy\ (mpg)$
PSAT	0.70	0.62	45.4
	0.6	0.6	**42.8**
Nonlinear MPC	0.70	0.69	42.49
	0.69	0.69	**46.01**
SC03 cycle			
Controller	*Initial SOC*	*Final SOC*	$FuelEconomy\ (mpg)$
PSAT	0.70	0.68	71.29
	0.68	0.68	**69**
Nonlinear MPC	0.70	0.69	76.66
	0.69	0.69	**74.77**
JC08 cycle			
Controller	*Initial SOC*	*Final SOC*	$FuelEconomy\ (mpg)$
PSAT	0.70	0.67	85.67
	0.67	0.67	**81**
Nonlinear MPC	0.70	0.71	82
	0.71	0.71	**83.6**
NY City cycle			
Controller	*Initial SOC*	*Final SOC*	$FuelEconomy\ (mpg)$
PSAT	0.70	0.66	68.68
	0.64	0.64	**52.6**
Nonlinear MPC	0.70	0.67	66.47
	0.67	0.67	**58.25**

Chapter 5

MPC-Based Power Management of a Ford HEV: Influence of Powertarin Dynamics

Before applying MPC with the 2-state dynamics, we first review the MPC formulation with just the battery dynamics referred here as the 1-state MPC and present its results over the closed-loop Ford HEV model. The 1-state MPC results will be used later in this chapter to evaluate a 2-state MPC performance. For this purpose, the inertial effects of the engine, motor, and generator, i.e. $J_{eng}\frac{d\omega_{eng}}{dt}$, $J_{mot}\frac{d\omega_{mot}}{dt}$, and $J_{gen}\frac{d\omega_{gen}}{dt}$, are ignored and set to zero. Thus the only state in the control-oriented model becomes the battery dynamics as presented in equation (2.6). In chapter 4 and [26, 29], we have discussed the 1-state MPC formulation in details and the results over a high-fidelity HEV model of a Toyota Prius were presented. We observed that by applying the 1-state MPC, an average of 8 percent fuel economy improvement is obtained with respect to the base-controller of the PSAT software. In this chapter, we first apply the same MPC formulation on a Ford high-fidelity HEV model. Because in the 1-state MPC, the powertrain inertial dynamics are ignored, an equivalent engine stop and start cost, $\Delta J_{on/off}$, is added to the cost function whenever the engine stop/start status is changed (the engine is in stop status when the engine speed becomes less than an idle engine speed). The 1-state MPC formulation for the optimal power management of the Ford power-split HEV is formulated

as

$$
\begin{aligned}
&\min_{\substack{u(\tau)\\ t\le\tau\le t+\Delta t}} J=\int_{t}^{t+\Delta t}\left(\dot{m}_f(\tau)+\Delta J_{on/off}\right)d\tau+\lambda(SOC(t),t)\cdot(SOC(t+\Delta t)-SOC(t))\\
&\dot{\bar{x}}(\tau)=\bar{f}(\bar{x}(\tau),\bar{u}(\tau),v(\tau))=-\frac{V_{oc}-\sqrt{V_{oc}^2-4R_{batt}P_{batt}(\tau)}}{2C_{batt}R_{batt}}\\
&h(\bar{x}(\tau),\bar{u}(\tau),y(\tau))\le 0\\
&\bar{x}(\tau)=SOC(\tau);\bar{u}(\tau)=\begin{bmatrix}T_{eng}(\tau)\\ \omega_{eng}(\tau)\end{bmatrix};v(\tau)=\begin{bmatrix}T_{driver}(\tau)\\ V(\tau)\end{bmatrix}
\end{aligned}
\tag{5.1}
$$

where h includes the inequality constraints defined in (2.9) and (2.11) with the following equality constraints derived by ignoring the powertrain inertial dynamics in (2.1)

$$
\begin{aligned}
T_{gen}&=-\left(\frac{N_S}{N_S+N_R}\right)T_{eng}\\
T_{mot}&=-\rho_{m2r}\left(\frac{N_R}{N_S+N_R}\right)T_{eng}+\rho_{m2d}T_{out}
\end{aligned}
\tag{5.2}
$$

Problem (5.1) is solved online using the method of dynamic programming and in the framework of MPC as explained in chapter 4 and [26, 29]. Because driver power demand over the future horizon is unknown, we assume a constant driver demand torque over the 5 steps prediction horizon. The receding horizon problem is solved numerically by employing DP over the 5-step horizon. Because of the short-horizon length the DP computations can be done in real-time. The 1-state MPC results over the closed-loop high-fidelity model of the Ford power-split HEV are presented in Table 5.1. The MPC results are updated at every sampling time of 1 second.

Table 5.1: Performance of the nonlinear 1-state MPC results over the Ford HEV model

Driving Cycle	*Fuel Economy* (mpg)
UDDS cycle	57.25
Highway FET cycle	50.36

These fuel economy values of the 1-state MPC are comparable to those of a Ford-base controller [1]. However further improvement in the fuel economy was desired. In the next section, these 1-state MPC fuel economy values are shown to be close enough to the *best achievable fuel economy of this formulation* and consequently further improvement is not expected by further calibration of the 1-state MPC (tuning parameter λ or the engine on/off penalty value $\Delta J_{on/off}$). Therefore adding the lumped powertrain inertial dynamics to

[1] Because of confidentially restrictions, the Ford-base controller results are not presented.

the MPC control-oriented model is proposed and done later in this chapter.

5.1 Fuel Economy Ceiling of the Nonlinear MPC with Battery Dynamics (1-State MPC)

In this section, we explain how to estimate the best achievable fuel economy of the nonlinear MPC with the 1-state Dynamics referred here as the 1-state MPC over the closed-loop high-fidelity model of the HEV. The best possible fuel economy can be obtained if the power demands over future horizons are known and that is what we will assume to find the theoretically achievable ceiling. We propose the following methodology: First the globally optimal solutions of (5.1) are obtained for a given driving cycle by using one dynamic programming sweep over the entire cycle for the 1-state control-oriented model. The global optimal input history of the energy management problem with 1-state dynamics is not the global optimal inputs history with respect to the Ford model with more modeling details and dynamics[2]. Therefore, the fuel economy value that is obtained from DP over the control-oriented model may be far from a realistic one and cannot be used as comparison for the MPC results. Therefore, we propose to apply the DP history of inputs to the high-fidelity model of the HEV to get a more realistic evaluation of fuel economy ceiling. However, we note that because of the differences between the control-oriented model of the MPC and the high-fidelity model of the HEV (the plant model), the time history of the optimal control inputs, obtained by running DP over the 1-state control-oriented model and for a driving cycle, cannot be applied directly over the high-fidelity model in an open-loop scheme. Instead we define a feedback control law based on the DP optimal solutions as presented in Figure 5.1. Let us indicate the globally optimal solutions for the 1-state control-oriented model by

$$u^* = \left\{ \begin{array}{c} T^*_{eng}(SOC(t),t) \\ \omega^*_{eng}(SOC(t),t) \end{array} \right\} \tag{5.3}$$

From these optimal inputs at each time and state value, a look-up table, a function of time and SOC, is defined in the closed-loop model in order to calculate the control inputs to the high-fidelity model from the feedback value of SOC at each time (see Figure 5.1). The closed-loop model is simulated for the same drive cycle to obtain the fuel economy resulting in the best achievable fuel economy, the fuel economy ceiling, of the 1-state MPC.

[2]Note that the global optimal solutions of an optimal control problem is optimal with respect to the defined *cost function* and the *control-oriented model*.

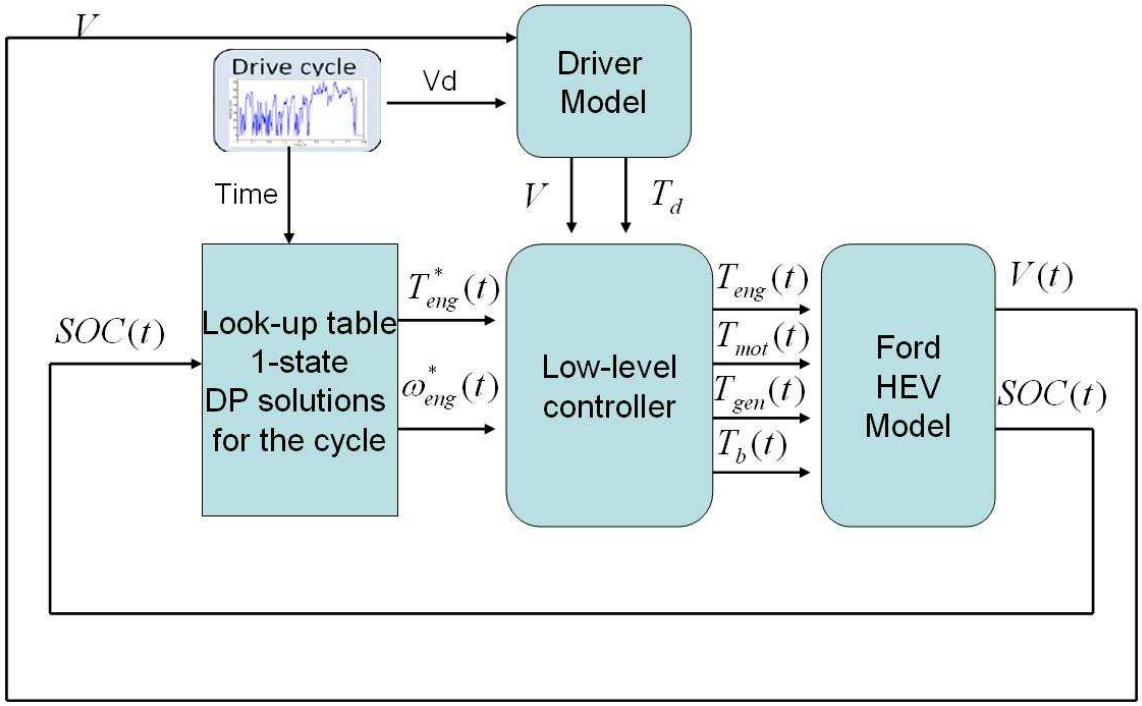

Figure 5.1: Closed-loop model with global optimal solutions feedback law.

The only calibration factor in finding the fuel economy ceiling of the 1-state MPC is the engine on/off cost, $\Delta J_{on/off}$. By tuning this value, the best fuel economy of the 1-state MPC over UDDS cycle is reported in the plot presented in Figure 5.2. This process can be performed for different driving cycles to find the corresponding fuel economy ceiling of the MPC over the high-fidelity model. *We emphasize that this process is performed to obtain a realistic evaluation criterion for the MPC results and is not used as the energy management strategy*. Considering the 1-state MPC results presented in Table 5.1 and the fuel economy ceiling results presented in Figure 5.2, it is observed that the fuel economy of the 1-state MPC for the UDDS cycle is very close to its ceiling value and additional calibration of the 1-state MPC (parameter λ or the engine on/off cost $\Delta J_{on/off}$) cannot improve the fuel economy. Furthermore from Figure 5.2, it is observed that engine stop and start has a considerable effect on the fuel economy. Therefore, in the next section, we add the powertrain inertial dynamics in the control-oriented model of the MPC in order to calculate the effect of engine speed transients.

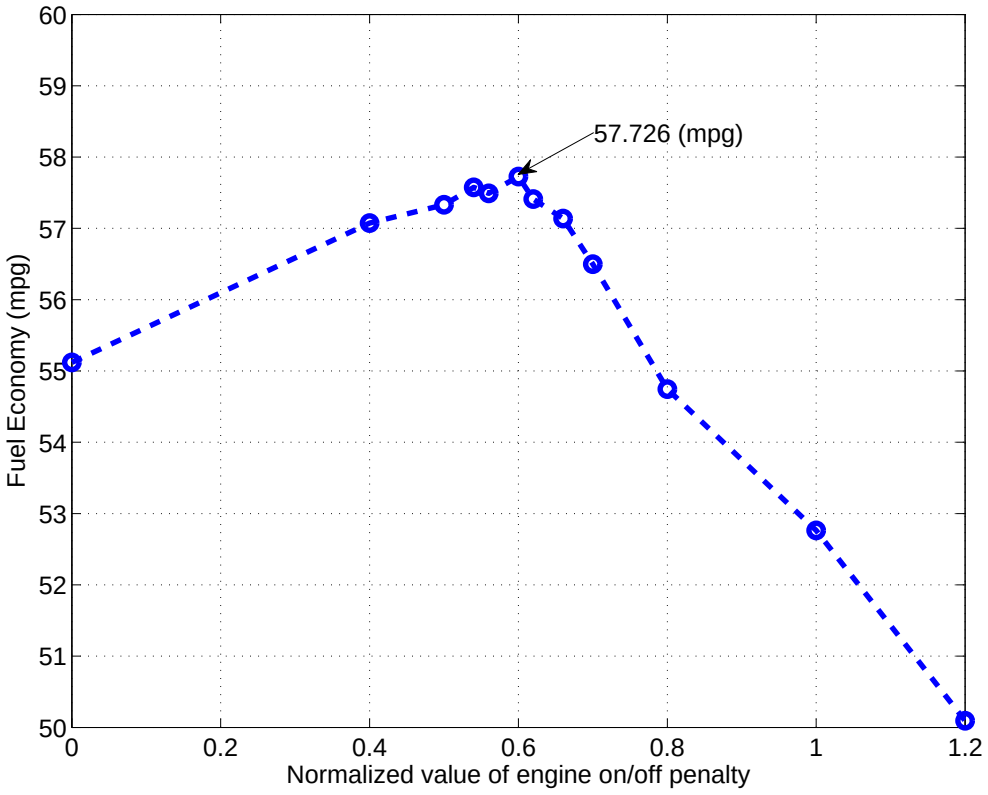

Figure 5.2: Fuel economy ceiling of the 1-state MPC.

5.2 A 2-State MPC-Based Power Management with Battery and Powertrain Dynamics

As it was shown in the previous section, engine transients have an important effect on the HEV fuel economy. This observation gives us the motivation to study the effect of including the lumped powertrain dynamics in the MPC. In order to model the transient dynamics of the powertrain in the MPC energy management decisions, both SOC and engine speed are defined as the states of control model as presented in (2.13). Assuming the same approximation of cost-to-go described in [29, 26], the 2-state MPC fuel minimization

problem is formulated by,

$$\begin{aligned}
&\min_{\substack{u(\tau)\\ t\le\tau\le t+\Delta t}} \quad J=\int_{t}^{t+\Delta t}\dot{m}_f(\tau)d\tau+\lambda(SOC(t),t)\cdot(SOC(t+\Delta t)-SOC(t))\\
&\dot{x}(\tau)=f(x(\tau),u(\tau),v(\tau))\\
&h(x(\tau),u(\tau),y(\tau))\le 0\\
&x(\tau)=\begin{bmatrix} SOC(\tau)\\ \omega_{eng}(\tau)\end{bmatrix};\ u(\tau)=\begin{bmatrix} T_{eng}(\tau)\\ T_{gen}(\tau)\end{bmatrix};\ v(\tau)=\begin{bmatrix} T_{driver}\\ V\end{bmatrix}
\end{aligned} \tag{5.4}$$

where f is defined in (19) and h is the physical constraints of the system defined by (2.9) and (2.11). By considering engine speed dynamics in the control model, we do not need to define any additional heuristic strategy for engine start and stop. Furthermore, as shown in the HEV model (2.13), by adding the engine speed dynamics, the inertial dynamics of the powertrain are modeled and consequently, the battery power and SOC are calculated more accurately. We implemented the 2-state MPC with a DP numerical solver[3] in the C++ programming language, embedded in a Matlab C-mex function to allow fast closed-loop simulations. Since the effect of preview information is not the subject of this research, the driver demand torque is assumed constant over the prediction horizon in order to estimate the vehicle speed and the measured disturbance v.

5.3 Simulation Results of the 2-State MPC over a Ford High-Fidelity Model

To evaluate the 2-state MPC results and the effect of adding lumped powertrain dynamics in the MPC model, UDDS driving cycle is selected as the reference for the simulations. In this city cycle, there are frequent stop and start periods making the effect of powertrain transients more important. The control sample time and MPC prediction horizon are chosen to be 1 second and 2 steps, respectively and the driver demand torque is assumed to be constant over the prediction horizon meaning that *no preview (future) information is used in the simulations*. Furthermore, we observed that for the 2-state MPC, at least 2 steps for the prediction horizon should be defined in order to have enough feasible solutions to pull up the engine, otherwise, the only feasible path is just electric-only mode. The SOC constraint for the MPC is defined to be $0.40 \le SOC \le 0.60$.

[3]Note that we use the DP solver as a global optimizer for the MPC over the prediction horizon and we do not use any future information. This is different from using DP to get the fuel economy ceiling over the whole drive cycle which requires future information and is computationally challenging.

5.3.1 Optimal Calibration of the 2-State MPC over the Ford Model

As indicated in equation (5.4), λ is the calibration (tuning) parameter of the 2-state MPC. In references [29, 26] and Chapter 4, it was shown that this parameter can be approximated by piecewise linear functions. In this dissertation, we define two different λ curves. One, which is called λ_{off}, is used when the engine is currently off (engine speed less than idle engine speed). The other curve, called λ_{on}, is applied when the engine is currently on (engine speed greater than idle engine speed). To optimally calibrate these curves, we used modeFRONTIER software [1] from ESTECO over a parallel computing cluster. In brief, modeFRONTIER calibrates the piecewise linear λ curves by running the closed-loop HEV model in Matlab with different λ curves over a pre-defined range. FSIMPLEX of modeFRONTIER (see [1]) was chosen as the optimizer (calibrator) method to search for the optimal λ curves which result in the best fuel economy of the 2-state MPC. By this process, we could perform an optimization-based methodology for the 2-state MPC calibration and also save a considerable time with respect to manually tuning the MPC. In Figure 5.3, the calibrated curves obtained over UDDS cycle and Ford HEV closed-loop model are illustrated. Also, the fuel economy values and their convergence is shown in Figure 5.4.

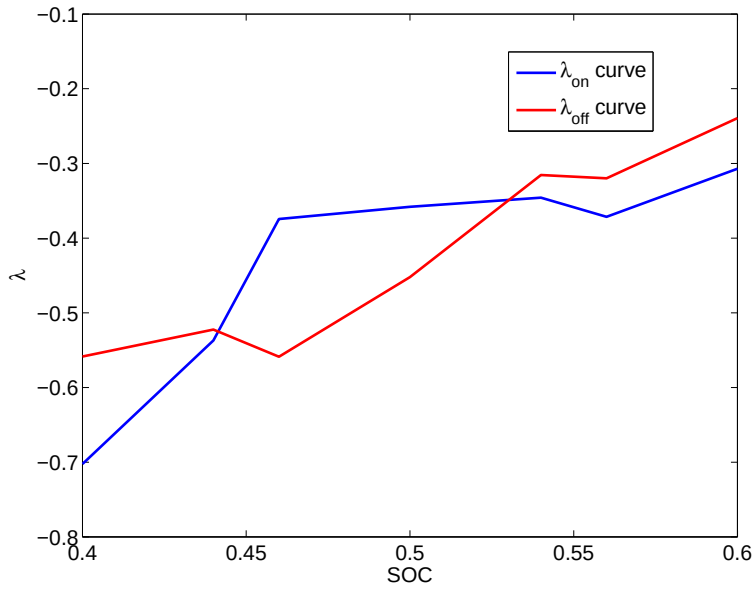

Figure 5.3: The calibrated λ in modeFRONTIER

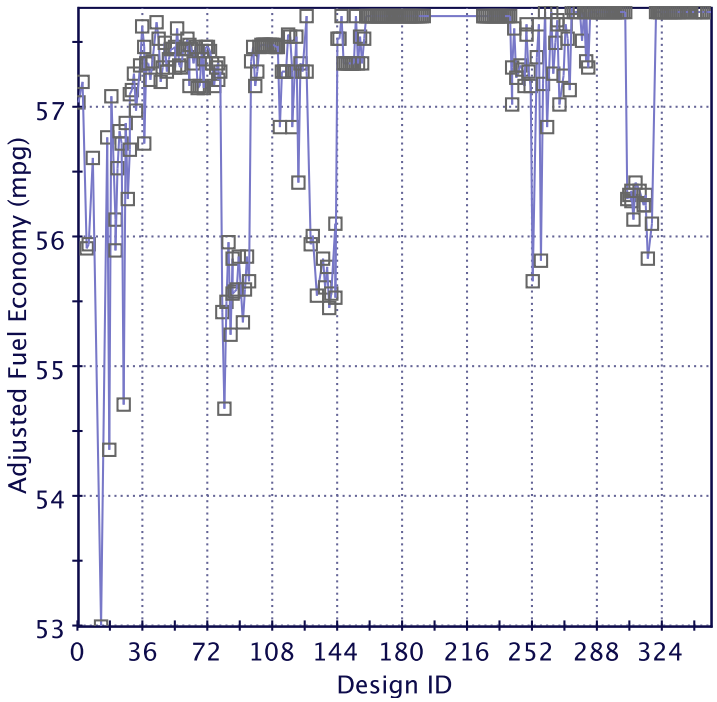

Figure 5.4: MPC calibration in modeFRONTIER

Table 5.2: 1-state versus 2-state MPC

Energy management	*Fuel economy (mpg)*
1-state MPC	57.25
1-state MPC ceiling	57.73
2-state MPC	57.71

5.3.2 Fuel Economy Analysis over the Ford Closed-Loop High-Fidelity Model

The fuel economy values of both the 1-state and 2-state MPC's over the UDDS cycle with the Ford closed-loop high-fidelity model are presented in Table 5.2.

We observed that 2-state MPC could enforce all the physical constraints. Also, the 2-state MPC fuel economy is improved with respect to the 1-state MPC and its value is close to the ceiling of 1-state MPC. Considering the fact that the ceiling of 1-state MPC is not easy to achieve (because of the uncertainty in the future vehicle operating conditions and also the error in the cost-to-go function approximation), 2-state MPC shows a noticeable improvement with respect to the 1-state MPC.

Chapter 6

Conclusions and Proposed Future Work for Part 1

6.1 Summary and Conclusions (Part 1)

In the first part of this dissertation, we demonstrated a successful application of MPC in the optimal power management of the power-split HEVs. For this purpose, first the control-oriented modeling of a power-split hybrid electric vehicle (Toyota Prius and Ford Fusion Hybrid) was done. It was shown that depending on the accuracy level, the dynamics of the system can be modeled by a 1-state or a 2-state model. In the 1-state model, battery state of charge (SOC) is the only state of the system. The battery dynamics which predicts the SOC trajectory over the prediction horizon are a nonlinear function of the control inputs. In the 2-state dynamics, in addition to the battery dynamics, the powertrain inertial dynamics are modeled and the engine speed is considered as an additional state of the system. In the 2-state model, the inertial power loss of the powertrain is modeled and SOC is predicted more accurately.

In addition to control-oriented modeling, another important element in designing the MPC controller is the performance index or the MPC cost function. In this work, first a quadratic cost function was defined and a standard linear MPC was employed to solve the power management problem online. Since the control-oriented model of the power-split HEV is nonlinear, the model is linearized and updated at each sampling time. This methodology is called the linear time-varying (LTV) MPC. The main advantage of LTV MPC is the available fast computational techniques for finding the solutions in real-time. To analyze the fuel economy of

the LTV MPC, a high-fidelity verified model of a power-split HEV extracted from the PSAT software is used in the closed-loop simulations and a PSAT rule-based controller is used as the reference controller. Regardless of the fact that the developed LTV MPC strategy is a systematic optimal control method for solving the power management problem, the fuel economy values over the standard drive cycles are not much improved with respect to the PSAT rule-base controller. We attribute this to the model error introduced by linearization of the control-oriented model. Furthermore, the feasible reference for the fuel consumption rate cannot be zero most of the time. Because of these issues, we observed that even increasing the prediction and control horizons of the LTV MPC with the current quadratic cost functional cannot noticeably improve the fuel economy.

In order to improve the fuel economy, a second cost function was introduced by dividing the fuel consumption cost into a stage cost and an approximation of cost-to-go as a function of the battery state of charge. The short horizon allows to solve the fuel minimization problem online in a nonlinear MPC framework. The proposed method is systematic in both design and calibration and also is predictive in nature. The results over a PSAT closed-loop model of a power-split HEV show that with the nonlinear MPC approach, the fuel economy is improved noticeably with respect to that of an available controller in the commercial PSAT software and compared to the LTV MPC. Based on the nonlinear MPC performance over the PSAT closed-loop model; this controller was redesigned and implemented on a Ford power-split HEV closed-loop model. The fuel economy ceiling of the MPC was also determined in closed-loop simulations. The nonlinear MPC fuel economy is very close to this ceiling, i.e. the best possible fuel economy. We also observed that changing the status of engine from on to off or vice versa (engine stop/start) considerably influences the fuel economy. Based on these observations and in order to further improve the MPC performance, the engine speed (powertrain) dynamics were added in the control-oriented model. With this addition, both the battery state of charge and the engine speed become the states of the control model. A nonlinear MPC based on this 2-state control model has been programmed using the C++ programming language and the results show improved fuel economy in the closed-loop simulations with the Ford high fidelity model. Furthermore, by using modeFRONTIER software and the parallel computing techniques, a systematic (optimal) calibration methodology of the MPC was presented. In summary, the MPC-based power management strategy developed in this work has the following features and advantages:

- is model-based,
- can be systematically designed and calibrated,
- its solutions are optimal with respect to the performance index and the control-oriented model,

- is adaptive with respect to the variable model parameters and constraints, and
- has a predictive nature and can also benefit from traffic and road preview information in its prediction.

Moving from the LTV MPC to the nonlinear MPC and then increasing the number of states in the control-oriented model increased the computational time. This should be another factor to consider in selection of any of these methods on a vehicle platform.

6.2 Future Research (Part 1)

In the following, a few research directions are proposed for enhancing the MPC power management strategy.

6.2.1 Tuning the approximated cost-to-go or parameter λ

In section 5.3.1, a systematic calibration method for the nonlinear MPC was presented. The MPC calibration presented in this dissertation was done based on the UDDS cycle and a piecewise linear λ curve. As we discussed in section 4.2, λ is related to both the global optimal solutions and also ECMS control method. We propose to tune the parameter λ over more driving cycles and to use the published strategies to tune ECMS for the MPC that may result in a better selection of λ function and further fuel economy improvement.

6.2.2 Analyzing the effect of future information

As it was mentioned before, one of the advantages of model predictive control is its ability to use preview information from road terrain and traffic. This ability comes from MPC's model-based prediction of the states and outputs. Recent advances in information technology and connectivity of modern vehicles present more opportunities for predicting the vehicle trip information with details such as the future road grade, the remaining distance to destination, and the speed constraints imposed by the traffic flow [54]. Use of preview information in the power management of hybrid electric vehicles has been discussed recently in the literature [57, 3]. Generally preview information in vehicle control can be divided into short- and long-horizon preview. For example, the speed of the vehicles in front of an HEV or the road speed limits can be considered as short-horizon future information while traffic flow information along a highway can be considered as long-horizon future information. In our nonlinear MPC, both of these types of future information can be employed

in a systematic manner. With the knowledge of the short-horizon future information, the system outputs over the prediction horizon are predicted more accurately and with the knowledge of longer horizon future information, the parameter λ or the cost-to-go approximation can be tuned more effectively. In an initial attempt, we tried to tune the 2-state MPC by assuming the HEV speed over a two-step (two-second) prediction horizon instead of a constant vehicle speed assumption. This calibration is done over the UDDS cycle with the methodology presented in section 5.3.1. The initial fuel economy (F.E.) results of this calibration are presented in table 6.1.

Table 6.1: Fuel economy analysis with future velocity information

$Control$	$Adjusted\ F.E.\ (mpg)$	$Charge-Balanced\ F.E.\ (mpg)$
2-state MPC without future speed	57.8	57.71
2-state MPC with future speed (2 steps)	58.4	-
Ford base controller	57.76	57.80

Due to the limited time, we could not finish the calibration and find the charge-balanced fuel economy of the 2-state MPC with the future vehicle speed. However, the adjusted fuel economy is promising. MPC calibration with known future information and its effect on the fuel economy can be performed in more detail in the future.

6.2.3 Linear MPC with a new quadratic cost function

As shown in chapter 3, with a quadratic cost function we can apply the well developed linear MPC methodologies with fast quadratic programming (QP) solvers. This reduces the computations with respect to the nonlinear MPC approach. The linear MPC approach can be implemented in Ford HEV PCM and compared to the rule-based control in vehicle tests. In this section, a quadratic cost function inspired by the one designed in [9] is proposed to be used in the MPC instead of the one proposed in chapter 3. In this proposed methodology, first the optimal engine speeds are calculated off-line based on maximizing the total efficiency of the system as

$$\omega^r_{eng}(k) = \omega^r_{eng}(V, T_d) = \arg\max_{P_{batt}} \left(\bar{\eta}^*\left(V, T_d, P_{batt}\right)\right) \tag{6.1}$$

where $\omega^r_{eng}(k)$ is the engine speed reference at sample time k ; V and T_d are the vehicle speed and demand wheel torque, respectively; P_{batt} is the battery power; and $\bar{\eta}^*$ is the maximum total efficiency of the power-split powertrain for a given vehicle speed, demand torque, and battery power. $\bar{\eta}^*$ can be obtained by (see

[30, 42, 2] for more details)

$$\bar{\eta}^{*}\left(V, T_d, P_{batt}\right) = \max_{\omega_{eng}} \eta_{total}\left(V, T_d, P_{batt}, \omega_{eng}\right) \tag{6.2}$$

where ω_{eng} is the engine speed. Defining a reference for the engine speed, a quadratic cost function over a short horizon can be defined by

$$\begin{aligned} J = \sum_{i=1}^{N} \Big(q_{x1} \cdot \big(\omega_{eng}(k+i) - \omega^{r}_{eng}(k+i)\big)^2 + q_{x2} \cdot \left(SOC(k+i) - SOC_r\right)^2 \Big) + \\ \sum_{i=0}^{M-1} \left(q_{u1} \cdot \Delta T_{eng}(k+i)^2 + q_{u2} \cdot \Delta T_{mot}(k+i)^2 \right) \end{aligned} \tag{6.3}$$

where ΔT_{eng} and ΔT_{mot} are the increments in engine and motor torques, respectively; SOC and SOC_r are battery state of charge and reference; and q_{x1}, q_{x2}, q_{u1} and q_{u1} are the penalty weights. Basically, this cost function is defined to operate the engine at a reference operation line while the deviation of SOC from a nominal reference is penalized. Moreover, in the second summation term, the rate of change of the engine and motor torques are penalized in order to achieve a better performance smoothness. Considering the 2-state dynamics as the control-oriented model, it is observed that in the new cost function, the references of the states are defined. Furthermore, the engine speed and SOC are related to the control inputs (for example engine and motor torques here) through the dynamics of the system making the linear dynamic approximation more effective.

Part 2:

Optimization-Based Power Management of a Wind Farm with Battery Storage

Chapter 7

Control-Oriented Modeling

In this and next chapters, an optimization-based power management of a wind farm with battery storage is developed. In this strategy, the objectives of reducing the power error and also extending the battery life which are explained in section 1.3 are considered. A review of the strategy and this part of the dissertation were presented in section 1.4.

7.1 Modeling of the Power Error Objective

Let P_{out} denote the combined output power delivered by a wind farm with a battery storage. As shown in Figure 1.3, P_{out} is given by

$$P_{\text{out}} = P_{\text{wind}} + P_{\text{bs}} \tag{7.1}$$

where $P_{\text{wind}} \geq 0$ is the power of the wind farm and P_{bs} is the power of the battery storage. The average power error we seek to minimize over an optimization horizon of H units of time in the future is defined as

$$P_{\text{error}} = \frac{1}{H}\int_{t}^{t+H} |P_{\text{out}}(\tau) - P_{\text{ref}}(\tau)|\, d\tau \tag{7.2}$$

where $P_{\text{ref}}(\tau)$ is a desired reference power provided by an operator. Substituting (7.1) into (7.2), and defining $P_{\text{bs,ref}} = P_{\text{ref}} - P_{\text{wind}}$, we obtain

$$P_{\text{error}} = \frac{1}{H}\int_{t}^{t+H} |P_{\text{bs}}(\tau) - P_{\text{bs,ref}}(\tau)|\, d\tau \tag{7.3}$$

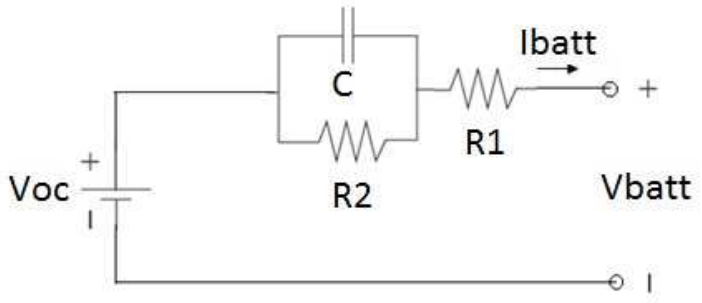

Figure 7.1: The Thevenin battery model [11]

If the power of the battery storage is distributed uniformly between n_{batt} identical batteries[1], we can rewrite equation (7.3) as

$$P_{\text{error}} = \frac{1}{H}\int_{t}^{t+H} |n_{\text{batt}} \cdot P_{\text{batt}}(\tau) - P_{\text{bs,ref}}(\tau)|\, d\tau \tag{7.4}$$

where P_{batt} is the power of each single battery and it is calculated as follows:

$$P_{\text{batt}} = V_{\text{batt}} \cdot I_{\text{batt}} \tag{7.5}$$

In (7.5), V_{batt} is the output voltage of a single battery and I_{batt} is the battery current. In order to calculate V_{batt}, we use the battery model in Figure 7.1 [11].

Based on this model, the battery output voltage is obtained from

$$V_{\text{batt}} = V_{\text{OC}} - V_{\text{cap}} - R_1 \cdot I_{\text{batt}} \tag{7.6}$$

where V_{OC} is the open circuit voltage, R_1 is the internal resistance, and V_{cap} is the overvoltage potential modeled by a capacitor. From this model, it follows that the overvoltage potential satisfies

$$\frac{dV_{\text{cap}}}{d\tau} = -\frac{1}{R_2 \cdot C} V_{\text{cap}}(\tau) + \frac{1}{C} I_{\text{batt}}(\tau) \tag{7.7}$$

where R_2 and C are the resistance and capacitance of the overvoltage potential model.

The battery model is also subject to battery constraints. Let *SOC* denote the state of charge of the battery, which is defined as the ratio of the stored battery charge to the battery capacity [55]. The battery is

[1] We assume that there is a battery management system (BMS) that uniformly distributes the power between the batteries of the storage.

subject to the following constraints:

$$\begin{aligned} SOC_{\min} \leq SOC(\tau) \leq SOC_{\max} \\ I_{\text{batt,min}} \leq I_{\text{batt}}(\tau) \leq I_{\text{batt,max}} \end{aligned} \tag{7.8}$$

where the lower and upper bounds in (7.8) are given. The state of charge is related to the battery current through the following dynamic equation [55]

$$\frac{dSOC}{d\tau} = -\frac{I_{\text{batt}}(\tau)}{C_{\text{batt}}} \tag{7.9}$$

where C_{batt} is the capacity of the battery.

The power error objective is to determine the battery current I_{batt} that minimizes the cost function (7.4) subject to the constraints in (7.5), (7.6), (7.7), (7.8), and (7.9). In order to reduce the state dimension in control design, we assume that $\frac{dV_{\text{cap}}}{d\tau} = 0$. Hence, equation (7.6) becomes

$$V_{\text{batt}} = V_{\text{OC}} - (R_1 + R_2) \cdot I_{\text{batt}} \tag{7.10}$$

A control objective is to minimize P_{error} in (7.4) subject to the model constraints in (7.5), (7.9), and (7.10) and the battery constraints in (7.8).

7.2 Battery Life Model

Another control objective is to operate the battery storage so as to extend its useful life. In order to quantify the battery life objective for the power management strategy, a battery life model is required. Modeling the battery life in applications such as wind energy with irregular operating conditions is challenging. These irregular operating conditions include operating at low state of charge, extremely high or low currents, extreme temperatures, and so forth. Furthermore, different types of electrochemical batteries have different aging processes, which determine the loss of life for a specific battery.

Based on a cost analysis method presented in reference [50], we observed that lead-acid batteries are still one of the cost effective options to be used in large-scale storage applications such as wind farms. Therefore, this type of batteries is selected for the wind farm storage.

In reference [49], three different approaches for the life prediction of the lead-acid batteries are discussed and compared. The first approach which is called physico-chemical model consists of a detailed

chemical and physical model of the aging processes in the lead-acid batteries. This model can accurately predict the loss of battery life. However, this model requires the knowledge of the interaction between electrochemical and physical measurements and the aging processes, which are usually not accessible with non-destructive measurements only. The second approach which is called weighted Amp-hour (Ah) throughput model is a computationally efficient model to predict the loss of battery life. This model is based on the observation that each battery can produce an expected total Ah throughput over its useful life. In this model, the effect of irregular operating conditions on the battery life are modeled with weight factors that take into account the deviation from regular, well-controlled, operating conditions. This model calculates aging continuously and can be coupled directly with battery performance models. Therefore, such models are suited for simulations and control. The third model which is called event-oriented model is based on an event-oriented aging model, which has been used in a number of mechanical engineering applications such as fatigue prediction. The event-oriented model separates the operation profile of the battery in a certain number of characteristics events. Then the incremental loss of the battery life is added up by counting the events over a time interval.

To illustrate our control strategy, the weighted Ah throughput model is used in this dissertation[2]. Based on this model. the growth rate of the weighted Ah throughput is calculated from

$$\frac{dwAh_{\text{batt}}}{d\tau} = \Pi_{\text{i}} f_{\text{i}}(\tau) \cdot I_{\text{batt}}(\tau) \cdot \text{H}(I_{\text{batt}}(\tau)) \tag{7.11}$$

where in this equation, wAh_{batt} is the weighted Ah throughput; the coefficients f_i are weight factors that model the effects of the irregular operating conditions; and $\text{H}(\cdot)$ is the Heaviside function defined by

$$\text{H}(I_{\text{batt}}(\tau)) = \begin{cases} 1 & if\ I_{\text{batt}}(\tau) > 0 \\ 0 & if\ I_{\text{batt}}(\tau) \leq 0 \end{cases} \tag{7.12}$$

Based on a model presented in reference [23], we consider the effect of SOC as a weight factor in equation (7.11) with the following model

$$f_{\text{SOC}}(t) = 1 + (c_{\text{SOC},0} + c_{\text{SOC,min}} \cdot (1 - SOC_{\min}(t)|_{t_0}^{t})) \sqrt{\frac{I_{\text{ref}}}{I}} \Delta t_{\text{SOC}}(t) \tag{7.13}$$

The variables in (7.13) are explained with the aid of Figures 7.2-7.4. The variable t_0 is the starting time

[2]Please note that the control strategy which is developed in this dissertation is modular and it allows to implement other battery life models for different battery technologies without any major change in the optimization.

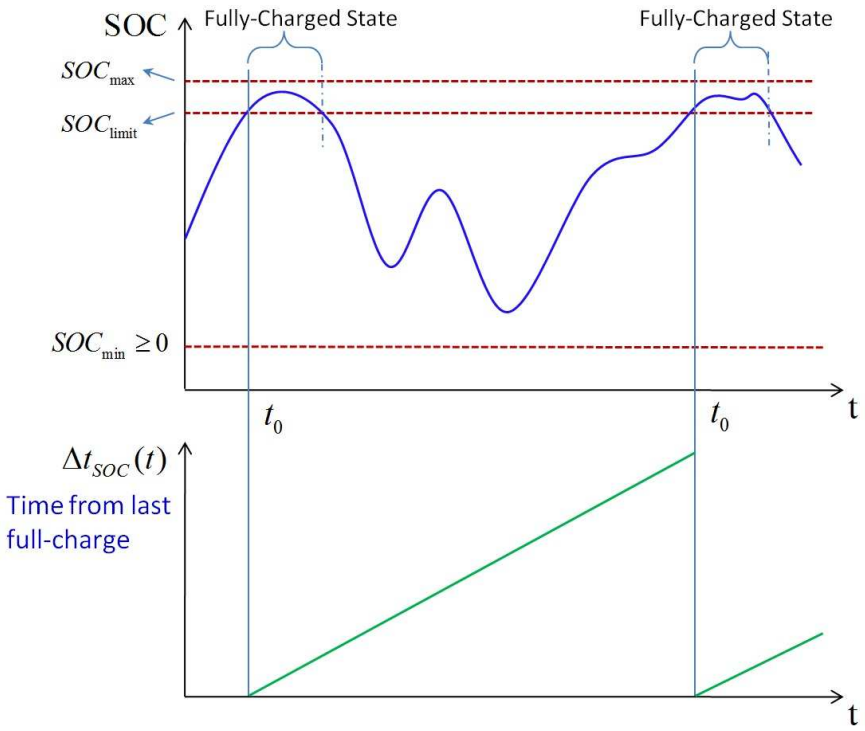

Figure 7.2: Schematic illustration of the full-charged state and the time from the last full-charged state

of a full-charged state, and the variable $\Delta t_{\mathrm{SOC}}(t) = t - t_0$ is the time from the last full-charged state; the full-charged state occurs when SOC becomes greater that a limit SOC_{limit}. The variable $SOC_{\mathrm{min}}(t)|_{t_0}^{t}$ is the minimum SOC from the start of the last full-charged state, and the variable I is the current factor, which is defined as the discharge current at the beginning of a discharge from a full-charged state; the variables $SOC_{\mathrm{min}}(t)|_{t_0}^{t}$ and I are shown schematically in Figures 7.3 and 7.4, respectively. The coefficients $c_{\mathrm{SOC},0}$, $c_{\mathrm{SOC,min}}$, and I_{ref} in equation (7.13) are constant parameters, which parameterize physical processes in the battery and are obtained either from expert guesses or from evaluating measured data of the battery [23].

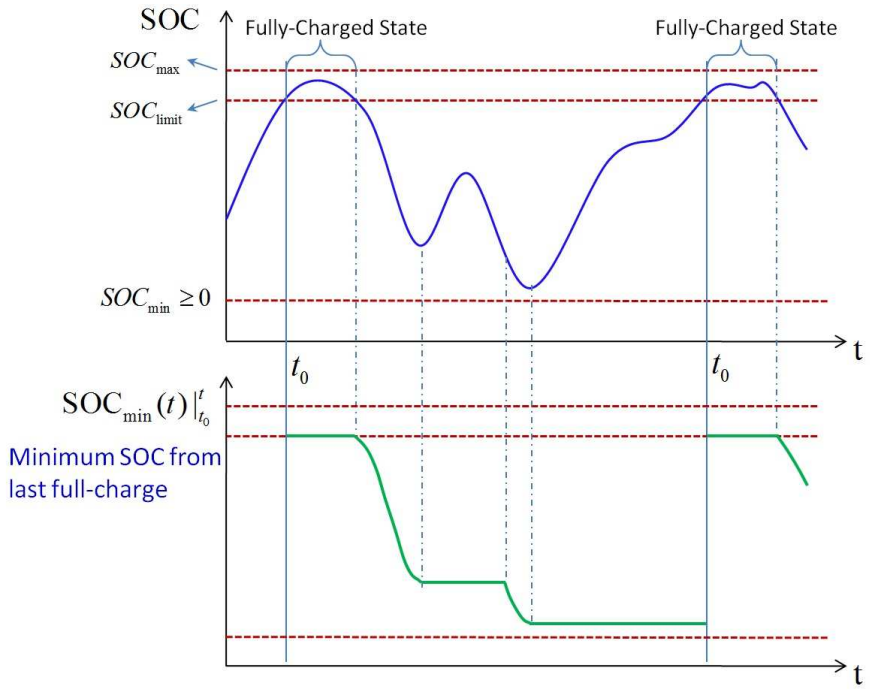

Figure 7.3: Schematic illustration of the minimum SOC from the last full-charged state

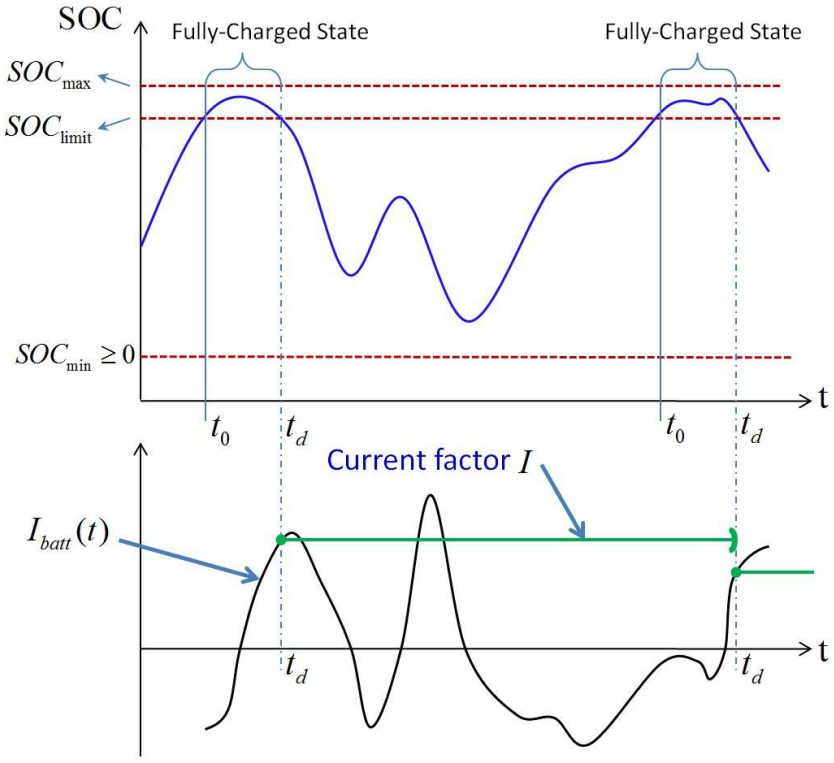

Figure 7.4: Schematic illustration of the current factor

Chapter 8

MPC-Based Power Management Strategy

8.1 The Optimal Power Management Problem

The goal of the control strategy is to command the battery current I_{batt} so that the power error and the loss of battery life are reduced simultaneously. In this dissertation, we quantify this goal by introducing the following cost function

$$J = w_{\text{error}} \frac{P_{\text{error}}}{P_{\text{n}}} + w_{\text{life}} \frac{wAh_{\text{batt}}(t+H)}{wAh_{\text{n}}} \tag{8.1}$$

where P_{error} and wAh_{batt} are defined in (7.4) and (7.11), respectively, and w_{error} and w_{life} are non-dimensional control weight factors for the power error and battery life objectives, respectively. The dimensional constants P_{n} and wAh_{n} normalize each term in equation (8.1).

Based on this cost function, the control problem we seek to solve is defined as follows:
Given a reference power demand $P_{\text{ref}}(\tau)$ for the wind farm over a given optimization horizon $t \leq \tau \leq t+H$; an estimate of the wind farm power production over the horizon $P_{\text{wind}}(\tau)$; and the current operating conditions

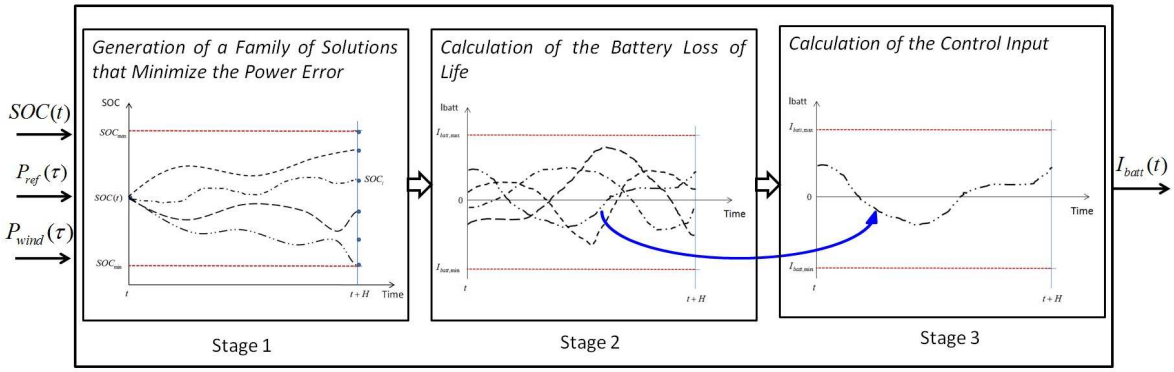

Figure 8.1: The flow chart of the power management strategy

of the battery storage solve

$$\min_{\substack{I_{\text{batt}}(\tau) \\ t\le\tau\le t+H}} \quad J(I_{\text{batt}}) \tag{8.2}$$

subject to (7.5), (7.8), (7.9), (7.10), and (7.11)

8.2 Optimization-Based Power Management Strategy

The optimization problem in (8.2) is a constrained nonlinear optimal control problem with two states. In [26], we have developed a dynamic programming solution (DP) in the framework of Model Predictive Control to the optimal power management problem of a Hybrid Electric Vehicle. Our goal is to use this strategy to solve the present problem. The DP algorithm in [26] assumes a one dimensional state space. Thus, the algorithm in [26] is not directly applicable to (8.2). In this dissertation, we provide a suboptimal solution to (8.2) by decomposing it into three subproblems solved in three separate stages. Figure 8.1 illustrates these three stages.

In stage 1, we calculate a family of control solutions (i.e., battery current profiles) to minimize the power error subject to the model and battery constraints and an additional constraint on the SOC at the end of the optimization horizon. In stage 2, the weighted Ah throughput at the end of the optimization horizon is calculated for each solution. Thus, stage 2 gives the loss of battery life incurred by each current profile from stage 1. In stage 3, we calculate the cost function defined in (8.1) for each solution and select the current profile with the smallest cost value. This approach gives a suboptimal solution to the optimization problem in (8.2). In what follows, these stages are described in detail.

Stage 1 *Generation of a Family of Control Solutions that Minimize the Power Error*

In this stage, we calculate a family of current profiles, $I^*_{\text{batt},0}(\tau), I^*_{\text{batt},1}(\tau), \cdots, I^*_{\text{batt,L}}(\tau)$, using the following procedure.

The current profile $I^*_{\text{batt},0}(\tau)$ is obtained by solving the following power error minimization problem:

$$\min_{\substack{I_{\text{batt}}(\tau) \\ t \le \tau \le t+H}} P_{\text{error}} \quad \textit{subject to: (7.5), (7.8), (7.9), and (7.10)} \tag{8.3}$$

The current profile $I^*_{\text{batt,i}}(\tau)$ with $i \geq 1$ is calculated by solving problem (8.3) with an additional terminal constraint

$$SOC(t+H) = SOC_{\text{i}} \tag{8.4}$$

where the values $SOC_{\text{i}},\ i \geq 1$, are given a priori. If the problem with this additional constraint is feasible, then we store the solution $I^*_{\text{batt,i}}(\tau)$. By changing the terminal *SOC* constraint in (8.4), we produce multiple feasible solutions, $I^*_{\text{batt},1}(\tau), I^*_{\text{batt},2}(\tau), \cdots, I^*_{\text{batt,L}}(\tau)$, which minimize the power error with different terminal *SOC* values. These solutions plus $I^*_{\text{batt},0}(\tau)$ generates the family of control solutions.

Stage 2 *Calculation of the Loss of Battery Life*

In this stage, the loss of battery life incurred by applying each current profile of the family of solutions from stage 1 is calculated. Based on the battery life model presented in Section 7.2, the terminal weighted Ah throughput of each $I^*_{\text{batt,i}}(\tau)$, for $i = 0 \cdots L$, is obtained from

$$wAh^*_{\text{batt,i}}(t+H) = \int_t^{t+H} f_{\text{SOC}}(\tau) \cdot I^*_{\text{batt,i}}(\tau) \cdot \text{H}(I^*_{\text{batt,i}}(\tau))\, d\tau \tag{8.5}$$

Stage 3 *Calculation of the Control Command*

According to the cost function defined in (8.1), the total cost of each current profile $I^*_{\text{batt,i}}(\tau)$, for $i = 0 \cdots L$, is calculated from

$$J^*_{\text{i}} = w_{\text{error}} \frac{P^*_{\text{error,i}}}{P_{\text{n}}} + w_{\text{life}} \frac{wAh^*_{\text{batt,i}}(t+H)}{wAh_{\text{n}}} \tag{8.6}$$

where $P^*_{\text{error,i}}$ is the corresponding power error of each current profile from (8.3) and (8.4), and $wAh^*_{\text{batt,i}}(t+H)$ is from (8.5).

The control input is obtained from

$$I_{\text{batt,opt}}(\tau) = \arg \min_{\{I^*_{\text{batt,0}}, I^*_{\text{batt,1}}, \ldots, I^*_{\text{batt,L}}\}} \{J^*_0, J^*_1, \ldots, J^*_{\text{L}}\} \tag{8.7}$$

The commanded battery current at time t is set to be

$$I_{\text{batt}}(t) = I_{\text{batt,opt}}(t) \tag{8.8}$$

To implement stages 1-3, we use a discrete-time Model Predictive Control (MPC) framework [34]. In this framework, the current $I_{\text{batt}}(t)$ is applied and held constant over the control sampling interval $[t,\ t+T_{\text{s}}]$ where $T_{\text{s}} \leq H$ is the control sampling interval. At the next control sampling time $t+T_{\text{s}}$ the state of the charge $SOC(t+T_{\text{s}})$, the wind farm power $P_{\text{wind}}(\tau)$ over the optimization horizon $t+T_{\text{s}} \leq \tau \leq t+T_{\text{s}}+H$, and the reference power $P_{\text{ref}}(\tau)$ are updated and stages 1-3 are repeated to calculate $I_{\text{batt}}(t+T_{\text{s}})$.

8.3 Simulation Conditions and Results

The power management strategy developed in Section 8.2 is tested using actual data from a wind farm in the state of Texas with maximum power production of 150 MW. The power produced by the wind farm (P_{wind}) is given over a 24-hour period. The block diagram of the system we simulate is shown in Figure 8.2.

The simulations are performed over a 24-hour period. The reference power P_{ref} is defined based on a one-hour power dispatching scenario as presented in reference [6][1]. In this scenario, a constant reference for

[1]This reference profile is an example to illustrate the performance of the control. However, other reference options can be handled in this framework.

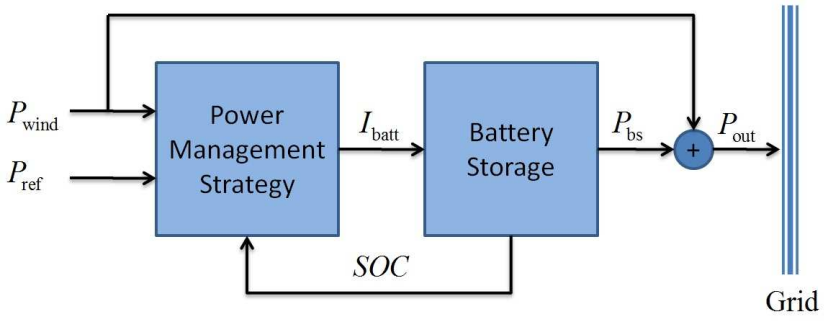

Figure 8.2: Block diagram of the storage system

Table 8.1: Battery Characteristics

$V_{OC}\ (V)$	$R_1\ (\Omega)$	$R_2\ (\Omega)$	$C\ (F)$	$C_{batt}\ (Amp-hr)$
2.135	0.0019	0.00041	12195121.0	500

the combined output power P_{out} over an hour is obtained by calculating the average of the wind farm power data P_{wind} over the one hour interval; see dash-dot trace in the top graph of Figure 8.3.

The model of the battery storage in Figure 8.2 consists of 22 parallel branches of 937 identical lead-acid batteries. To model each battery, we used the model presented in Figure 7.1 and described by equations (7.5), (7.6), (7.7), (7.9), and (7.11). The characteristics of the model for each single battery are chosen from reference [6] and are presented in Table 8.1[2].

The power management block in Figure 8.2 consists of the stages 1-3 presented in Section 8.2. Note that the power management strategy is implemented in discrete time and the stages 1-3 are discretized with a control sampling interval $T_s = 60\ sec$. The optimization horizon H is set to 10 control sampling steps. In order to generate the family of control solutions in the stage 1, we solve the power error minimization problem with dynamic programming (DP) [26]. For this purpose, the state, SOC, and the control input, I_{batt}, are quantized over their admissible range with the following quantization levels: $\Delta SOC = 0.001$ and $\Delta I_{batt} = 2.5\ Amp$. The battery constraints are set to be $SOC_{min} = 0.3$, $SOC_{max} = 1$, $I_{batt,min} = -400\ Amp$, and $I_{batt,max} = 400\ Amp$. To generate the family of control solutions, we define 10 terminal SOC values, which are uniformly distributed over the SOC range $[0.3,\ 1]$.

[2]This design is equivalent to a battery storage with power and energy capacities of 22 MW and 22 $MW-hr$, respectively. The optimal size of the battery storage is another important aspect of the system which is outside the scope of this dissertation.

8.3.1 Simulation Results for the Minimum Power Error Solution

We now present the time domain simulation results for the minimum power error solution. This corresponds to minimizing (8.6) with $w_{\text{life}=0}$, or equivalently to implementing the solution of (8.3). Figure 8.3 shows the time histories of the power signals, the state of charge, the current command, the error between the output power P_{out} and the reference power P_{ref}, and the growth of the weighted Ah throughput over the 24-hour simulation period. Three power signals are shown: the wind farm power P_{wind} (solid, red), the operator reference power P_{ref} (dash-dot. green), and the combined output power of the system P_{out} (solid, blue). It is observed that the battery is operated so that the combined output power P_{out} follows the operator reference power P_{ref} while the battery constraints on the SOC and I_{batt} are satisfied.

8.3.2 Simulation Results for a Solution with Battery Life Objective

In order to show the effect of penalizing the loss of battery life, the closed-loop simulation is repeated by defining a non-zero control weight factor for the battery life objective $w_{\text{life}>0}$; see equation (8.1). In this section, the simulation results with the control weight ratio $\frac{w_{\text{error}}}{w_{\text{life}}} = 175$ are presented. Figure 8.4 shows the time histories of the power signals, the state of charge, the current command, the error between the output power P_{out} and the reference power P_{ref}, and the growth of the weighted Ah throughput over the 24-hour simulation period. The power signals include the wind farm power P_{wind} (solid, red), the operator reference power P_{ref} (dash-dot. green), and the combined output power of the system P_{out} (solid, blue). It is observed that by penalizing the loss of battery life, the total weighted Ah throughput over the simulation period is decreased with respect to one of the minimum power error solution; however, the averaged power error between the output power and the reference power is increased with respect to one of the minimum power error solution. From the simulations, it follows that a 21% reduction of weighted Ah throughput leads to an increase of 67% in the value of the averaged power error over the 24-hour simulation period.

8.3.3 Power Management Performance with Different Control Weight Ratios

In this section, the closed-loop simulations over the 24-hour period are repeated by defining a range of control weight factors for the battery life and power error objectives. The results are plotted in Figure 8.5. This plot shows the averaged power error versus the total weighted Ah throughput over the simulation period. It is observed that by increasing the weight ratio $\frac{w_{\text{error}}}{w_{\text{life}}}$, which is equivalent to decreasing the control weight factor on the battery life objective w_{life}, the weighted Ah throughput is increased while the averaged power

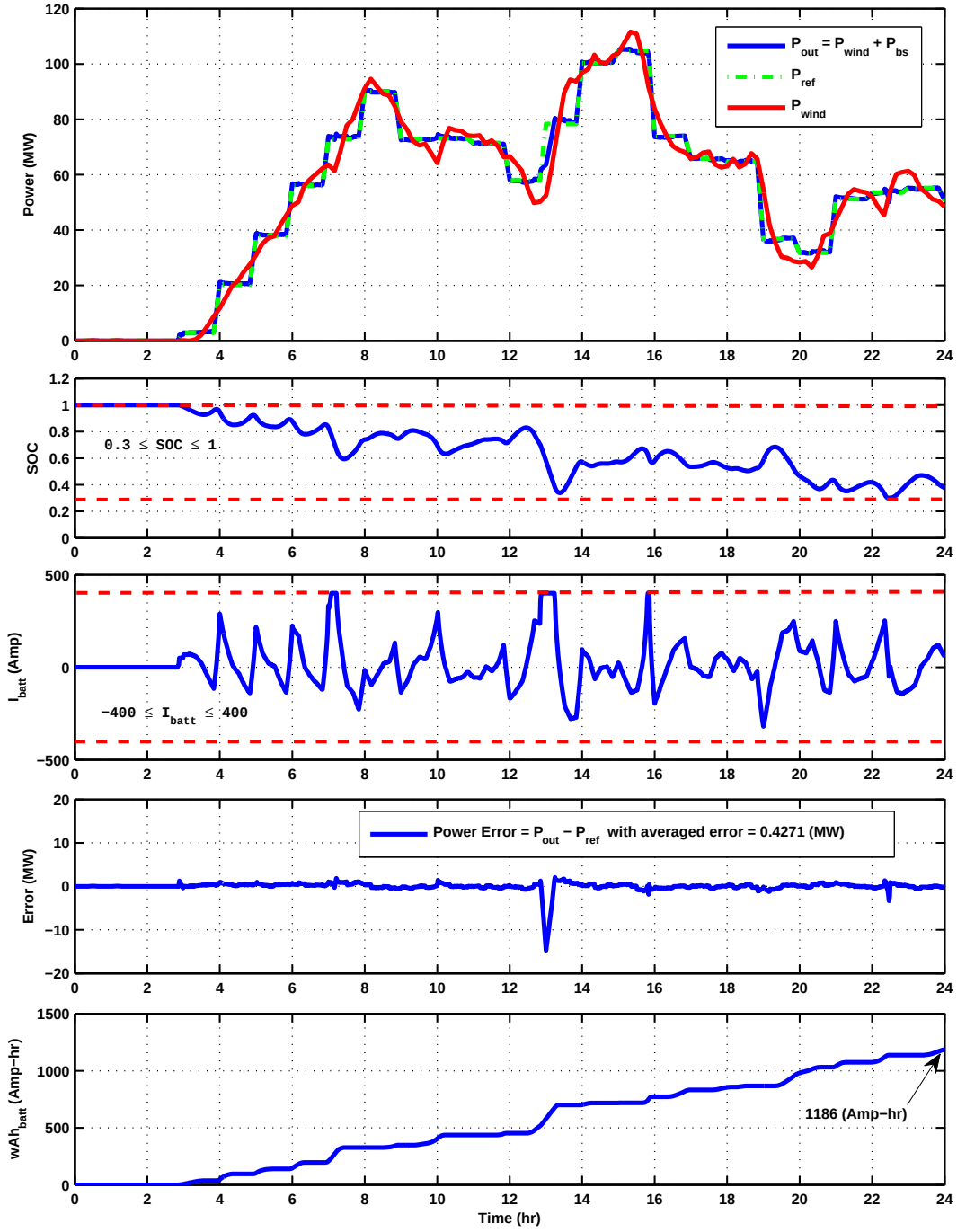

Figure 8.3: Simulation results for the minimum power error solution with the actual wind power data

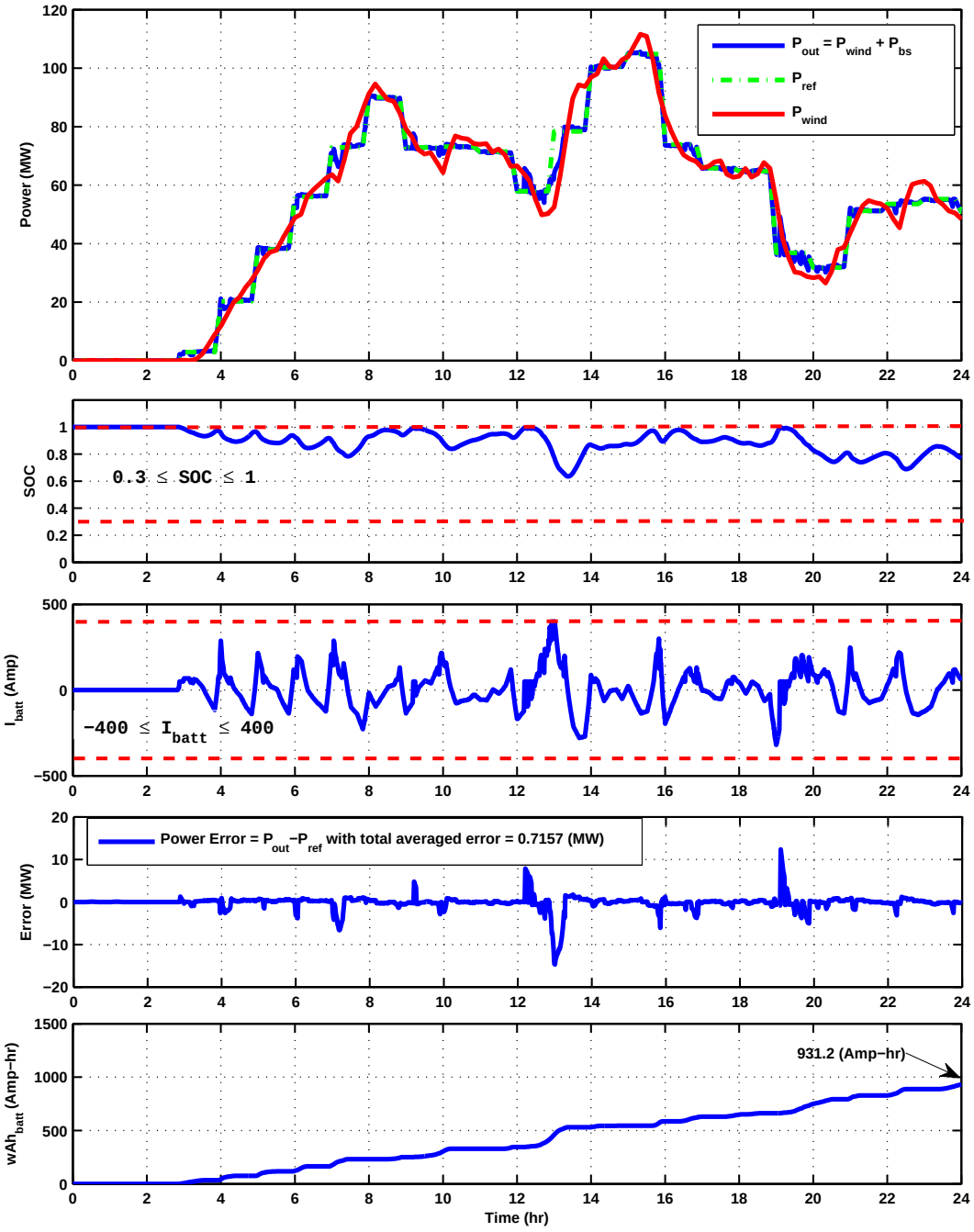

Figure 8.4: Simulation results for $\frac{w_{\text{error}}}{w_{\text{life}}} = 175$ with the actual wind farm power data

error is decreased. This is in accordance to the fact that the power error objective conflicts with the battery life objective. By tuning the weight factors, the operator has the freedom to do the tradeoff between the two objectives.

8.3.4 The Effect of Forecast Error

In the simulations we have done so far, it was assumed that the wind farm power profile is known over the simulation period. However, in wind applications such as firm capacity [15], the wind farm owner should forecast the wind farm power P_{wind} for the next 24 hours to set the reference power P_{ref} for the next day power production. Therefore, in order to show the effect of the forecast error in the performance of the control strategy, we generated a new wind power profile by adding a random error signal to our original wind power data and using the resulting randomly perturbed wind profile as the actual wind power production.

According to reference [16], for forecast horizons up to 48 *hr*, the wind power forecasting systems can predict a wind farm power with an error equal to $5-10\%$ of the wind farm maximum power production. Therefore, we added a random signal generated from the uniform distribution over the range $[-7.5\ MW,\ +7.5\ MW]$ to our original wind farm power profile. The new wind power profile with the additional error is used as the wind farm power P_{wind} in the simulations of this section. However, since we want to calculate the reference power P_{ref} based on the forecast wind power, the reference power profile remains the same as the one we had before. These power profiles are shown in Figure 8.6.

With these new simulation conditions, the one-hour power dispatching scenario over the 24-hour period was repeated with different values of weight factors and the results are plotted in Figure 8.7. It is observed that due to the forecast error in the calculation of the reference power P_{ref}, the averaged output power and the total Ah throughput over the simulation period is increased with respect to the case without forecast error. However, the overall trend remains the same as the case without the forecast error. The price paid for having uncertainty in the wind power forecast is clear; both averaged power error and battery weighted Ah throughput are increased, resulting in worse performance and decreased battery life. Taking into account the statistics of the wind power forecast error in the design of the power management strategy would likely lead to better results, but this is outside the scope of this research.

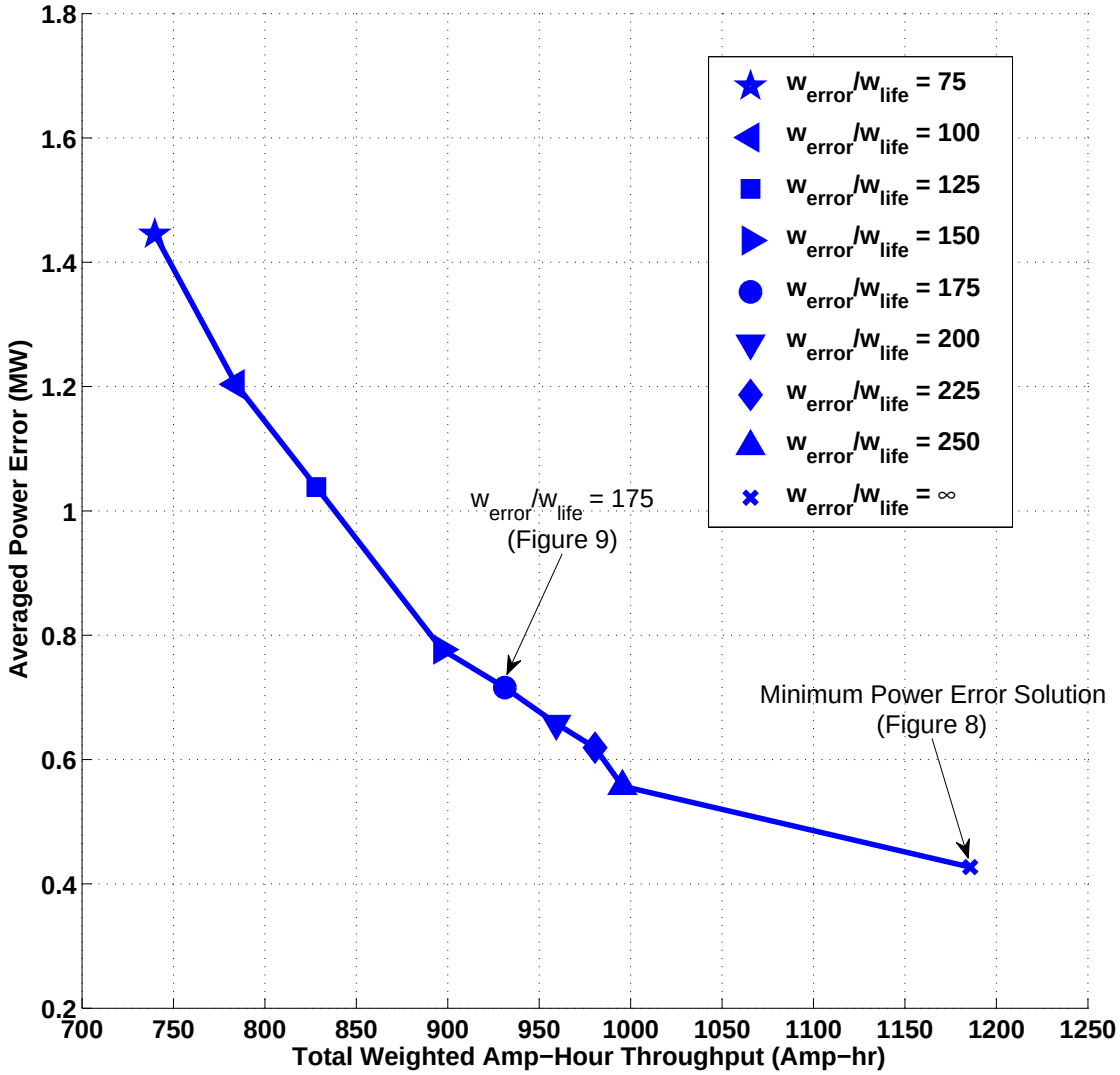

Figure 8.5: Averaged power error versus total weighted Ah throughput over the 24-hour power firming

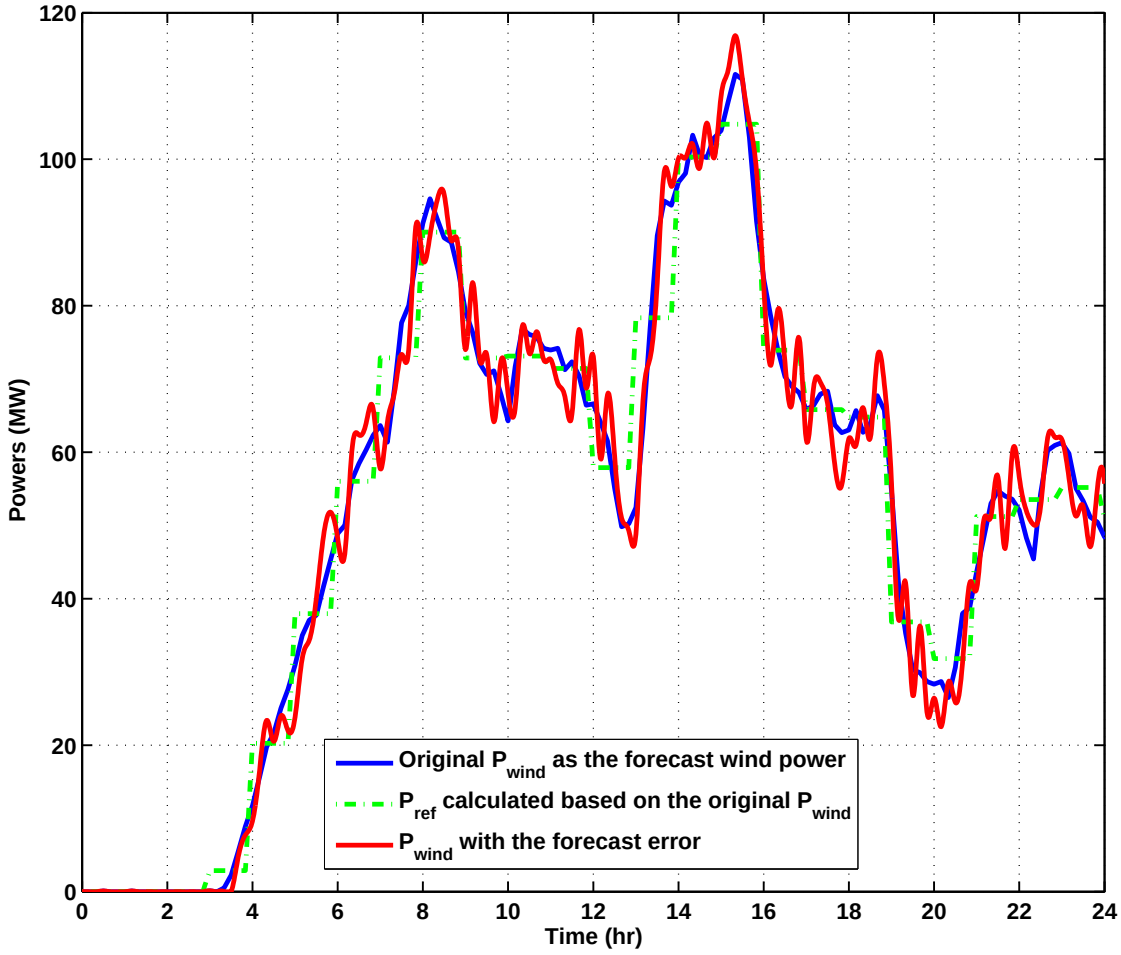

Figure 8.6: Wind farm power with forecast error

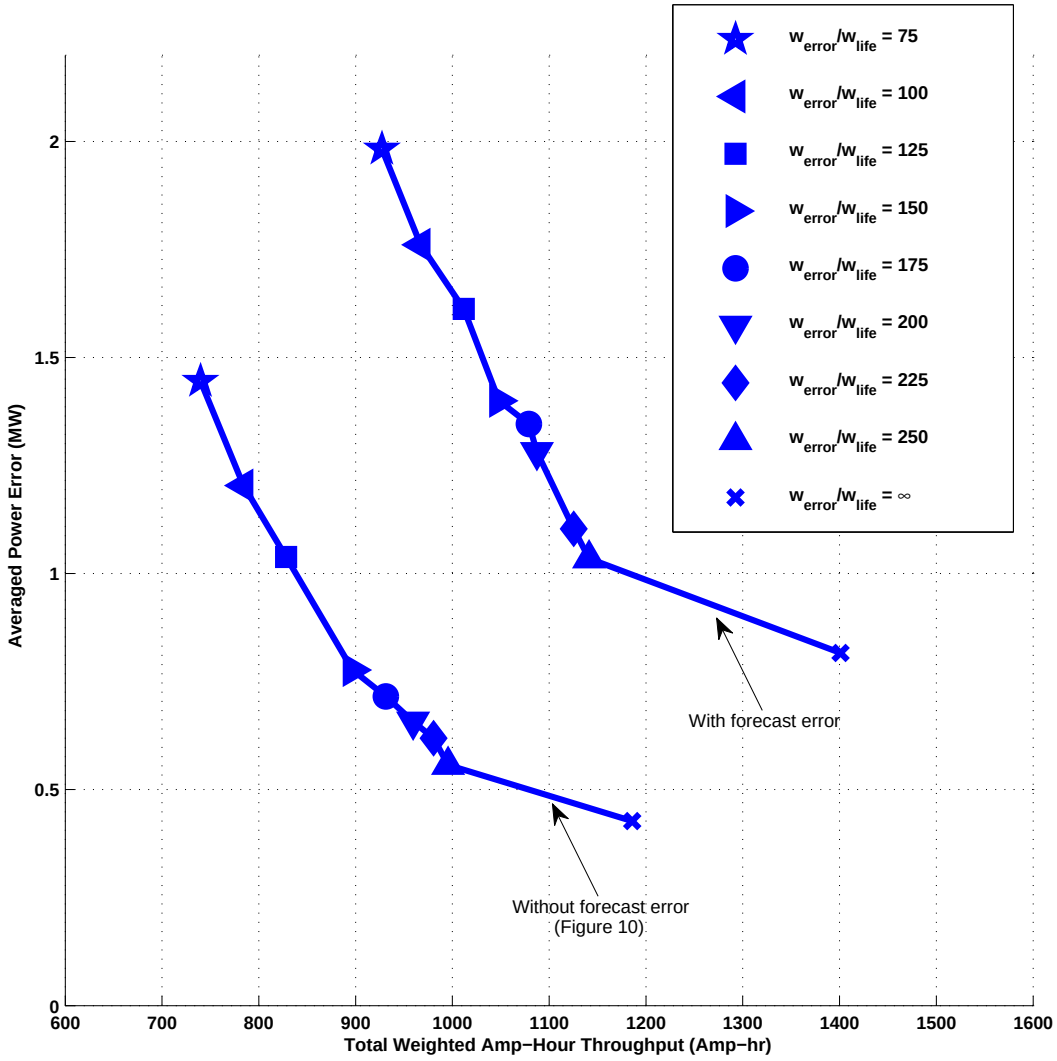

Figure 8.7: Averaged power error versus total weighted Ah throughput over the 24-hour power firming

Chapter 9

Conclusions and Proposed Future Work for Part 2

9.1 Summary and Conclusions (Part 2)

The second part of this dissertation presented an optimization-based control strategy for the real-time power management of battery storage in a wind farm. The strategy seeks to minimize the error between the power delivered by the storage-aided wind farm and a power reference from an operator. In addition, the proposed strategy attempts to maximize the useful life of the battery storage. The control strategy has two main stages. The first stage produces a family of control solutions that minimize the power error subject to the system constraints and a set of constraints on the battery state of charge (SOC), enforced at the end of an optimization horizon. The second stage screens the family of control solutions to select one attaining an optimal balance between power error and battery life. The battery life model used in this stage is a weighted Amp-hour (Ah) throughput model. *Modularity* is one of the most appealing features of the proposed power management strategy. That is, the formulation can accommodate more sophisticated optimization models in the first stage, as well as more elaborated battery life models in the second stage. The strategy is implemented in the framework of Model Predictive Control. Closed-loop simulation results using real wind farm data showed the effectiveness of the strategy.

9.2 Future Research (Part 2)

In the following section, a few research directions are proposed based on the developed methodology in the second part of this dissertation.

9.2.1 Communicating with the wind farm control

In this dissertation, it was assumed that there is not any control on the wind farm power generation by the power management strategy. Therefore, an increased power error may be observed when the battery storage is in a full-charge state while it needs to be charged to follow the reference power[1]. However, it is possible to reduce the power generation by the wind farm if it is required. By giving an additional degree of freedom to the power management strategy to control the wind farm power generation, it is possible to prevent any over charge of the battery which is harmful for its life, and also to reduce the power error from the reference. This additional control input can be defined with an upper limit constraint which is obtained by the forecast of the wind power along the optimization horizon. We have implemented an MPC with two inputs in the first part of this dissertation and the same methodology can be applied for the control of both the battery storage and the wind farm.

9.2.2 Stochastic MPC

Investigating the effect of forecast error on the real-time performance of the strategy is another important subject for research. In Section 8.3.4, we observed that the forecast error in the wind power prediction affects the strategy performance. One of the solutions that may improve the performance of the strategy is to apply stochastic optimal control theory with a wind power forecast model. Stochastic MPC has been used before for the power management of HEVs in references [48] and [9]. The same methodologies can be developed for the purpose of the wind farm power management.

9.2.3 Applying the strategy for the power management of hybrid electric vehicles

The basic idea of the power management strategy developed in Part 2 is to generate a family of solutions instead of one solution and to select the one which satisfies other control objectives. In Chapter 5 of this thesis, it was shown that powertrain dynamics specifically the engine start/stop transients have an important effect on the vehicle fuel economy. Therefore, the engine speed dynamics were added to the

[1] When the operator reference power is below the generated wind power, the battery should be charged to follow the reference.

MPC resulting in a 2-state MPC problem. However, we observed that by increasing the number of states of the nonlinear control-oriented model, the computational time of the DP solver is increased noticeability. Therefore, one way to reduce the computations and to increase the flexibility of the HEV power management is to implement the same idea presented for the wind farm; i.e. generating a family of solutions by solving the 1-state fuel minimization problem formulated in Section 4.3. Then in a post processing stage, other objectives such as reduction of the powertrain inertial losses or the battery life extension can be quantified with appropriate models. Finally, a solution that balances these control objectives of the HEV can be selected and applied in the framework of MPC in real-time.

Appendices

Appendix A LTV MPC Power Management of an HEV with Combined Battery and Supercapacitor

In all different types of hybrid electric vehicles, the energy storage system (ESS) is one of the degrees of freedom used to assist the engine or to recover the vehicle kinetic energy in the regenerative braking mode. In general, the ESS unit in hybrid vehicles should have the ability to provide both enough energy and also energy rate (power) over different driving conditions. Table 1 compares energy and power characteristics of supercapacitors versus a few batteries [8]. As can be seen, batteries have better energy density than supercapacitors but their power density or their ability to release energy in a very short time is typically poor. In addition, besides the fact that cycling life of a battery is much shorter than a supercapacitor, cycling the battery with high currents and depth of discharge (DOD) can significantly reduce the life of the battery [36], [35]. On the other hand, although the energy density of supercapacitors is less than the batteries, their power density is generally much higher than the battery. Moreover, the cycle life of supercapacitors is very long with respect to the electrochemical batteries. Based on the discussed advantages and disadvantages of batteries and supercapacitors, using a combination of them in the ESS unit of hybrid electric vehicles has attracted attention recently [8],[35], [5].

The purpose of this section is to analyze potential merits of integrating a supercapacitor in the ESS unit of a power-split hybrid electric vehicle (HEV) with the developed LTV MPC power management in Chapter 3. Inclusion of a supercapacitor bank adds one additional degree of freedom to the power management of an HEV. The number of states also increases by one, which is the state-of-charge of the supercapacitor. Therefore, using dynamic programming to find the optimal solution for the HEV power management problem becomes more computationally intensive due to the added state and input. Furthermore, dynamic programming based solutions are drive cycle dependent. On the other hand, optimization methods like ECMS ([47]) may be sensitive to their tuning parameter and having one more additional tuning factor adds further to the complexity of an ECMS approach [39]. Rule-based strategies have also been proposed in some papers that have considered integration of ulracapacitors with batteries. In [5], a table look-up approach determines the power split between the battery and supercapacitor. The outcomes of their simulations in a commercial software tool illustrate the capabilities of improving the battery's life due to decreasing current output of the battery. Also in [35], based on an optimal engine operating map of Toyota Prius and the demanded power of a standard drive cycle, the ESS power in different segments of a vehicle trip is derived and a Maxwell D-cell supercapacitor module is sized to reduce discharging power rate of the battery. In this section, we develop

Table 1: Performance comparison of batteries and supercapacitors

	NIMH Battery	Li-ion Battery	supercapacitor
Energy density (Wh/kg)	40-50	50-80	1-5
Power density (W/kg)	900-1100	1000-4000	1000-30,000
Number of cycles at 80% DOD	≈ 3000	≈ 3000	$\gg 100{,}000$

a real-time control strategy based on Model Predictive Control for the power management of a power-split HEV with combined battery and supercapacitor.

A.1 Control-Oriented Modeling

Among different configurations of a hybrid electric powertrain, the power-split configuration that provides both series and parallel functionality has been used in production by several auto-makers. The Toyota Prius, Ford Fusion Hybrid, and Ford Escape Hybrid are among the produced HEV's with a power-split powertrain. Figure 1 shows a schematic view of a power-split HEV. In this configuration, the engine and the generator are connected to the planet carrier and the sun gear of a planetary gear set which functions as a speed coupler, respectively. The output of the speed coupler is combined with a motor through a counter shaft which functions as a torque coupler to power the vehicle driveline. Because of the different possible power flows in a power-split powertrain, the engine operating point can be seen as decoupled from the vehicle operating point. In addition, the energy storage system provides another degree of freedom to accumulate or deliver energy. Since in the HEV, the energy storage system consists of a battery and an ultracapacitor, totally there are three degrees of freedom to drive the HEV. The power-split HEV consists of a power transmission system, an internal combustion (I.C.) engine and an energy storage system. Each of these components has different parts with their interactions shown schematically in Figure 1. In the following sections, a model of each component is derived to obtain a control-oriented model of the HEV which is used to design the optimal power management strategy.

A.1.1 Vehicle Speed Dynamics and the Power Transmission System Model

In this section, dynamical models of the power transmission system and the vehicle are presented. More details are available in ([33] and [12]). As it is shown in Figure 1, the power transmission system includes a planetary gear set which combines the powers of the engine, the motor, and the generator. In order to model this system, the following assumptions are made:

- The internal dynamics of the motor and generator are fast enough to be ignored.

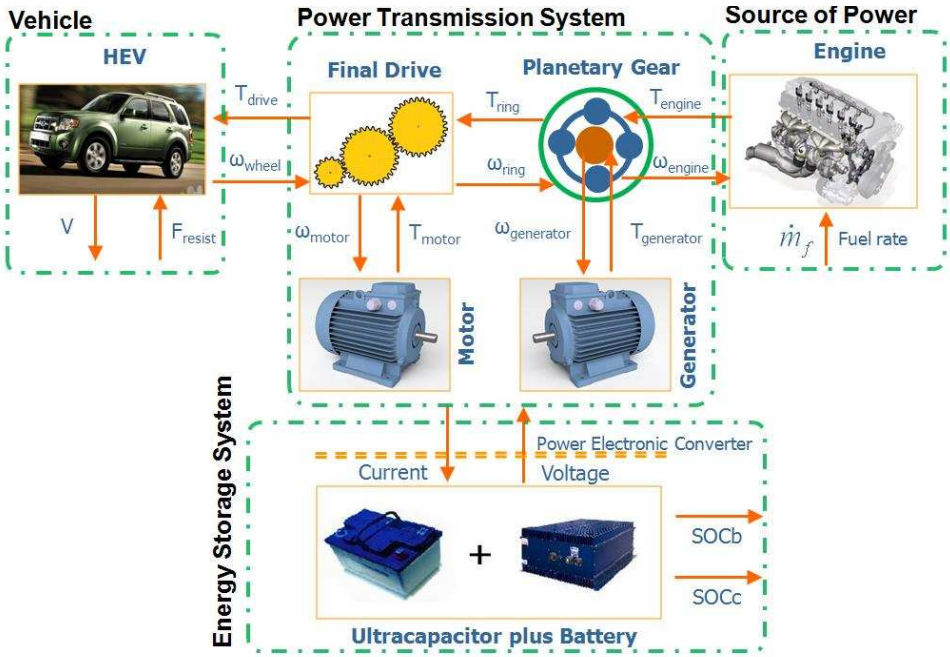

Figure 1: Power-split HEV configuration

- The vehicle is modeled as a lumped mass and its speed dynamics are presented by its longitudinal dynamics.
- All connecting shafts in the power transmission system are rigid.
- The inertial of the pinion gears in the planetary gear set are neglected.
- The inertial of the engine, generator, and motor are lumped with the one of the carrier, sun, and ring gears respectively.
- The inertial of the final transmission system and the wheels are lumped with the ring gear.

By applying Newton's laws of motion on both the planetary gear set and considering the lumped mass longitudinal dynamics of the vehicle, we obtain

$$\begin{aligned}
J_{gen}\frac{d\omega_{gen}}{dt} &= T_{gen} + F \times N_S \\
J_{eng}\frac{d\omega_{eng}}{dt} &= T_{eng} - F \times (N_S + N_R) \\
J_{mot}\frac{d\omega_{mot}}{dt} &= T_{mot} - \frac{T_{out}}{g_f} + F \times N_R \\
m\frac{dV}{dt} &= \frac{T_{out} + T_{brake}}{r_w} - \frac{1}{2}\rho A_f C_d V^2 - C_r mg\cos(\theta) + mg\sin(\theta)
\end{aligned} \tag{1}$$

In equations (1), J_{eng}, J_{gen}, and J_{mot} are lumped inertial of the engine, generator, and motor, respectively; N_S, and N_R are the radii of the sun and ring gears, respectively; T_{eng}, T_{gen}, and T_{mot} are the engine, generator, and motor torques, respectively; ω_{eng}, ω_{gen}, and ω_{mot} are the engine, generator, and motor speeds, respectively; T_{out} is the output torque of the power transmission system; T_{brake} is the friction brake torque; V, m, and A_f are the speed, mass, and frontal area of the vehicle, respectively; r_w is the wheel radius; C_r is the rolling friction coefficient; C_d and ρ are the drag coefficient and air density; g_f is the final derive ratio; θ is the road grade which is assumed to be positive when vehicle goes down a hill; and g is the gravitational acceleration. Also in (1), F is the interaction force between the gears of the planetary gear set. There are also two kinematic equality constraints including

$$N_s\omega_{gen} + N_R\omega_{mot} = (N_s + N_R)\,\omega_{eng} \tag{2}$$

$$\omega_{mot} = \frac{g_f}{r_w}V \tag{3}$$

By combining equations (2) and (3) with (1) we obtain

$$\begin{aligned}
&\left(J_{eng} + \left(\tfrac{N_S+N_R}{N_S}\right)J_{gen}\right)\tfrac{d\omega_{eng}}{dt} = T_{eng} + \left(\tfrac{N_S+N_R}{N_S}\right)T_{gen} + \\
&\left(\tfrac{N_S+N_R}{N_S}\right)\left(\tfrac{N_R}{N_S}\right)J_{gen}\tfrac{d\omega_{mot}}{dt} \\
&T_{mot} = \tfrac{T_{out}}{g_f} - \left(\tfrac{N_R}{N_S+N_R}\right)\left(T_{eng} - J_{eng}\tfrac{d\omega_{eng}}{dt}\right) + J_{mot}\tfrac{d\omega_{mot}}{dt} \\
&\tfrac{d\omega_{mot}}{dt} = \tfrac{g_f}{mr_w}\left(\tfrac{T_{out}+T_{brake}}{r_w} - \tfrac{1}{2}\rho A_f C_d V^2 - C_r mg\cos(\theta) + mg\sin(\theta)\right)
\end{aligned} \tag{4}$$

In addition to the dynamics in (4), the following constraints are applied on the power transmission system:

$$\begin{aligned} T_{eng}^{\min} \leq T_{eng} \leq T_{eng}^{\max};\ 0 \leq \omega_{eng} \leq \omega_{eng}^{\max} \\ T_{mot}^{\min} \leq T_{mot} \leq T_{mot}^{\max};\ \omega_{mot}^{\min} \leq \omega_{mot} \leq \omega_{mot}^{\max} \\ T_{gen}^{\min} \leq T_{gen} \leq T_{gen}^{\max};\ \omega_{gen}^{\min} \leq \omega_{gen} \leq \omega_{gen}^{\max} \end{aligned} \tag{5}$$

In (5), $.^{\min}$ and $.^{\max}$ denote the minimum and maximum bounds which may vary with respect to the operating conditions of the system.

A.1.2 Energy Storage System Model

The energy storage system (ESS) of the HEV we study in this paper Appendix includes a battery plus an ultracapacitor. By this combination, the power capabilities of the ESS is improved. Depending on the application, different topologies are proposed in the literature to combine batteries with ultracapacitors ([36] and [38]). In this dissertation, a parallel topology shown schematically in Figure 2 is used. In this topology, the battery and the ultracapacitor are placed in a direct parallel configuration to divide the total power demand from the ESS between them. Adding a DC-to-DC convertor to control the ratio of the power delivered from each element is a common practice as shown in Figure 2. In the following, a model of the energy storage system is derived. For this purpose, the following assumptions are made:

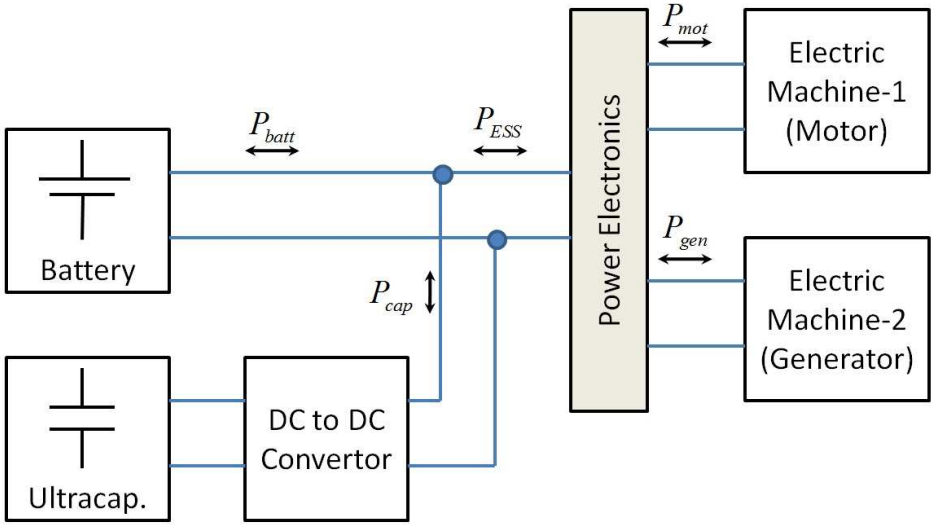

Figure 2: Schematic view of the energy storage system (ESS)

- Equivalent circuit models are used to model the battery and the ultracapacitor.
- The dynamics of the power electronics including the DC-to-DC convertor are ignored.
- The power loss in the power electronics is modeled by an efficiency factor.
- Positive power denotes discharge and negative power denotes charge.

In the electrical storage systems including batteries and ultracapacitors, the state of charge (SOC) is defined as the ratio between the stored charge in the storage and the charge capacity of the storage. Based on the assumptions we made above, the SOC dynamics of the battery and the ultracapacitor are modeled by ([13], [18]):

$$\frac{dSOC_{batt}}{dt} = -\frac{V_{oc} - \sqrt{V_{oc}^2 - 4P_{batt}R_{batt}}}{2C_{batt}R_{batt}} \tag{6}$$

$$\frac{dSOC_{cap}}{dt} = -\frac{SOC_{cap}V_{max} - \sqrt{(SOC_{cap}V_{max})^2 - 4P_{cap}R_{cap}}}{2R_{cap}C_{cap}V_{max}} \tag{7}$$

where SOC_{batt} and SOC_{cap} are the state of charge of the battery and the ultracapacitor, respectively; V_{oc}, R_{batt}, C_{batt}, and P_{batt} are the open-circuit voltage, internal resistance, capacity, and power of the battery, respectively; and V_{max}, R_{cap}, C_{cap}, and P_{cap} are the maximum rated voltage, internal resistance, capacitance, and power of the ultracapacitor, respectively. Since the conversion of the electrical power of the ESS is performed through the motor and generator, we can write

$$P_{ESS} = \begin{cases} \eta_{discharge}P_{mot/gen} & if\ P_{mot/gen} \geq 0 \\ \eta_{charge}P_{mot/gen} & if\ P_{mot/gen} < 0 \end{cases} \tag{8}$$

where

$$P_{mot/gen} = P_{mot} + P_{mot}^{loss} + P_{gen} + P_{gen}^{loss} \tag{9}$$

In equations (8) and (9), $\eta_{discharge}$ and η_{charge} are the energy storage efficiency in charge and discharge, respectively; $P_{mot} = T_{mot}\omega_{mot}$ is the motor power; $P_{gen} = T_{gen}\omega_{gen}$ is the generator power; and P_{motor}^{loss} and P_{gen}^{loss} are the motor and generator power losses, respectively. Denoting P_{batt} and P_{cap} as the battery and ultracapacitor powers, respectively, and r as the power splitting factor controlled by the power management

system, we can write

$$P_{ESS} = P_{batt} + P_{cap} \tag{10}$$

$$P_{batt} = rP_{ESS} \tag{11}$$

$$P_{cap} = (1-r)P_{ESS} \tag{12}$$

In addition to the ESS dynamics presented in (6) and (7) and equations (8-12), the following constraints are applied on the energy storage system:

$$\begin{aligned} SOC_{batt}^{\min} \leq SOC_{batt} \leq SOC_{batt}^{\max} \\ SOC_{cap}^{\min} \leq SOC_{cap} \leq SOC_{cap}^{\max} \\ P_{batt}^{\min} \leq P_{batt} \leq P_{batt}^{\max} \\ P_{cap}^{\min} \leq P_{cap} \leq P_{cap}^{\max} \end{aligned} \tag{13}$$

A.2 Control-Oriented Model

With the models presented in Sections A.1.1 and A.1.2, a control-oriented model of the HEV is derived in this section. For this purpose, we first present a few simplifications we made to reduce the number of the states in the system.

The first simplification is done based on the driveability constraint. The driveability constraint requires that the total torque at the wheels, which is the sum of the output torque of the power transmission system T_{out} and the friction brake torque T_{brake}, to be equal to the driver demand torque as

$$T_{out} + T_{brake} = T_{driver} \tag{14}$$

Assuming that this driveability constraint is enforced, the vehicle speed dynamics in (1) can be uniquely determined for an initial vehicle velocity and a driver torque profile. The vehicle speed dynamics are used to calculate the vehicle velocity V along the prediction horizon, but it does not add a state to the control-oriented model.

The second simplification is made by setting the inertial effects of the engine, motor, and generator,

i.e. $J_{eng}\frac{d\omega_{eng}}{dt}$, $J_{mot}\frac{d\omega_{mot}}{dt}$, and $J_{gen}\frac{d\omega_{gen}}{dt}$ to zero. With this setting and the driveability constraint in (14), the equations in (4) are simplified to the following equality constraints:

$$\begin{aligned} T_{gen} &= -\left(\frac{N_S}{N_S+N_R}\right) T_{eng} \\ T_{mot} &= \frac{T_{driver}-T_{brake}}{g_f} - \left(\frac{N_R}{N_S+N_R}\right) T_{eng} \end{aligned} \tag{15}$$

The third simplification is to ignore the dynamics of the engine and to calculate the engine fuel consumption from the engine empirical fuel flow map. This map is used to relate the fuel consumption rate $\dot{m}_f$ to the engine speed and torque as

$$\dot{m}_f = \varphi\left(\omega_{eng}, T_{eng}\right). \tag{16}$$

Based on the above simplifications and also the models presented in Sections A.1.1 and A.1.2, the control-oriented model of the HEV is represented as

$$\begin{aligned} \dot{x} &= f\left(x,u,v\right) \\ y &= g\left(x,u,v\right), \end{aligned} \tag{17}$$

where x, u, v, and y are the state, input, measured disturbance, and output vectors of the system, respectively. These vectors are defined by

$$x = \begin{bmatrix} SOC_{batt} \\ SOC_{cap} \end{bmatrix},\ u = \begin{bmatrix} T_{eng} \\ \omega_{eng} \\ r \\ T_{brake} \end{bmatrix},\ v = \begin{bmatrix} T_{driver} \\ V \end{bmatrix},\ y = \begin{bmatrix} \dot{m}_f \\ P_{batt} \\ P_{cap} \\ \omega_{gen} \\ T_{mot} \end{bmatrix} \tag{18}$$

In equation (17) f is defined by

$$f = \begin{bmatrix} f_1(x,u,v) \\ f_2(x,u,v) \end{bmatrix}, \tag{19}$$

where

$$f_1 = -\frac{V_{OC}-\sqrt{V_{OC}^2-4P_{batt}R_{batt}}}{2C_{batt}R_{batt}} \tag{20}$$

$$f_2 = -\frac{SOC_c V_{max} - \sqrt{(SOC_c V_{max})^2 - 4P_{cap}R_{cap}}}{2R_{cap}C_{cap}V_{max}} \tag{21}$$

A.3 The HEV Power Management Problem

The power (energy) management problem of an HEV is to find the control inputs of the system so that the total fuel consumption over an interval is minimized while the battery charge is sustained and the constraints of the system are enforced. Based on these objectives, the following quadratic cost function is defined

$$J = \int_t^{t+H} \|L(x,u,v)\|_2^2 \, d\tau \tag{22}$$

In (22), $||.||_2^2$ is the 2-norm operator, H is the prediction (optimization) horizon, and the vector L is defined by

$$\begin{aligned} L(x,u,v) = [&w_{batt} \cdot (SOC_b - SOC_b^r) \ , \ w_{cap} \cdot (SOC_c - SOC_c^r) \ , \\ &w_f \cdot \dot{m}_f \ , \ w_b \cdot T_{brake}]^T \end{aligned} \tag{23}$$

where SOC_{batt}^r and SOC_{cap}^r are the reference values for the battery and ultracapacitor state of charge, and w_{batt}, w_{cap}, w_f, and w_b are control weigh factors. With this cost function and the control-oriented model developed in Section A.2. the optimal power management problem of the HEV is defined as the following optimal control problem

$$\begin{aligned} &\min_{\substack{u(\tau) \\ t \le \tau \le t+H}} \quad J(u) \\ &\textit{subject to (17), (5), and (13)} \end{aligned} \tag{24}$$

In the next section, based on linear Model Predictive Control theory, a real-time solution to this problem is developed.

A.4 LTV MPC Power Management

Since the defined cost function in equation (22) is quadratic, a linear time-varying (LTV) MPC methodology is employed to solve the problem in real-time. An power management strategy based on LTV MPC was reported before by the authors to manage the power in a power-split HEV without ultracapacitor ([28], [26]). Here, a similar approach is employed to develop a power management controller for the HEV

with combined battery and ultracapacitor. In the following, this strategy is explained in details.

A.4.1 Linear Model Predictive Control (MPC)

The LTV MPC control strategy is based on the linear MPC theory which is briefly reviewed in this section. More details can be found in ([**?**, 52]). In the standard MPC, a finite-horizon quadratic cost function penalizes deviation of the output vector y from the corresponding reference vector r. In a general form, the associated optimization problem can be formulated in discrete-time as

$$\begin{aligned}\min_{\Delta U} J = \sum_{i=0}^{P-1} \|u(k+i|k) - u_{target}(k)\|^2_{w_i^u} + \\ \|\Delta u(k+i|k)\|^2_{w_i^{\Delta u}} + \|y(k+i+1|k) - r(k+i+1)\|^2_{w_{i+1}^y} + \rho_\varepsilon \varepsilon^2\end{aligned} \tag{25}$$

subject to

$$\begin{cases} x(k+i+1|k) = Ax(k+i|k) + B_u u(k+i|k) + B_v v(k+i|k) \\ y(k+i|k) = Cx(k+i|k) + D_v v(k+|k) \end{cases}$$

$$u_i^{\min} \leq u(k+i|k) \leq u_i^{\max}$$

$$\Delta u_i^{\min} \leq \Delta u(k+i|k) \leq \Delta u_i^{\max}$$

$$-\varepsilon + y_i^{\min} \leq y(k+i+1|k) \leq y_i^{\max} + \varepsilon$$

$$\Delta u(k+i|k) = 0 \; for \; i = M, ..., P$$

$$\varepsilon \geq 0$$

where P is the prediction horizon, M is the control horizon, $\Delta U = [\Delta u(k|k), ..., \Delta u(k+M-1|k)]^T$ is the sequence of input increments to be optimized, v is the vector of known inputs or measured disturbances, w_i^u, $w_i^{\Delta u}$, w_{i+1}^y and ρ_ε are the weighting factors at the i^{th} sample time, $x(k+i|k) \in R^n$ is the predicted state vector, $u(k+i|k) \in R^m$ is the vector of the manipulated variables, $y(k+i|k)$ is the vector of the predicted outputs, $r(k)$ is the vector of the output references, $u_{target}(k)$ is the vector of the input steady-state references, and ε is the softening (slack) variable used to avoid infeasibility. Using the discrete model of the system, the

outputs over a finite future horizon are predicted by

$$\begin{aligned} & y(k+i+1|k) = C[A^{i+1}x(k) + \\ & \sum_{l=0}^{i} A^{i}B_u \left(u(k-1) + \sum_{j=0}^{l} \Delta u(k+j|k) \right) + \\ & B_v v(k+l|k)] + D_v v(k). \end{aligned} \tag{26}$$

Substituting predicted trajectories of the outputs into the performance index J and output constraints, the optimization problem can be formulated as a Quadratic Program (QP) with linear inequality constraints,

$$[\Delta U^*, \varepsilon] = \arg\min_{\Delta U, \varepsilon} \frac{1}{2}\Delta U^T H \Delta U + F^T \Delta U \tag{27}$$

subject to

$$G_u \Delta U + G_\varepsilon \varepsilon \leq W$$

where H, F, G_u, G_ε, and W are constant matrices and are function of references, measured inputs, input targets, the last control input, and states value at current sampling time. After solving QP problem (27) and obtaining the optimal input sequence ΔU^*, the control input to the plant is obtained by

$$u^*(k) = u(k-1) + \Delta u^*(k|k). \tag{28}$$

A.4.2 The Power Management Strategy

In order to apply the linear MPC to solve the power management problem in (24), the nonlinear control-oriented model is linearized around the current operating conditions and the control inputs are obtained by applying the linear MPC to the linearized control-oriented model. Therefore, at each control sampling step, the following steps are proposed for the power management of the HEV:

- Measurement/estimation of system states including SOC_{batt} and SOC_{cap}.
- Prediction of the torque demand and vehicle speed (measured disturbances) over the prediction horizon.
- Linearization of the nonlinear control-oriented model presented in Section A.2 around the current operating conditions as

$$\begin{cases} \dot{x} = \tilde{A}x + \tilde{B}_u u + \tilde{B}_v v + \tilde{F} \\ y = \tilde{C}x + \tilde{D}_u u + \tilde{D}_v v + \tilde{G} \end{cases} \tag{29}$$

where

$$\begin{aligned}
\tilde{A} &= \left(\frac{\partial f}{\partial x}\right)_{(x_0,u_0,v_0)}; \tilde{B}_u = \left(\frac{\partial f}{\partial u}\right)_{(x_0,u_0,v_0)} \\
\tilde{B}_v &= \left(\frac{\partial f}{\partial v}\right)_{(x_0,u_0,v_0)}; \tilde{C} = \left(\frac{\partial g}{\partial x}\right)_{(x_0,u_0,v_0)} \\
\tilde{D}_u &= \left(\frac{\partial g}{\partial u}\right)_{(x_0,u_0,v_0)}; \tilde{D}_v = \left(\frac{\partial g}{\partial v}\right)_{(x_0,u_0,v_0)} \\
\tilde{F} &= f(x_0,u_0,v_0) - \tilde{A}x_0 - \tilde{B}_u u_0 - \tilde{B}_v v_0 \\
\tilde{G} &= g(x_0,u_0,v_0) - \tilde{C}x_0 - \tilde{D}_u u_0 - \tilde{D}_v v_0
\end{aligned} \tag{30}$$

x_0, u_0 and v_0 are the current values of the state, input and measured disturbance vectors, respectively. To remove direct injection of the control inputs in the output equations in accordance to the MPC formulation presented in section A.4.1, the linearized system can be augmented with fast filters ([28]).

- Application of the linear MPC explained in the previous section to the resulting discrete-time model to calculate the optimal control input as

$$u^*(k) = \begin{bmatrix} T^*_{eng}(k) \\ \omega^*_{eng}(k) \\ r^*(k) \\ T^*_{brake}(k) \end{bmatrix} \tag{31}$$

The control input $u^*(k)$ is applied and held constant over the control sampling interval and the above steps with the updated state feedbacks from the HEV are repeated at the next control sampling step in the framework of the Model Predictive Control.

A.5 Simulation Conditions

In order to analyze the performance of the developed power management strategy, a closed-loop model of a power-split HEV was developed in MATLAB Simulink. The block diagram of the model is shown in Figure 3.

The driver model block in Figure 3 consists of a PI controller which calculates the required torque by the driver T_{driver} to follow a desired speed profile or driving cycle. The power management block in Figure 3 receives T_{driver} and feedbacks from a high-fidelity model of the HEV and the set points to the computation block based on the LTV MPC strategy developed in Section A.4. The set points to the computation blocks

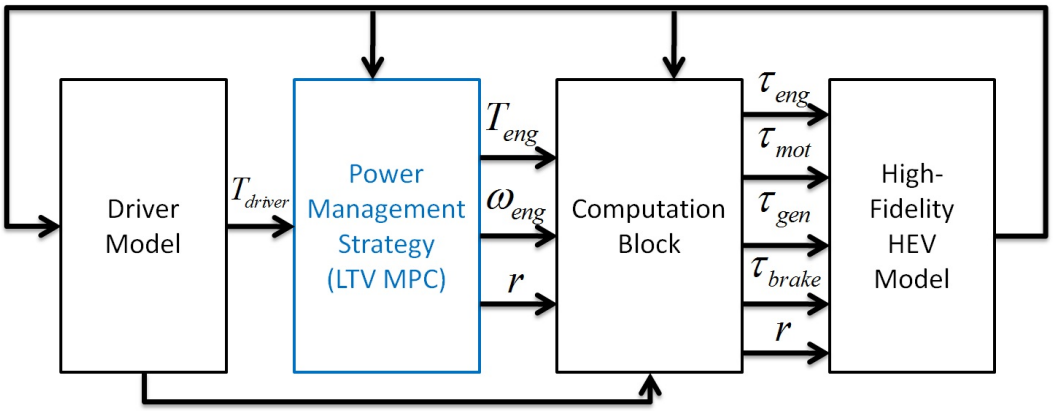

Figure 3: The closed-loop model in Simulink

Table 2: The characteristics of a Panasonic ultracapacitor module

Rated Voltage (V)	Capacitance (F)	Resistance (Ω)	Weight (gram)
2.5	1200	1	340

are the engine torque T_{eng}, engine speed ω_{eng}, frication brake torque T_{brake}, and the power splitting factor r. In the computation block, there is a PI controller which calculates the required generator torque T_{gen} in order to follow the engine speed set point with delivering T_{driver}. With the generator torque, the motor torque T_{mot} and the frication brake torque T_{brake} are computed from the models presented in Section (A.1.1). The driver and the computation blocks are extracted from a model of Toyota Prius hybrid in Powertrain System Analysis Toolkit (PSAT) ([31]).

In the block diagram of Figure 3, a high-fidelity model of Toyota Prius hybrid developed in PSAT software is used to model the HEV. The Toyota Prius has the power-split configuration discussed here. In the energy storage system of the model, we added the ultracapacitor model discussed in Section A.1.2. This capacitor is designed so that its maximum charge capacity becomes one tenth of the battery capacity. This means that a relatively small ultracapacitor is combined with the battery[2]. Based on this assumption, 100 modules of an ultracapacitor from Panasonic are arranged in series. The specifications of the ultracapacitor module is presented in Table 2.

In the power management block of Figure 3, the power management strategy presented in Section A.4 is performed in discrete time with control sampling interval T_s equal to 1 second. The prediction and control horizons H are set to 5 steps of the control sampling interval. The reference values for the states, SOC^r_{batt} and SOC^r_{cap}, are set to 0.7 and 0.8, respectively and the constraints on the states are set to $0.6 \leq SOC_{batt} \leq 0.9$

[2]Optimal sizing of the battery with an ultracapacitor is an important subject which is out of the scope of this study

and $0.6 \leq SOC_{cap} \leq 0.8$. The weight values in the cost function (22) are set to be tuned with the following rules ([7]):

In the propelling operation mode where $T_{driver} \geq 0$

if $SOC_{batt} \leq SOC^r_{batt}$

if $|SOC_{batt} - SOC^r_{batt}| \leq 0.1$

$w_{batt} = 1, w_{cap} = 0, w_f = 100 \cdot e^{(18 \cdot |SOC_{batt} - SOC^r_{batt}|)}, w_b = 1$

elseif $|SOC_{batt} - SOC^r_{batt}| > 0.1$

$w_{SOC_{batt}} = 1, w_{SOC_{cap}} = 0, w_f = 100, w_b = 1$

elseif $SOC_{batt} > SOC^r_{batt}$

$w_{batt} = 0, w_{cap} = 0, w_f = 500, w_b = 1$

In the braking operation mode where $T_{driver} < 0$

$w_{batt} = 1, w_{cap} = 10, w_f = 5000, w_b = 0$

Based on the above weight selection, in the HEV propelling operation, where the demand torque by the deriver is positive $T_{driver} \geq 0$, the weight on the ultracapacitor w_{cap} is set to zero and the power management system is allowed to use the energy in the ultracapacitor as long as SOC_{cap} constraints are satisfied. Also in this mode, when SOC_{batt} is less than its reference value SOC^r_{batt}, the weight on the fuel consumption is set to increase exponentially from 10 until SOC_{batt} becomes less than 0.6 where the fuel consumption weight is fixed at 100. However, when SOC_{batt} becomes greater than its reference value SOC^r_{batt} , a large weight is put on the fuel consumption and the weight on the battery is removed to increase the battery usage. In the braking operation mode, since the ultracapacitor can be charged faster and with higher power density, a larger weight is defined on the SOC_{cap} deviations from its reference value SOC^r_{cap} than the battery one. The fuel consumption rate and the constraints on the engine, motor, and generator are obtained from the PSAT model. In Figure 2.6, the fuel consumption rate of the model $\dot{m}_f$ and the engine maximum torque T^{max}_{eng} are presented as an illustration. Finally, since we do not want to consider any preview information in the power management of the HEV, the future driver torque profile is assumed to be exponentially decaying along the prediction horizon as

$$T_{driver}(k+i) = T_{driver}(k) e^{\left(\frac{-iT_s}{\tau_d}\right)} \qquad i = 1,\ 2,\ \cdots,\ P \tag{32}$$

where $T_{driver}(k)$ is the known value of the driver torque demand at the beginning of the prediction horizon and

τ_d determines the decay rate. Due to frequent variation of torque demand in a driving cycle and the integrative nature of the system dynamics with respect to the torque, assumption of a decaying torque demand leads to a stable numerical calculation of the MPC. However, constant-torque assumption is also another option if preview information is not provided ([10]). With the above torque profile and by numerical integration of the vehicle longitudinal dynamics in equation (1) over the future time horizon, the future velocity profile is predicted in the power management block.

A.6 Simulation Results

In this section, the closed-loop model with the simulation conditions presented in Section A.5 is simulated over different driving cycles with vehicle speed profiles shown in Figure 4. Considering the high power but low energy density specification of the ultracapacitor, it is important to analyze the performance of the power management strategy over driving cycles with different speed transients. Also, to compare the performance of the strategy over the HEV with and without ultracapacitor, a power management strategy based on LTV MPC developed by the authors in reference ([28]) for an HEV without ultracapacitor is used. We tuned the LTV MPC strategy of the HEV without ultracapacitor with the same parameters discussed in Section A.5.

To compare the results over a driving cycle, we calculate the charge-balanced fuel economy and also the averaged C-rate of the battery in charge and discharge modes of operation. The charge-balanced fuel economy which is also called equivalent fuel economy is obtained by repeating simulations over a driving cycle until the initial and final SOC's become equal. This fuel economy is reported to compare the results.

The battery C-rate is another parameter used to evaluate the power management performance. We use the following definition of the C-rate based on the battery power from reference ([35])

$$C_p = \frac{P_{batt}}{V_{oc} \cdot C_{batt}} \tag{33}$$

This parameter describes the charge/discharge intensity of a battery as a function of battery power. Generally, cycling a battery at higher C-rates reduces the life of a battery ([36]); Reduced C-rate is expected by combining the battery with the ultracapacitor. In this study, the averaged C_p in charge and discharge are reported to compare the results. The averaged C-rates in charge and discharge over a driving cycle with driving period

Table 3: The power management performance over UDDS driving cycle

UDDS driving cycle			
ESS	$FuelEconomy(mpg)$	$\bar{C}_{p,d}$	$\bar{C}_{p,c}$
with ultracap.	79.83	0.4953	-0.5546
without ultracap.	76.81	1.1760	-1.3290

equal to t_f are respectively obtained from

$$\bar{C}_{p,c} = \frac{\int_0^{t_f} C_p(t)\,dt}{t_f} \quad if \quad C_p(t) < 0 \tag{34}$$

$$\bar{C}_{p,d} = \frac{\int_0^{t_f} C_p(t)\,dt}{t_f} \quad if \quad C_p(t) \geq 0 \tag{35}$$

A.6.1 Power Management Performance over the UDDS Driving Cycle with and without Ultracapacitor

In order to compare the performance of the power management strategy over an urban driving cycle with frequent speed transients and stop/start events, the closed-loop model is simulated over the UDDS standard driving cycle and the results are presented in this section. Figure 5 shows the time histories of the vehicle speed V, battery state of charge SOC_{batt}, ultracapacitor state of charge SOC_{cap}, battery power P_{batt}, and motor, generator, and engine speeds and torques. As it is observed from the figure, vehicle speed follows the driving cycle and all the constrains of the system are enforced over time. Furthermore in Figure 6, the time history, statistics specifications, and the histogram of the battery C-rate in charge and discharge are shown. To compare the results with the HEV without the ultracapacitor, the same simulation scenario is performed over the model of the HEV without the ultracapacitor and the results are presented in Figures 7 and 8. Furthermore, the charge-balanced fuel economy and the averaged battery C-rate in charge and discharge for both cases are presented in Table 3. From these simulation results, it is observed that the C-rate of the battery in both charge and discharge are improved noticeably. Also, for this driving cycle, the fuel economy is also improved even with the additional weight of the ultracapacitor.

Table 4: The power management performance over Highway FET driving cycle

Highway FET driving cycle			
ESS	$FuelEconomy(mpg)$	$\bar{C}_{p,d}$	$\bar{C}_{p,c}$
with ultracap.	69.07	0.7659	-0.8490
without ultracap.	69.31	1.052	-1.1840

A.6.2 Power Management Performance over the Highway FET Driving Cycle with and without Ultracapacitor

In order to compare the performance of the power management strategy over a highway driving cycle with less speed transients, the closed-loop model is simulated over the Highway FET standard driving cycle and the results are presented in this section. Figure 9 shows the time histories of the vehicle speed V, battery state of charge SOC_{batt}, ultracapacitor state of charge SOC_{cap}, battery power P_{batt}, and motor, generator, and engine speeds and torques. As it is observed from the Figure 9, vehicle speed follows the driving cycle and all the constrains of the system are enforced over time. Furthermore in Figure 10, the time history, statistics specifications, and the histogram of the battery C-rate in charge and discharge mode over the cycle period is shown. To compare the results with the case without the ultracapacitor, the same simulation scenario is performed over the model of the HEV without the ultracapacitor and the results are presented in Figures 11 and 12. With these simulation results, the charge-balanced fuel economy and the averaged battery C-rate in charge and discharge are calculated and the results are presented in Table 4. From these simulation results, it is observed that the C-rate of the battery in both charge and discharge are improved. However, the improvement is not as much as the results over the urban driving cycle. This is because of the fact that ultracapacitors have high power density but low energy density. Therefore, in driving cycles with less speed transients and fewer stop/start events, the ultracapacitor is depleted most of the time and can not assist the battery to drive the vehicle. Also, due to the additional weight of the ultracapacitor, the fuel economy is not improved, noticeably.

A.6.3 Power Management Performance Comparison over Multiple Driving Cycles

In this section, the power management strategy over the power-split HEV with and without ultracapacitor are simulated over more standard driving cycles. The charge-balanced fuel economy and the battery averaged C-rate in charge and discharge are presented in Table 5. It is observed that the battery C-rate is improved with the ultracapacitor consistently. However, the C-rate improvement in the cycles with more speed transients and stop/start events is more than the ones with less speed transients and fewer stop/start.

Table 5: The LTV-MPC power management performance over multiple driving cycles

SC03 driving cycle			
ESS	$FuelEconomy(mpg)$	$\bar{C}_{p,d}$	$\bar{C}_{p,c}$
with ultracap.	73.77	0.5350	-0.6362
without ultracap.	71.82	2.0749	-2.5447
US06 driving cycle			
ESS	$FuelEconomy(mpg)$	$\bar{C}_{p,d}$	$\bar{C}_{p,c}$
with ultracap.	43.64	1.7071	-2.5822
without ultracap.	43.51	2.8500	-4.4492
NY driving cycle			
ESS	$FuelEconomy(mpg)$	$\bar{C}_{p,d}$	$\bar{C}_{p,c}$
with ultracap.	63.94	0.2597	-0.3050
without ultracap.	63.28	0.7996	-0.9196
JC08 driving cycle			
ESS	$FuelEconomy(mpg)$	$\bar{C}_{p,d}$	$\bar{C}_{p,c}$
with ultracap.	88.49	0.2859	-0.3136
without ultracap.	86.16	0.8678	-0.9544
EUDC driving cycle			
ESS	$FuelEconomy(mpg)$	$\bar{C}_{p,d}$	$\bar{C}_{p,c}$
with ultracap.	74.79	0.5128	-0.5740
without ultracap.	74.76	0.9105	-1.0196

As we discussed in the last section, this is due to the fact that the ultracapacitors have low energy density and in the cycles with less speed transients, they are depleted quickly and are not charged frequently to assist the battery. Also, from the fuel economy results presented in Table 5, it is observed that for driving cycles with less speed transients, the fuel economy is not improved noticeably due to the additional weight of the ultracapacitor.

A.7 Conclusions of the Appendix

In this study, a combination of an ultracapacitor and a battery as the energy storage unit of a power-split HEV was analyzed. First, the plant model of a power-split HEV with an ultracapacitor and battery was developed. Then, based on the control objectives to minimize both the fuel consumption and also cycling the battery at high peak powers, an online supervisory controller based on model predictive control was developed. The closed-loop simulation results show that the controller is able to manage the energy such that all control objectives and constraints are satisfied over a finite prediction horizon. It was observed that by combining an ultracapacitor with a battery, cycling the battery at high C-rates (peak powers) is reduced significantly especially over driving cycles with more stop and start durations. The improved C-rate of the battery are expected to extend battery life and reliability.

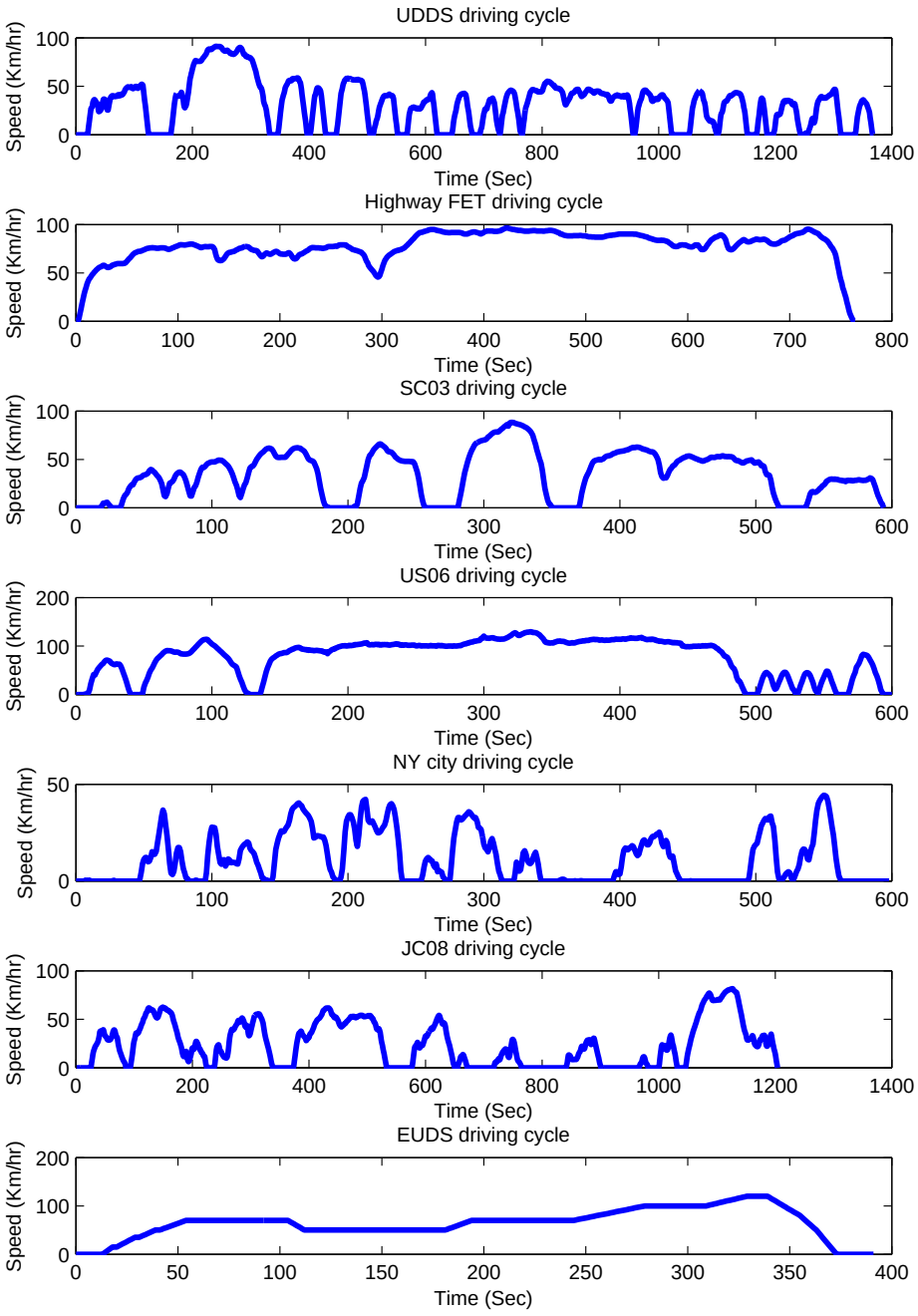

Figure 4: Standard driving cycles

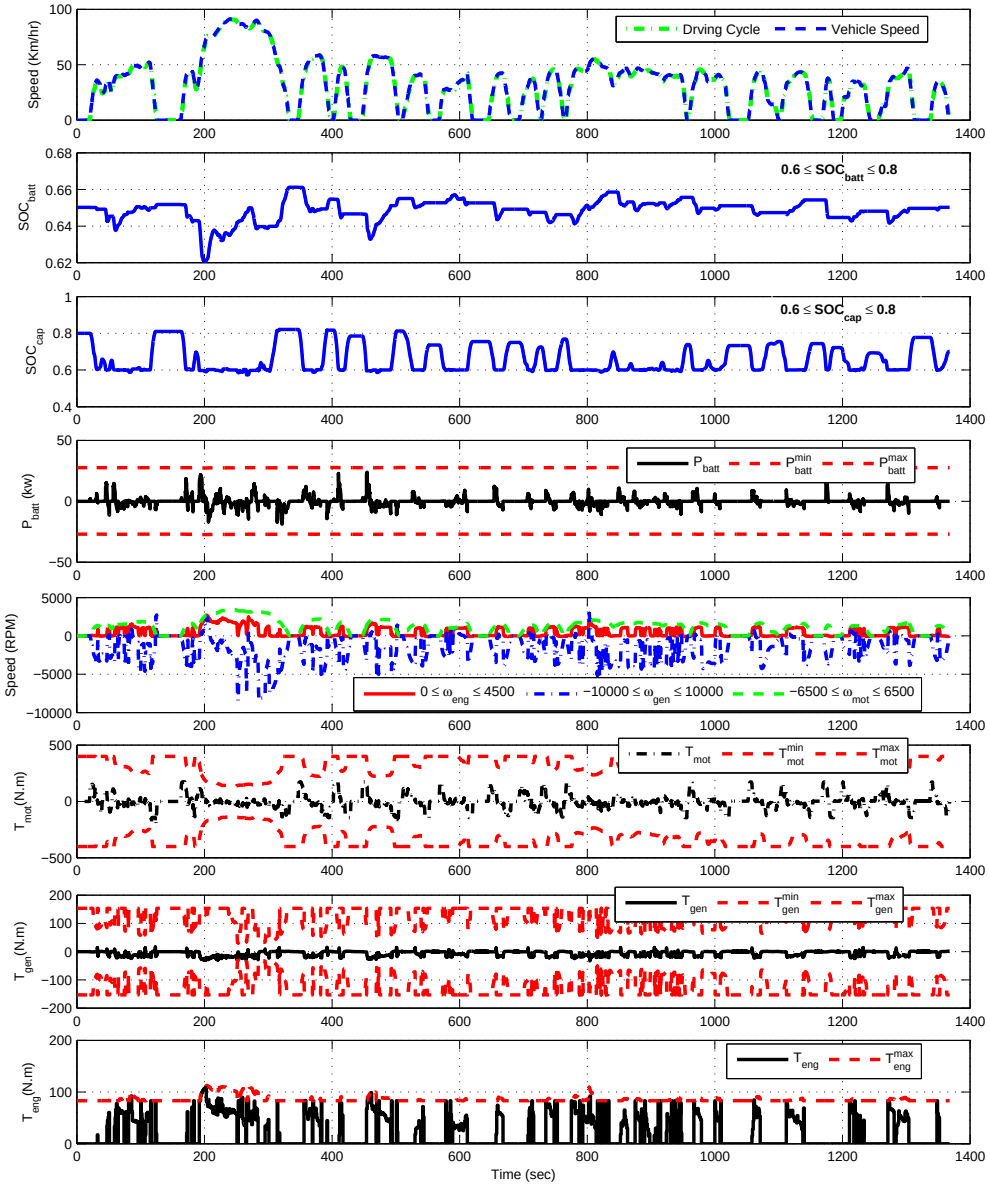

Figure 5: Simulation results over the urban driving cycle for the ESS with the Ultracapacitor

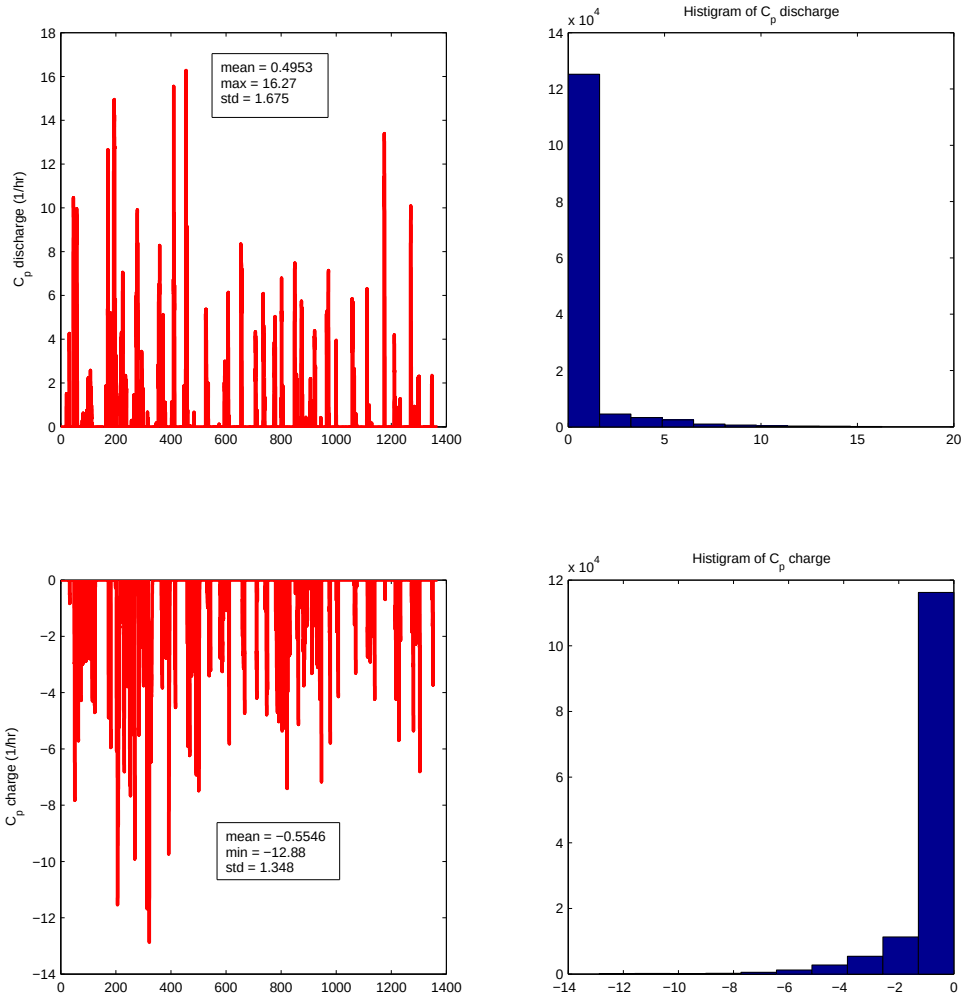

Figure 6: C-rate results over the urban driving cycle for the ESS with the Ultracapacitor

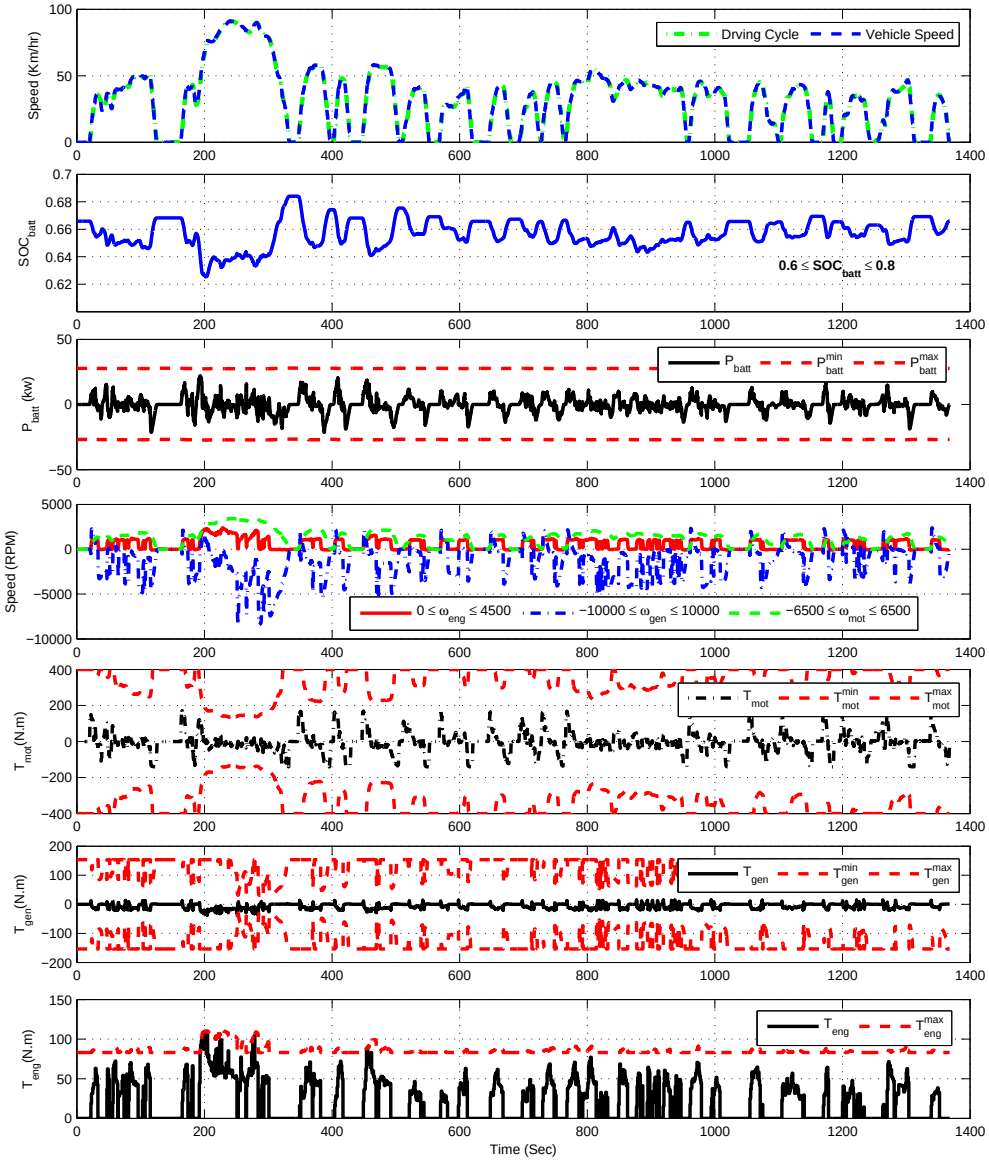

Figure 7: Simulation results over the urban driving cycle for the ESS without the Ultracapacitor

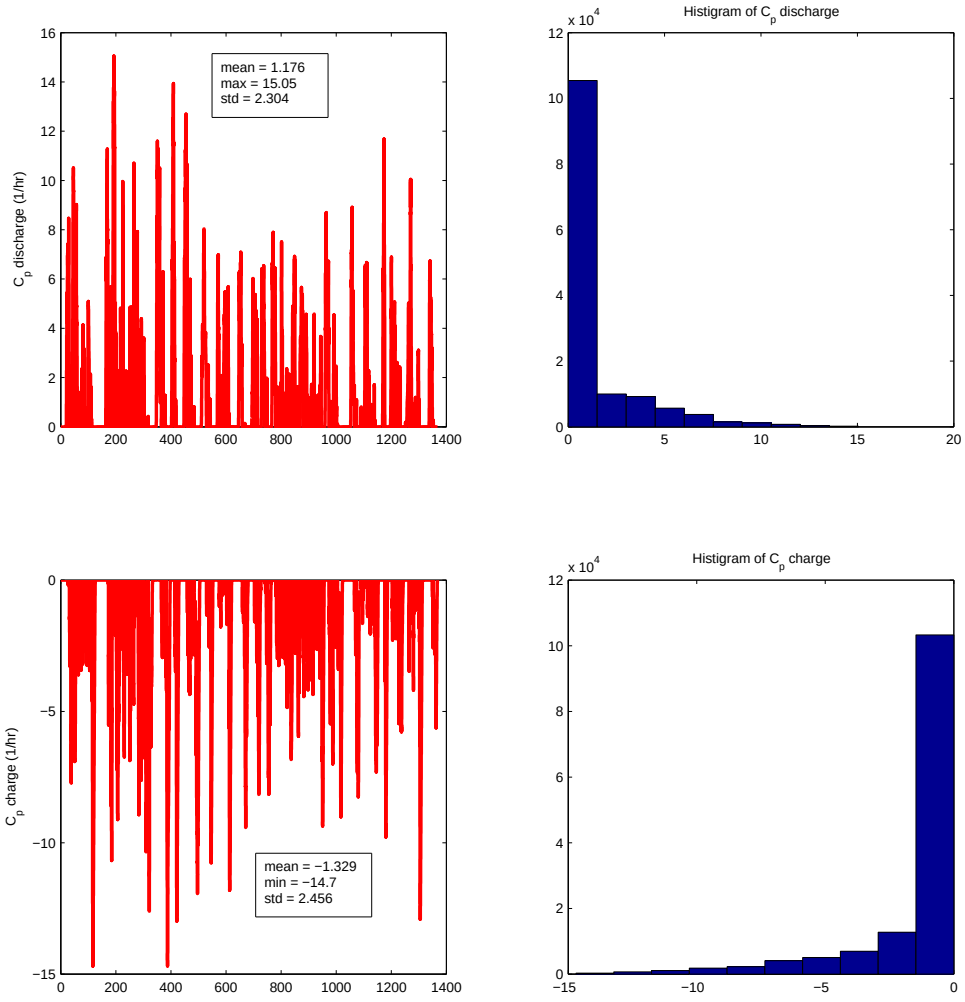

Figure 8: C-rate results over the urban driving cycle for the ESS without the Ultracapacitor

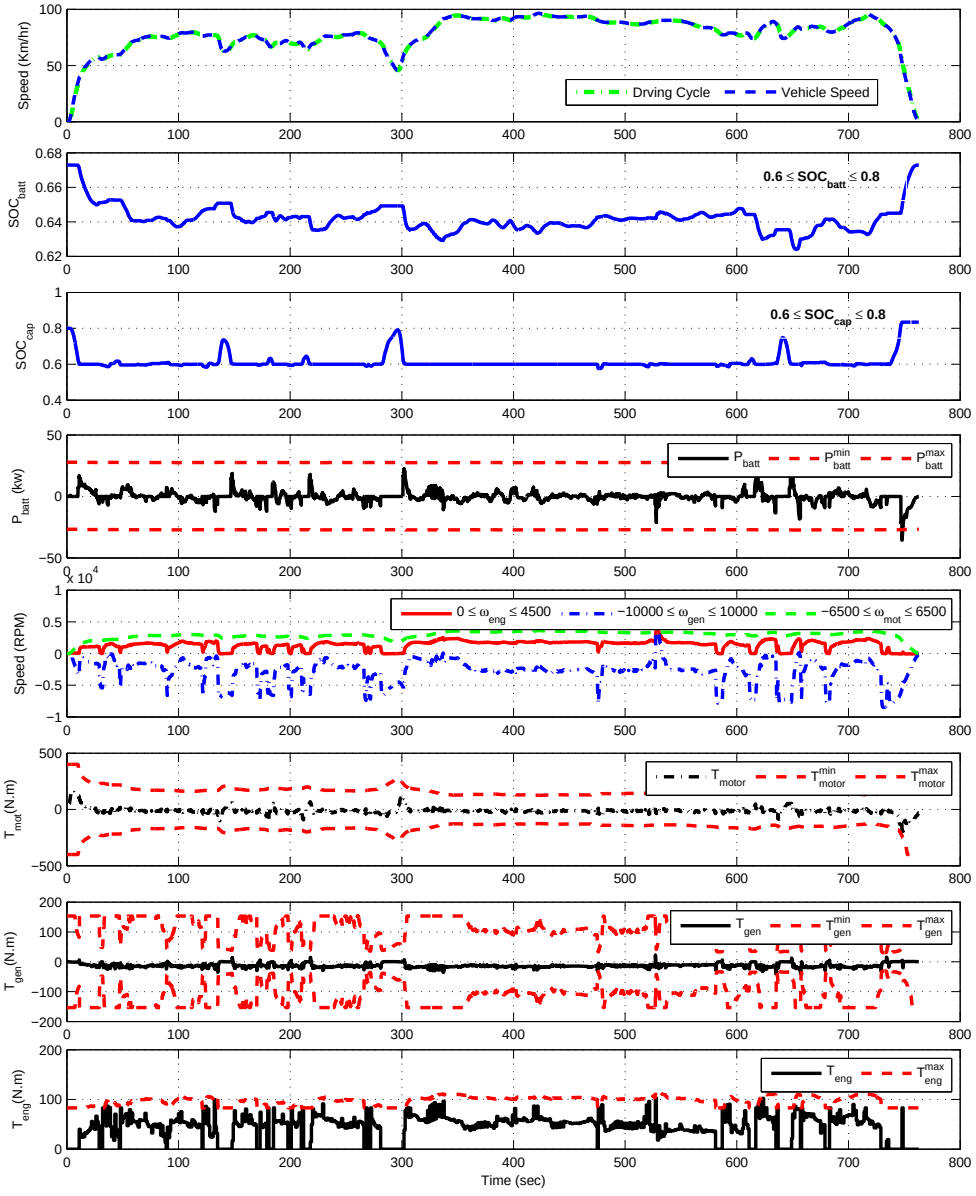

Figure 9: Simulation results over the Highway driving cycle for the ESS with the Ultracapacitor

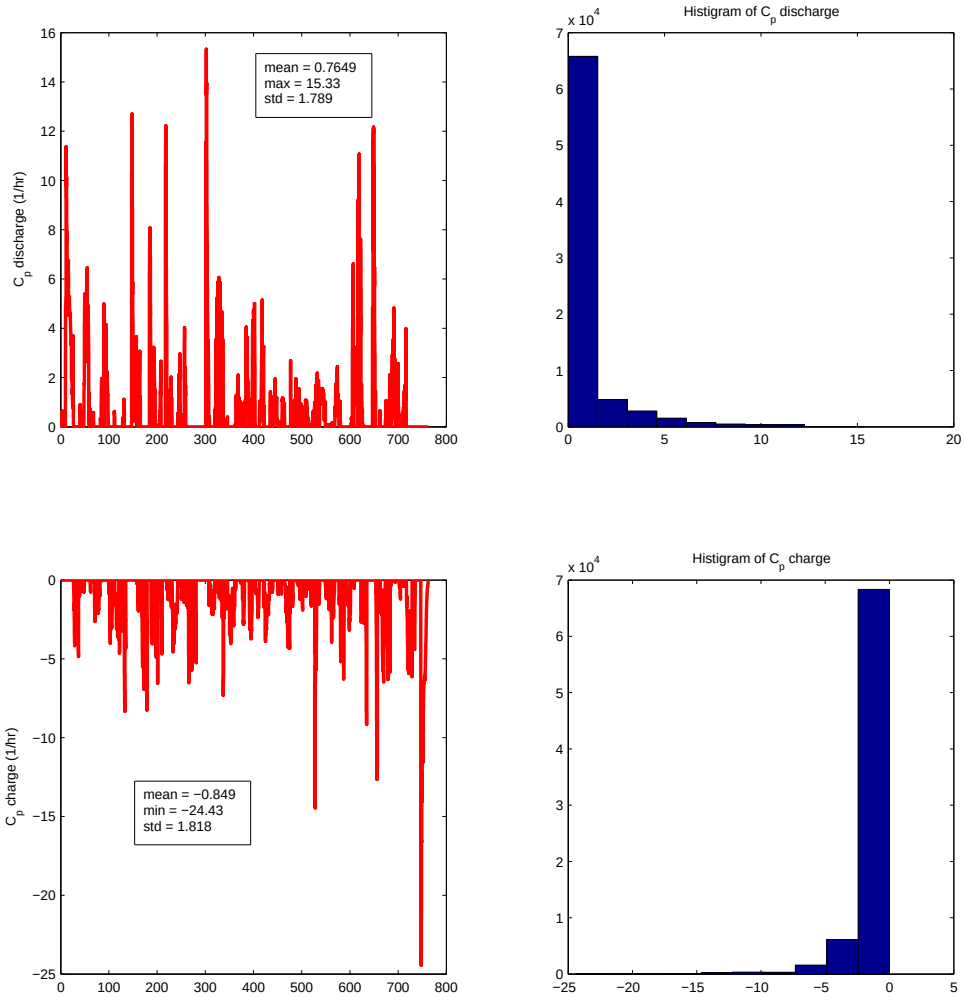

Figure 10: C-rate results over the Highway driving cycle for the ESS with the Ultracapacitor

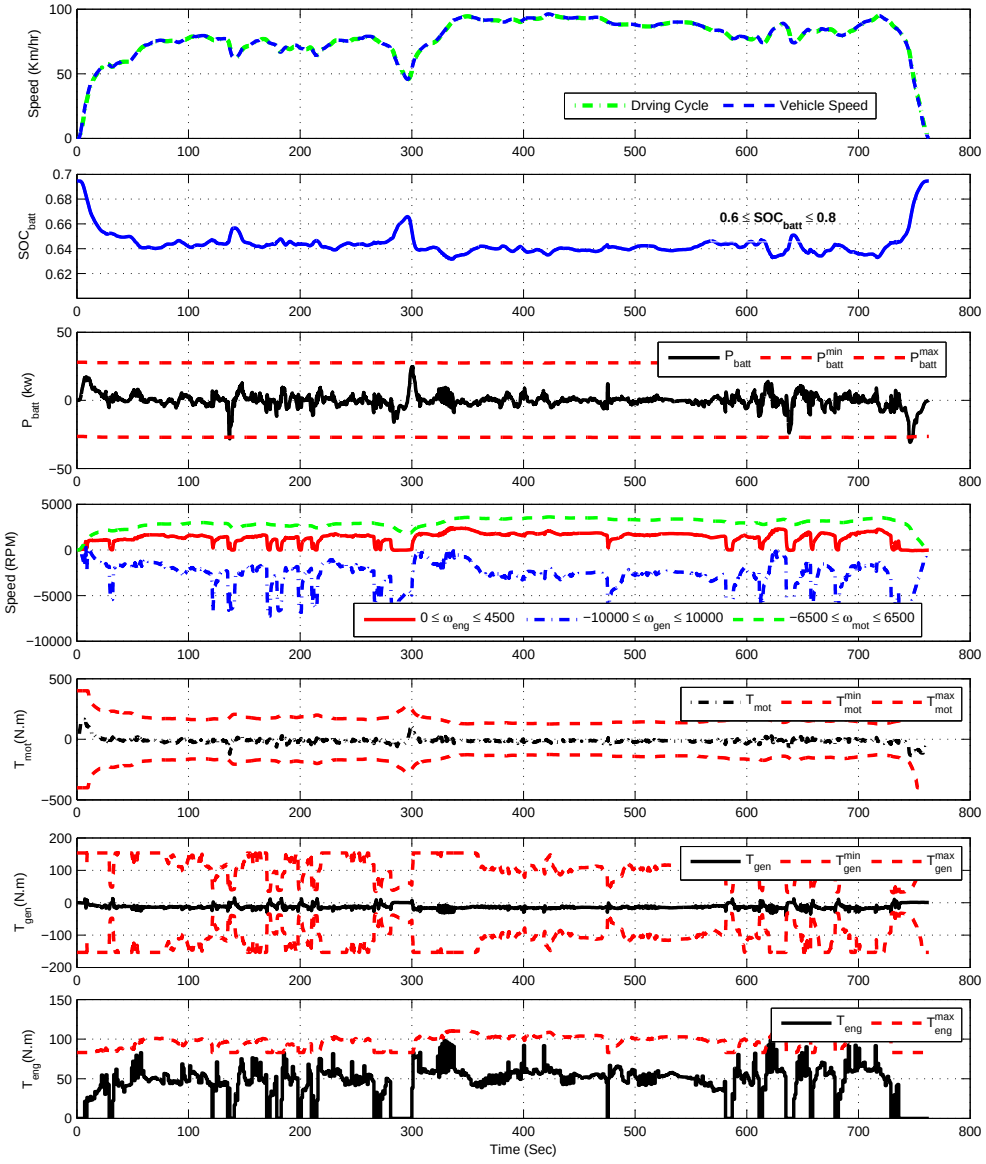

Figure 11: Simulation results over the Highway driving cycle for the ESS without the Ultracapacitor

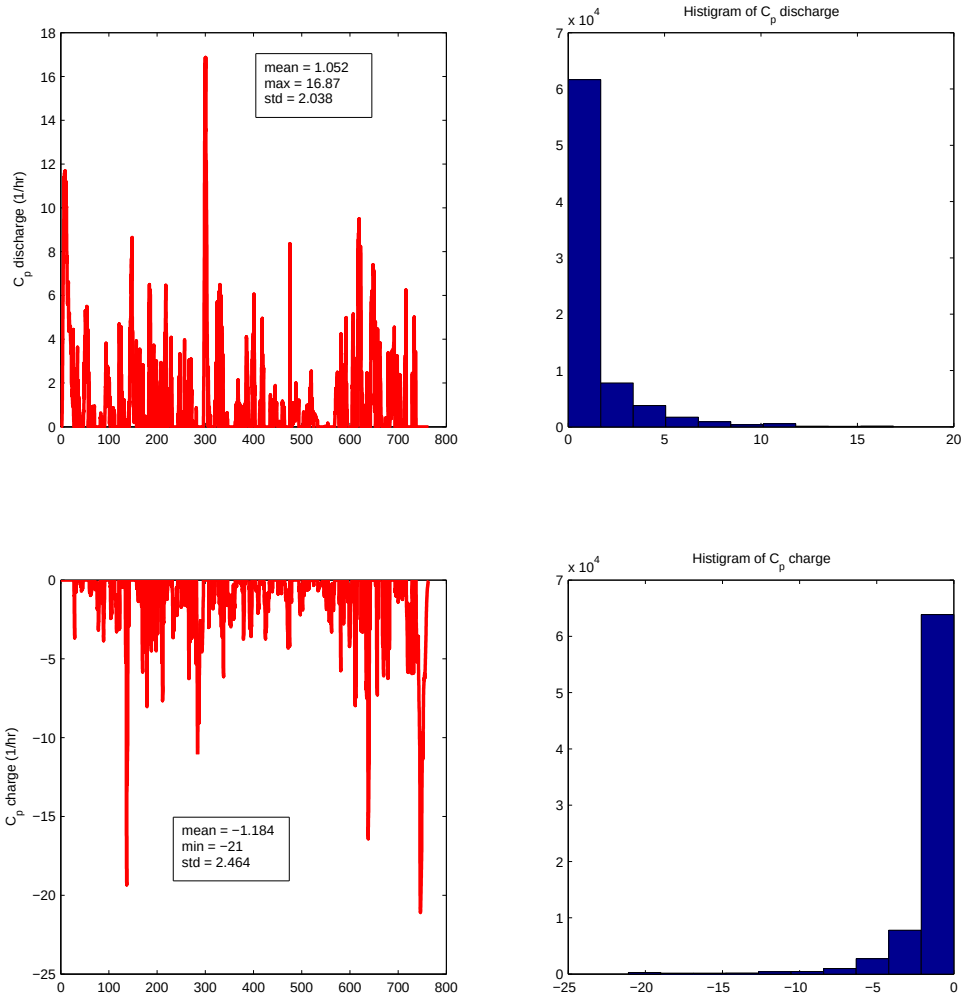

Figure 12: C-rate results over the Highway driving cycle for the ESS without the Ultracapacitor

Appendix B Minimum Principle and the HEV Power Management Problem

The necessary conditions for the optimality can be obtained by applying the variational approach (Pontryagin minimum principle [25]) to the HEV power management problem with the objective of fuel minimization. The Hamiltonian for this problem is defined,

$$H(SOC(\tau),u(\tau),p(\tau),\tau) = \dot{m}_f(u(\tau)) + p(\tau)[f^c(u(\tau),\tau)] \tag{36}$$

where $\tau \in [t,\ t_f]$. Using this notation, the necessary conditions for the optimality from current time t and an initial value of $SOC(t)$ to the end of the drive cycle are,

$$\begin{aligned}
&H = \dot{m}_f(u(\tau)) + p(\tau)[f^c(u(\tau),\tau)] = H(u(\tau),p(\tau),\tau)\\
&S\dot{O}C^*(\tau) = \tfrac{\partial H}{\partial p}(u^*(\tau),p^*(\tau),\tau)\\
&\dot{p}^*(\tau) = -\tfrac{\partial H}{\partial SOC}(u^*(\tau),p^*(\tau),\tau) = 0\\
&H(SOC^*(\tau),u^*(\tau),p^*(\tau),\tau) \le H(SOC^*(\tau),u(\tau),p^*(\tau),\tau)
\end{aligned} \tag{37}$$

These conditions need to be satisfied for all admissible $u(\tau)$ in $t \le \tau \le t_f$. Since $\frac{\partial H}{\partial SOC} = 0$, we have $p^*(\tau) = \lambda(SOC(t),t)$. The relationship between HJB equations and the minimum principle implies that [25],

$$p^*(\tau) = \frac{\partial J^*(SOC^*(\tau),\tau)}{\partial SOC} = \frac{\partial J^*(SOC(t),t)}{\partial SOC} = \lambda(SOC(t),t) \tag{38}$$

Thus for an initial time, t, and a state of the charge, $SOC(t)$, by replacing $\tau = t + \Delta t$ we get

$$\frac{\partial J^*}{\partial SOC}(SOC^*(t+\Delta t),t+\Delta t) = \frac{\partial J^*}{\partial SOC}(SOC(t),t) \tag{39}$$

where $\frac{\partial J^*}{\partial SOC}(SOC(t),t) = \lambda(SOC(t),t)$. Notice that $SOC^*(\tau)$ is derived by relaxing the constraints which are enforced online by MPC along the finite prediction horizon.

Appendix C Relationship between MPC and Equivalent Consumption Minimization Strategy (ECMS)

In the Equivalent Consumption Minimization Strategy (ECMS) [46, 53] for the power management of an HEV, an instantaneous cost function is defined by,

$$J = \dot{m}_f(t) + S \cdot \frac{Pbatt(t)}{H_f} \tag{40}$$

where S is the ECMS factor. In Appendix B, the Hamiltonian is,

$$H = \dot{m}_f(u(t)) + p(t)S\dot{O}C(t) \tag{41}$$

According to the Pontryagin's Minimum Principle, [25],

$$J = H(SOC(t), u(t), p^*(t), t) = \dot{m}_f(u(t)) + p^*(t)S\dot{O}C(t) \tag{42}$$

By considering the dynamics of the battery and ignoring the power losses due to the internal resistance,

$$S\dot{O}C(t) \cong -\frac{P_{batt}}{C_{batt}V_{oc}}. \tag{43}$$

Hence it can be implied that,

$$p^*(t) = \left(\frac{C_{batt}V_{oc}}{H_f}\right) \cdot S \tag{44}$$

From the relationship between HJB equation and the minimum principle ([25]), it is obtained that,

$$\lambda(SOC(t), t) = p^*(t) = \left(\frac{C_{batt}V_{oc}}{H_f}\right) \cdot S \tag{45}$$

Bibliography

[1] modeFRONTIER version 4.2.1 Documentation. *see URL http://www.esteco.com*.

[2] Kukhyun Ahn and P Y Papalambros. Engine optimal operation lines for power-split hybrid electric vehicles. *Journal of Automobile Engineering*, 223 (9), 2009.

[3] D. Ambuhl and L. Guzzella. Predictive reference signal generator for hybrid electric vehicles. *IEEE Transactions on Vehicular Technology*, 58 (9):4730 – 4740, 2009.

[4] P. Falcone, F. Borrelli, H. E. Tseng, J. Asgari and D. Hrovat. Linear time-varying model predictive control and its application to active steering systems: Stability analysis and experimental validation. *International Journal of Robust and Nonlinear Control*, 18(8):1172–1177, 2004.

[5] A. Baisden and A. Emadi. Advisor-based model of a battery and an ultra-capacitor energy source for hybrid electric vehicles. *IEEE Transactions on Vehicular Technology*, 53(1):199–205, 2004.

[6] S. Teleke, M. Baran, S. Bhattacharya and A. Q. Huang. Optimal control of battery energy storage for wind farm dispatching. *IEEE Transactions on Energy Conversion*, 25(3):787–794, 2010.

[7] H. Borhan and A. Vahidi. Model predictive control of a power-split hybrid electric vehicle with combined battery and ultracapacitor energy storage. *American Control Conference*, pages 5031–5036, 2010.

[8] A. F. Burke. Batteries and ultracapacitors for electric, hybrid, and fuel cell vehicles. *Proceedings of the IEEE*, 95(4):806 – 820, 2007.

[9] G. Ripaccioli, A. Bemporad, F. Assadian, C. Dextreit, S. Di Cairano and I. V. Kolmanovsky. Hybrid modeling, identification, and predictive control: An application to hybrid electric vehicle energy management. *Lecture Notes in Computer Science*, 5469:321–335, 2009.

[10] H. Borhan, W. Liang, A. Vahidi, A. Phillips, M. Kuang, S. Di Cairano, and R. McGee. Nonlinear model predictive control of a power-split hybrid electric vehicle: Influence of inclusion of powertrain dynamics. *ASME Dynamic Systems and Control conference, Arlington, VA, USA*, 2011.

[11] Z. M. Salameh, M. A. Casacca and W. A. Lynch. A mathematical model for lead-acid batteries. *IEEE Transactions on Energy Conversion*, 7(1):93–98, 1992.

[12] F. U. Syed, M. L. Kuang, J. Czubay and H. Ying. Derivation and experimental validation of a power-split hybrid electric vehicle model. *IEEE Transactions on Control Systems Technology*, 54(6):1731–1747, 2006.

[13] A. Vahidi D. Rotenberg and I. Kolmanovsky. Ultracapacitor assisted powertrains: Modeling, control, sizing, and the impact on fuel economy. *American Control Conference*, pages 981–987, 2008.

[14] U.S. Energy Information Administrations (EIA). Annual energy review. *Technical report (http://www.eia.gov/aer)*, 2009.

[15] J. Eyer and G. Corey. Energy storage for the electricity grid benefits and market potential assessment guide. *Technical report, Sandia National Laboratories*, 2010.

[16] P. Sorensen G. Giebel and H. Holttinen. Forecast error of aggregated wind power. *Technical report, TradeWind*, 2007.

[17] M. Ehsani, Y. Gao, S. E. Gay and A. Emadi. *Modern Electric, Hybrid Electric, and Fuel Cell Vehicles: Fundamentals, Theory, and Design*. CRC, 2004.

[18] W. Greenwell and A. Vahidi. Predictive control of voltage and current in a fuel cellultracapacitor hybrid. *IEEE Transactions on Industrial Electronics*, 57:1954–1963, 2010.

[19] C. Lin, H. Peng, J. W. Grizzle and J. Kang. Power management strategy for a parallel hybrid electric truck. *IEEE Transactions on Control Systems Technology*, 11(6):839 – 849, 2003.

[20] L. Guzzella and A. Sciarretta. *Vehicle Propusion Systems:Introduction to Modeling and Opitmization*. Springer, 2005, pp.190-203.

[21] S. Teleke, M. Baran, A. Q. Huang and S. Bhattacharya. Control strategies for battery energy storage for wind farm dispatching. *IEEE Transactions on Energy Conversion*, 24(3):725–732, 2009.

[22] G. Zini, J. Kern, J. and M. Duoba. Honda insight validation using PSAT. *SAE Paper 2001-01-2538*, 2001.

[23] H. Bindner T. Cronin P. Lundsager J. Schiffer, D. U. Sauer and R. Kaiser. Model prediction for ranking lead-acid batteries according to expected lifetime in renewable energy systems and autonomous power-supply systems. *Journal of Power Sources*, 168:66–78, 2007.

[24] P. Denholm, E. Era, B. Kirby and M. Milligan. The role of energy storage with renewable electricity generation. *Technical Report, NREL/TP-6A2-47181*, 2010.

[25] Donald E. Kirk. *Optimal Control Theory: An Introduction*. Dover, 2004.

[26] H. Borhan, A. Vahidi, A. Phillips, M. Kuang , I. Kolmanovsky and S. Di Cairano. MPC-based energy management of a power-split hybrid electric vehicle. *IEEE Transactions on Control Systems Technology, in press. (Article first published online. doi:10.1109/TCST.2011.2134852)*, 2011.

[27] H. Borhan, A. Vahidi, A. Phillips, M. Kuang, Ilya V. Kolmanovsky and S. De Cairano. Mpc-based energy management of a power-split hybrid electric vehicle. *Accepted in the IEEE Transactions on Control Systems Technology*, 2011.

[28] H. Borhan, A. Vahidi, A. Phillips, M. Kuang and I. Kolmanovsky. Predictive energy management of a power-split hybrid electric vehicle. *American Control Conference*, pages 3970 – 3976, 2009.

[29] H. Borhan, C. Zhang, A. Vahidi, A. Phillips, M. Kuang and S. Di Cairano. Nonlinear model predictive control for power-split hybrid electric vehicles. *49th IEEE conference of Decision and Control (CDC)*, 2010.

[30] W. Liang; Q. Wang; X. Wang; J. Supina; R. McGee; M. Kuang. Power split hev engine speed determination for optimal powertrain efficiency using 4d ems table. *Ford Patent Application*, 2010.

[31] Argonne National Laboratory. Powertrain System Analysis Toolkit (PSAT) documentation. commercial software.

[32] J. H. Lee and N. L. Ricker. Extended Kalman filter based nonlinear model predictive control. *Industrial Engineering and Chemical Research*, 33(6):1530–1541, 1994.

[33] J. Liu and H. Peng. Modeling and control of a power-split hybrid vehicle. *IEEE Transactions on Control Systems Technology*, 16(6):1242 – 1251, 2008.

[34] J. M. Maciejowski. *Predictive Control with Constraints*. Prentice Hall, 2002.

[35] J. Miller, P. McCleer and M. Everett. Comparative assessment of ultra-capacitors and advanced battery energy storage systems in powersplit electronic-cvt vehicle powertrains. *IEEE International Conference on Electric Machines and Drives*, pages 1513 – 1520, 2005.

[36] J. Miller. Energy storage technology markets and application's: Ultracapacitors in combination with lithiumion. *The 7th International Conference on Power Electronics*, pages 16–22, 2007.

[37] S. Oliveira. *Model Predictive Control for Constrained Nonlinear Systems*. vdf Hochschulverlag AG, 1996.

[38] O. Onar and A. Khaligh. Dynamic modeling and control of a cascaded active battery/ultra-capacitor based vehicular power system. *IEEE Vehicle Power and Propulsion Conference*, pages 1–4, 2008.

[39] G. Rizzoni P. Pisu. A supervisory control strategy for series hybrid electric vehicles with two energy storage systems. *2005 IEEE Conference Vehicle Power and Propulsion*, page pp. 8, 2005.

[40] G. Paganelli, S. Delprat, T.M. Guerra, J. Rimaux, and J.J. Santin. Equivalent consumption minimization strategy for parallel hybrid powertrains. *Vehicular Technology Conference*, 4:2076–2081, 2002.

[41] A. Rousseau, J. Kwon, P. Sharer, S. Pagerit and M. Duoba. Integrating data, performing quality assurance, and validating the vehicle model for the 2004 Prius using PSAT. *SAE Paper 2006-01-0667*, 2006.

[42] J-Y Park; Y-K Park; and J-H Park. Optimal power distribution strategy for series-parallel hybrid electric vehicles. *Journal of Automobile Engineering*, 222 (6), 2008.

[43] C. Lin, H. Peng and J. W. Grizzle. A stochastic control strategy for hybrid electric vehicles. *Proceedings of the 2004 American Control Conference*, 5:4710– 4715, 2004.

[44] L. Johannesson, S. Pettersson, and B. Egardt. Predictive energy management of a 4QT series-parallel hybrid electric bus. *Control Engineering Practice*, 17:1440–1453, 2009.

[45] P. Pisu and G. Rizzoni. A comparative study of supervisory control strategies for hybrid electric vehicles. *IEEE Transactions on Control Systems Technology*, 15(3):506–518, 2007.

[46] G. Paganelli, S. Delprat, T. M. Guerra, J. Rimaux and J. J. Santin. Equivalent consumption minimization strategy for parallel hybrid powertrains. *Proceedings of the Vehicular Technology Conference*, 4:2076–2081, 2002.

[47] C. Musardo, G. Rizzoni and B. Staccia. A-ECMS: An adaptive algorithm for hybrid electric vehicle energy management. *Proceedings of the IEEE Conference on Decision and Control*, pages 1816– 1823, 2005.

[48] D. S. Callaway S. J. Moura, H. K. Fathy and J. L. Stein. A stochastic optimal control approach for power management in plug-in hybrid electric vehicles. *IEEE Transactions on Control Systems Technology (Article first published online)*, page PP, 2010.

[49] D. U. Sauer and H. Wenzl. Comparison of different approaches for lifetime prediction of electrochemical systems-using lead-acid batteries as example. *Journal of Power Sources*, 176:534–546, 2008.

[50] S. M. Schoenung and M. V. Hassenzahl. Long- vs. short- term energy storage technologies analysis: A life-cycle cost study. *Technical Report (Sandia National Labaratories)*, 2003.

[51] A. Sciarretta and L. Guzzella. Control of hybrid electric vehicles. *IEEE Control Systems Magazine*, 27(2):60–70, 2007.

[52] G. C. Goodwin, M. Seron and J. A. Dona. *Constrained Control and Estimation*. Springer, 2005.

[53] L. Serrao, S. Onori, and G. Rizzoni. ECMS as a realization of Pontryagin's minimum principle for HEV control. *American Control Conference, 2009. ACC '09.*, pages 3964 –3969, 2009.

[54] C. Zhang; A. Vahidi; P. Pisu; L. Xiaopeng; K. Tennant. Role of terrain preview in energy management of hybrid electric vehicles. *IEEE Transactions on Vehicular Technology*, 59 (3):1139 – 1147, 2010.

[55] W. Waag and D. U. Sauer. Secondary batteries - lead-acid systems — state-of-charge/health. *Encyclopedia of electrochemical power sources*, pages 793–804, 2009.

[56] Z. Wan and M. V. Kothare. Efficient scheduled stabilizing output feedback model predictive control for constrained nonlinear systems. *IEEE Transactions on Automatic Control*, 49(7):862 – 875, 2004.

[57] C. Zhang and A. Vahidi. Trip preview in energy management of plug-in hybrid vehicles. *IEEE Transactions on Control Systems Technology (Article first published online)*, page PP, 2011.